



Unsupported and silica-supported nickel nanoparticles: synthesis and application in catalysis

Mohamed Abboud · Reem Alnefaie · Abdullah Alhanash

Received: 30 March 2021 / Accepted: 18 October 2021 / Published online: 19 January 2022
© The Author(s), under exclusive licence to Springer Nature B.V. 2022

Abstract In recent years, nickel nanoparticles (Ni NPs) have attracted a growing attention from the scientific research community, because they are inexpensive, eco-friendly, facile to prepare, and they could be used in a panoply of applications, ranging from catalysis to sensors and from fuel cells to photoelectrochemical devices. This review article recapitulates different synthesis methods which have been used to prepare unsupported and silica-supported Ni NPs and their utilisation as nanocatalysts in heterogeneous catalysis and photocatalysis. Firstly, various widely used techniques to synthesize unsupported Ni NPs have been briefly discussed. This includes ball milling, mechanochemical synthesis, laser ablation, and ion sputtering as top-down methods, and physical vapour deposition, chemical vapour deposition, sol-gel method, chemical precipitation, chemical reduction, hydrothermal method, solvothermal, spray pyrolysis, and biological techniques as bottom-up methods. Subsequently, the widely applied methods to incorporate Ni NPs in different types of silica (e.g. SBA-15, MCM-41, MCM-48, TUD-1) are briefly reviewed including impregnation, precipitation, and colloid methods. Finally, recent applications of both unsupported and supported Ni NPs in heterogeneous catalysis and photocatalysis have been discussed, with brief investigation of the effect of Ni NP size and aggregation on their catalytic activity and reusability.

Keywords Unsupported Ni NPs · Silica-supported Ni NPs · Preparation methods · Heterogeneous catalysis · Heterogeneous photocatalysis · Mesoporous silica · Nanocomposites

Introduction

Catalysis is a fundamental process for many chemical protocols. A catalyst is mostly required to increase the rate of a chemical reaction in modern organic synthesis and to produce chemicals and materials at milder conditions (Sheldon and Dakka 1994; Sachdeva et al. 2013; Clark and Macquarrie 1998). In the last 10 years, research has become more intense on developing new and effective catalytic systems.

Catalysis has been applied in different areas including bio-, electro-, heterogeneous-, and homogeneous catalysis. Catalysts applied in electrochemical reactions are labelled electrocatalysts (e.g. fuel cells). Natural catalysts, involving cells or enzymes, are themed biocatalysts.

The terms heterogeneous and homogeneous catalyses are used if the catalyst and reactant (s) are in different phases (e.g. solid/liquid, solid/gas) or same (e.g. liquid/liquid), respectively. When performing heterogeneous catalysis, two reaction set-ups can be employed: continuous flow or batch methods. The present review focuses on heterogeneous catalysis, in which the catalyst is present in the solid phase, and the reactants are in the liquid or gas phase.

M. Abboud (✉) · R. Alnefaie · A. Alhanash
Catalysis Research Group, Chemistry Department, College of Science, King Khalid University, P.O. Box 9004, Abha 61413, Saudi Arabia
e-mail: Abboud_med@yahoo.fr

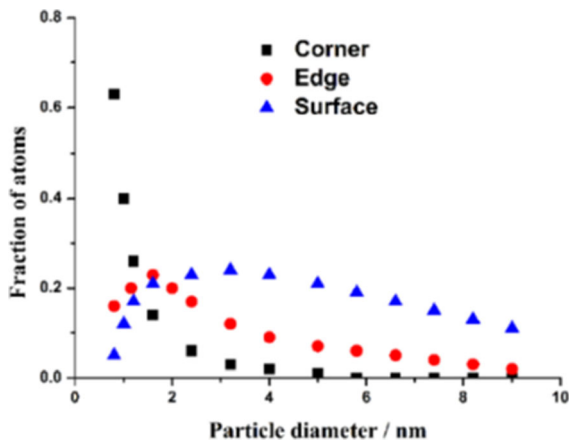
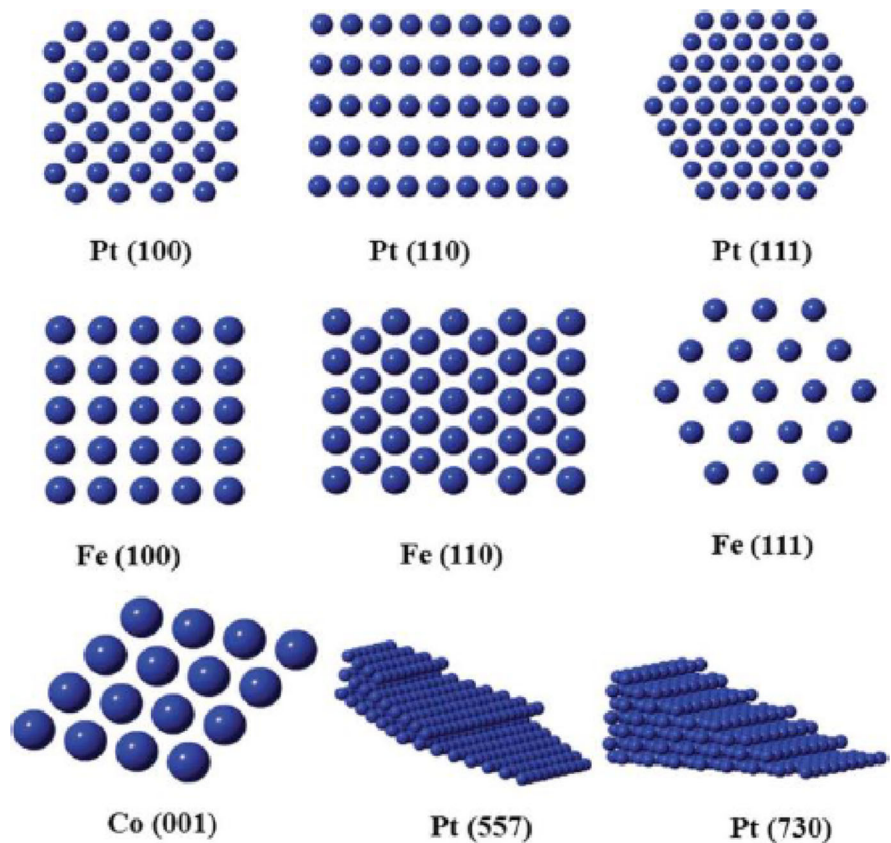


Fig. 1 The fraction of atoms located on surface, corner or edge sites as a function of particle diameter (Lin et al. 2004)

The heterogeneous catalysis contributes to a sustainable future because it has many economic and environmental benefits. It enables large-scale and faster production compared to homogeneous catalysis, and usually, the catalyst is easily separable and recyclable (Sachdeva et al. 2013; Liu and Corma 2018).

Fig. 2 Atomic arrangements of low index with highly coordinated atoms (e.g. (100), (110), (111)) and high index with lowly coordinated atoms (e.g. (557), (730)) (Demello 2006)



The development in the area of heterogeneous catalysis over the last 30 years has mainly focused on engineering catalysts in nanoscale, as well as developing new effective and practical preparation methods. A particular interest has been devoted to metal nanoparticles (NPs) due to their favourable properties, including (i) high available surface area per mass unit, (ii) different fraction of the types of available active sites, (iii) the surface energy can be altered by the ultra-fine NPs, and (iv) reduction of metal NP load is required.

The important characteristics governing the catalytic activity of the metal NPs include particles size, structure, and shape. To disperse and stabilize the metal NPs, and to avoid their aggregation and deactivation, they are often incorporated into a solid matrix, and so the interaction between metal NPs and support is an additional factor to consider.

Transition metal oxides are a large class of materials that has been widely investigated due to their important electronic, magnetic, and catalytic properties (Kung 1989; Henrich and Cox 1996; Noguera 1996; Salem 2003). In recent years, transition metal nanoparticles

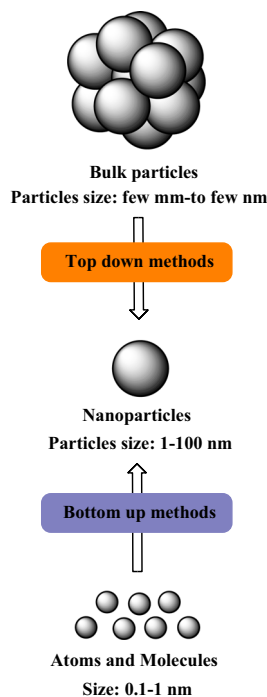


Fig. 3 An overview of top–down and bottom–up methods to prepare nickel nanoparticles

(TMNs) have attracted much attention in many technological and scientific fields, including heterogeneous catalysis (Ornelas et al. 2005; Astruc 2007). Many publications reported the utilisation of TMNs as catalysts for different important reactions (Zhong et al. 2007; Moreno-Manas and Pleixats 2003; Li et al. 2002). They have exhibited a high performance in terms of conversion, selectivity, and yields of products. In fact, the high surface/volume ratio of NPs affords a greater number of active sites per unit area compared to their bulky counterparts. In addition, TMNs have attracted a considerable interest in catalysis because usually, they are efficient catalysts, inexpensive, eco-friendly, and easy to prepare (Astruc (Ed.) (2008); Djakovitch et al. 2007; Durand et al. 2008). To extend the application of TMNs as nanocatalysts, many efforts have been devoted to tailor their nanostructure and minimize their size to ultrafine NPs and hence their surface chemistry (Yang et al. 2017; Astruc 2020).

One of the most promising TMNs is nickel. Due to its relative abundance, Ni is more cost-effective than most of the metals in use as a catalyst (Bian et al. 2017). Numerous research efforts have been recently devoted

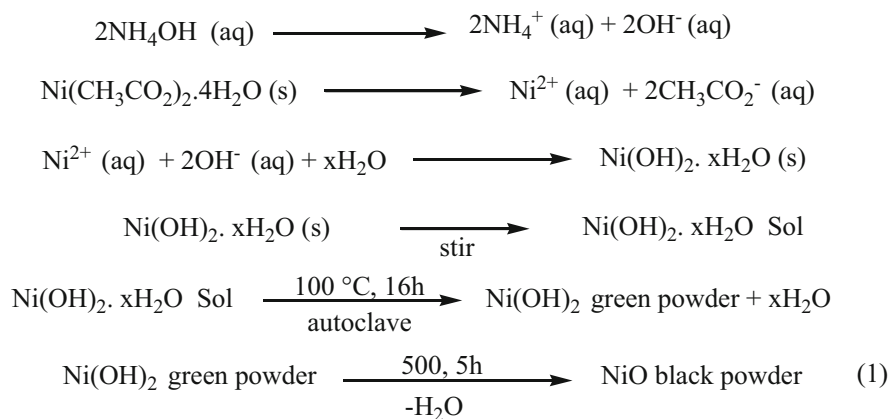
Table 1 Top–down methods used to prepare nickel nanoparticles

Method	Advantages	Disadvantages
Ball milling (Balamurugan et al. 2015; Ahmadsoltansaraei and Moghaddam 2014)	- Useful for large production of NPs with high purity	- Requires high energy and long time - Contamination is possible by steel balls
Mechanochemical synthesis (Fiss et al. 2020; Tang et al. 2014)	- Simple and efficient technique	- The formed microstructures are highly sensitive to grinding conditions - Contamination by milling media and atmosphere - Long time is required to synthesis very small NPs (size less than 20 nm)
Laser ablation (Gondal et al. 2012; Khashan et al. 2017; Mahdi et al. 2020; Safa et al. 2019)	-Simple and useful for large production of small nickel NPs in the form of suspension - Properties of NPs can be changed by changing laser parameters and liquid nature accordingly - No surfactant is needed in liquid media	-Prolonged time can lead to the blockage of the laser path by the formed NPs and reduction of ablation rate
Ion sputtering (Karpinski et al. 2012; Li et al. 2017; Salunkhe and AV, M. A., & Kekuda, D. 2020; Peng et al. 2010)	- Economical technique - No change in the composition of sputtered material compared to the targeted NPs - Suitable method for intermetallic compounds and refractory metals - Generates less impurity - Composition of alloy NPs can be easily controlled compared to other chemical methods - Appropriate for the preparation of ionic NPs with a large range of size and compositions	- The nature of sputtering gas (Ar, He, Ne, Xe, and Kr) can affect the morphology, texture, and composition of the obtained nanocrystalline nickel oxide films

Table 2 Bottom-up methods used to prepare nickel nanoparticles

Method	Advantages	Disadvantages	
Solid-state methods	Physical vapour deposition (Lin et al. 2017)	- Simple technique for the synthesis of thin films	- Expensive technique - Produces a low quantity of material - For the implementation of this method at industrial level, high throughput with lower cost is necessary
	Chemical vapour deposition (Moravec et al. 2011; Napari et al. 2020)	- NP properties can be controlled, such as crystal structure and surface morphology - High film durability can be obtained - Easy to scale-up	- Corrosive, toxic, and explosive gases - Deposition of multicomponent material is difficult
Liquid-state synthesis methods	Sol-gel method (Pooyandeh et al. 2020; Shamim et al. 2019; Zorkipli et al. 2016)	- Simple technique - NP size and morphology can be controlled by monitoring reaction parameters	-
	Chemical precipitation (Abboud et al. 2020; Ebin 2018; Mahaleh and Y., Sadmezhaad, S. K., & Hosseini, D. 2008)	- Simple and efficient approach to prepare metal NPs - Abundant bases can be used as precipitation agents (e.g. NaOH, NH ₄ OH) - Hydrothermal treatment can be used to accelerate the precipitation - High purity NPs can be obtained - Particle shape and size can be controlled using different complexation and protection agents, respectively	-
	Chemical reduction (Ebin 2018; El-Kemary et al. 2013)	- Simple technique - Abundant reducing agents can be used such as NaBH ₄ , ethylene glycol, glucose, ethanol, urea, hydrazine hydrate, citrate of sodium	- Reducing agents are usually toxic and contain impurities
	Hydrothermal method (Cao et al. 2020; Zhou et al. 2018; Ahire et al. 2012)	- Produces NPs with suitable size and shape, and high crystallinity	- Limitation of reproducibility and reliability
	Solvothermal (Gu et al. 2019; Beach et al. 2009)	- Produces monodispersed NPs with high crystallinity - Appropriate technique to prepare NPs with narrow size distribution using simple heating apparatus	-
Gas-phase methods	Spray pyrolysis (Ukoba et al. 2018; Desai 2016)	- Relatively simple technique - Inexpensive method - Reproducible - NP size is controllable	-
	Flame pyrolysis (Dillon et al. 2013; Seo et al. 2003)	- Promising method for the production of Ni NPs - Efficient for less volatile nickel precursors	-
Biological methods	Using fungi proteins (Salvadori et al. 2015; Yang et al. 2014)	- Easy to scale up - Economical flexibility - Large surface area	- Safety problem - NPs formed are of different sizes
	Using plant and plant products (Habtemariam and Oumer 2020; Sabouri et al. 2019; Helan et al. 2016; Ramalingam et al. 2019)	- No pathogenicity risk as that of bacteria and fungi methods - Formation of homogenous NPs	- Heating is required which increases the NP production cost
Other methods	Electrochemical deposition (Zhang et al. 2013; Moghaddam et al. 2008)	- Fast, simple and low-cost method - Produces NPs of controlled size and morphology - NPs attach directly to the substrate	-
	Microwave-assisted method (Azhagu Raj et al. 2017; Jena and Shivashankar 2008; Nadagouda et al. 2011)	- Simple, rapid, and highly effective technique - Homogeneous heating	- Short crystallisation time
	Ultrasound technique (Vargas et al. 2016)	- Eco-friendly, easy, and fast method - Useful for less volatile materials - Different forms of NPs can be synthesized by changing reaction conditions	- The sonochemical reduction rate completely depends on the ultrasound frequency

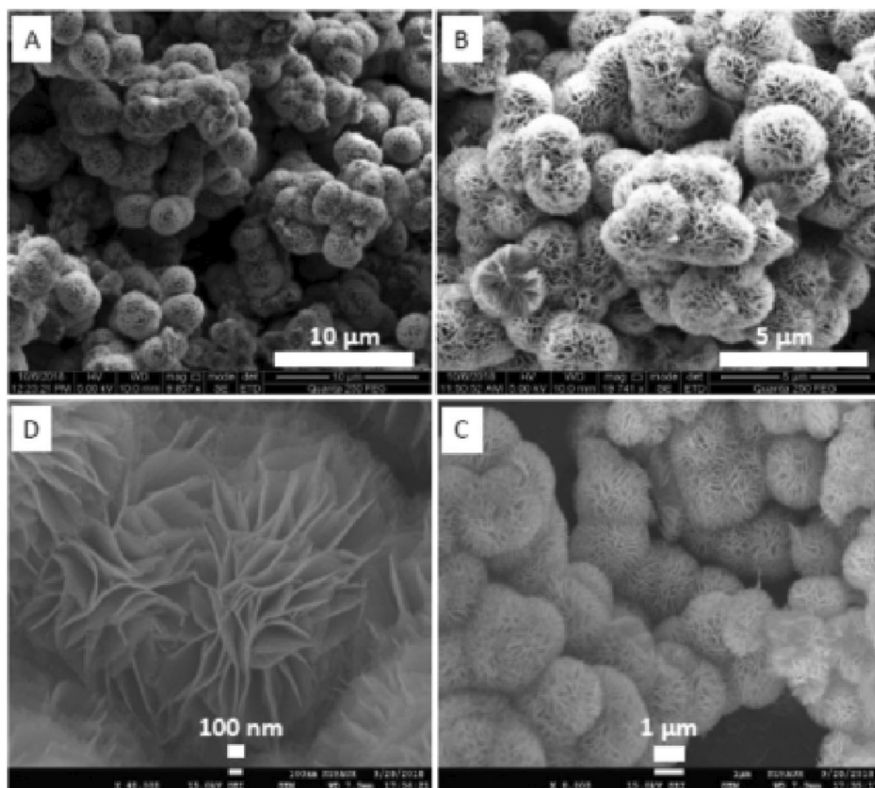
Fig. 4 Principal steps involved in this the synthesis of flower-like NiO NPs



to the preparation of nickel nanoparticles (Ni NPs) with tailored features, because of their unique electronic, optical, and mechanical properties and their widespread potential applications in many fields including catalysis, nanoelectronics, optoelectronics, adsorption of dyes from industrial water, development of supercapacitors, fabrication of dye-sensitized solar cells, and sensors and biomedical applications (Jaji et al. 2020; Vollath and Szabó 2009; Schubert and Hüsing 2019; Ozin et al.

2009a; Lai et al. 2006, 2008; Christoskova and Stoyanova 2001; Ashik et al. 2017; Guo et al. 2011; Solsona et al. 2016; Vikraman and Park 2016; Sasaki et al. 2018; Gao et al. 2012; El-Safty et al. 2008; Adil et al. 2017; Arora et al. 2017; Pike et al. 2017; Chand and Sandhu 2015; Sun et al. 2016). Due to their unique magnetic, chemical, and physical properties, we believe that Ni NPs will gain more attention in future in various technological fields such as nanocatalysis, battery

Fig. 5 SEM images of the flower-like NiO microspheres



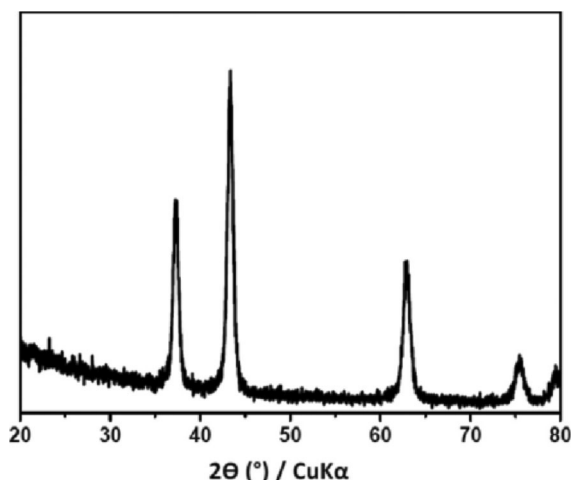


Fig. 6 XRD pattern of the NiO NPs obtained with CTAB

manufacture, dye-sensitized solar cells, enhanced pseudo-capacitance, and drug delivery.

Recently, Ni NP-based heterogeneous nanocatalysts have been employed for various organic transformations such as hydrogenation reaction of aromatics (Grosso et al. 2004), production of synthesis gas (Zou et al. 2005), steam reforming (Ying et al. 1999), methanation (Jia et al. 2003), isomerisation of hydrocarbons (Basha et al. 2006), and hydrocracking (Moreno-Tost et al. 2002) (Polshettiwar et al. 2009; Kalbasi and Mosaddegh 2011; Alonso et al. 2011). Ni NPs are considered as promising nanocatalysts because they are eco-friendly, nonexpensive, easy to prepare, and easily recoverable and recyclable.

Ni NPs have been also employed in photocatalysis. Nickel oxide is one of the promising intrinsic p-type transparent electrically conducting oxides (TCOs) that exhibit several interesting features such as wide band gap (3.5 to 4 eV), excellent durability, chemical stability, and large span optical density (Sriram et al. 2016).

Despite the importance of Ni NPs as efficient economic and eco-friendly nanocatalysts, characteristics such as optical and catalytic activity may be lost if the dispersion of these particles is not adequately modulated. Several efforts have been deployed to overcome their aggregation problem, low durability, low dispersibility, and electrons and holes recombination by incorporating them into a solid matrix, like mesoporous silica, zeolites, carbon, metal oxides, or polymers (Kumar et al. 2016; Wang et al. 2017; Jin et al. 2009; Martín-Jimeno et al. 2021).

Throughout this review, we will discuss the most common techniques used to prepare unsupported and silica-supported Ni NPs and their recent applications in heterogeneous catalysis, including photocatalysis. The effect of Ni NP size and aggregation on the catalytic activity of the reported catalysts will be briefly studied.

Designing metal nanoparticles

Effect of nanoparticle size and shape

Increasing the number of active sites in a surface unit of a metal by increasing the surface area per gram of the catalyst, by reducing the metal particles size, not only minimizes the cost of catalyst preparation but also reduces the associated side effects on the environment and public health of the catalytic process. It has been found that the reduced particle size has also a higher fraction of corner and edge sites as shown in Fig. 1 (Martín-Jimeno et al. 2021), which can affect the binding properties of reactants on the catalyst. Some reports mentioned that the catalysis occurs especially on isolated active sites, and thus, decreasing the NP size is recommended. This behaviour was observed for the oxidation reaction of

Fig. 7 TEM images of the obtained NiO nanoflakes. Red cycles in panel A show uniform and highly ordered channels

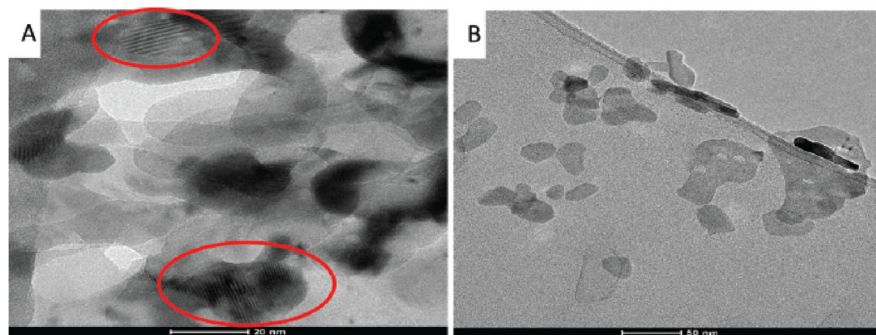
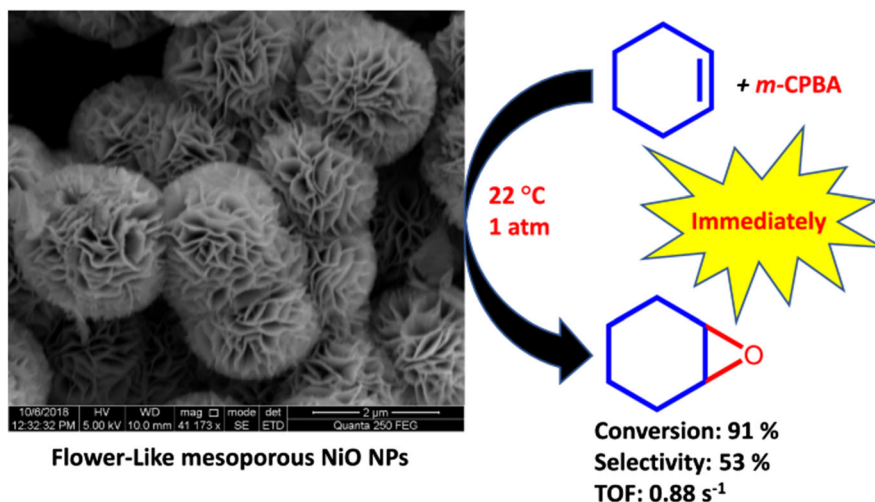


Fig. 8 Transformation of cyclohexene to cyclohexene oxide over flower-like NiO NPs (Abboud 2020)



CO over Au NPs, in which the catalysis occurred in the isolated active sites located in corners and edges, where the Au atoms were lowly coordinated, and were able to bind both CO and oxygen (Lin et al. 2004). Conversely, Giordano et al. (Tsunoyama et al. 2008) reported that the oxygen reduction reaction (ORR) catalysed by Pt NPs preferably occurred in the active sites located in the planes, where each O₂ molecule was bound on two adjacent Pt atoms. This could lead to a mass normalized catalytic activity. The smallest NPs contain a low and isolated number of active sites, and the larger NPs have small surface area. Therefore, a compromised size

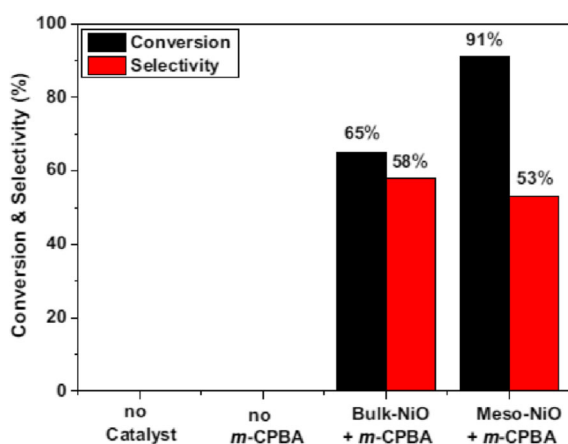


Fig. 9 The calculated conversion of the cyclohexene oxidation reaction at different blank reactions. 10 mg of NiO catalyst, 0.06 mL of cyclohexene, 156 mg of *m*-CPBA (1.5 equivalent), 3 mL of solvent: CH₃CN/CH₂Cl₂ (1:1 v/v), *T* = 22 °C, 1 atm

distribution could afford the highest mass normalized catalytic activity.

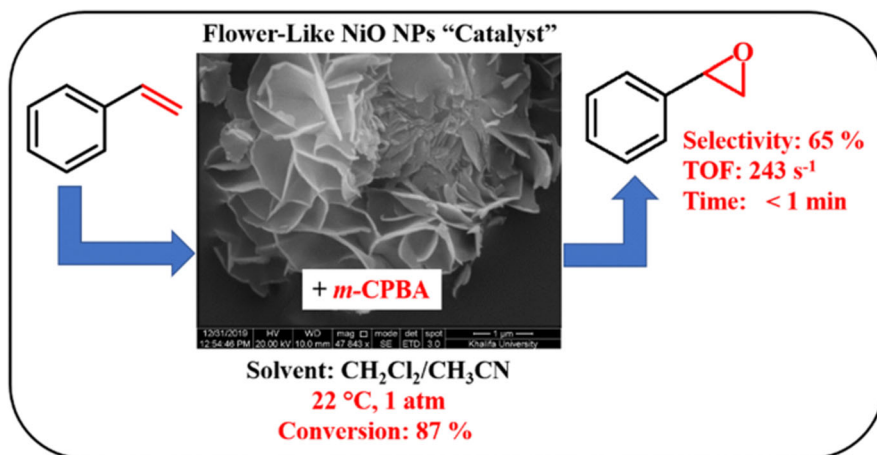
Particles shape is another important parameter which can affect the active sites distribution in the catalyst NPs. Controlling the metal NP shape is an ongoing challenge. However, using colloidal methods, this aim has been relatively achieved (Glasnov 2013; Rogers 2017). The obtained metal NP shapes are a result of the arrangement of different crystal planes (facets). NP shape could have a direct effect on reactants adsorption/desorption properties, reactant binding, and metal/support interactions. During the catalyst synthesis, different possible facet arrangements could be formed. But, typically, low index facets, such as (100), (110), and (111), are predominant, because these facet arrangements are characterized by low energy and high atomic coordination (Fig. 2). However, if the active species are located in corners and edges, it is preferable to prepare facet arrangements with high indexes (e.g. (557), (730), Fig. 2) (Baumgard et al. 2013).

The metal/support contact surface area and the number of active sites in the periphery depend on the shape of metal NPs. As mentioned above, the CO oxidation reaction over Au NPs preferentially occurred in the periphery active sites, and the catalytic performance was shape dependent (Woehl et al. 2012).

Support effect

The physical and chemical stability, good reusability, and high turnover numbers are important factors

Fig. 10 Epoxidation reaction of styrene oxide over flower-like NiO NPs



defining an efficient catalyst. To overcome metal NP deactivation due to the aggregation, low durability and dispersibility, electron–hole recombination, and degradation, metal NPs have been incorporated and immobilized into a support. However, the support can also affect the catalyst activity and performance either by (1) changing the shape and structure of NPs, (2) redox transforming the metal ions which have two or more redox states (e.g. MnO₂, Fe₂O₃, and CeO₂), and (3) support-metal NP charge transferring (Bönnemann and Richards 2001).

The choice of the type of support is usually governed by the application. Carbon is often used as a support for fuel cell owing to its high conductivity (Polte et al.

2010a), and titanium dioxide (TiO₂) has been widely used as a support in photocatalysis as it is a semiconductor characterized by an appropriate band gap (McKenzie et al. 2010), whereas silica (Polshettiwar et al. 2010), alumina, and other transition metal oxides (Gniewek et al. 2008) have demonstrated to be very appropriate supports for various applications, even for nanocatalysts, due to their high thermal and chemical stabilities and high surface areas (Polte et al. 2010b, 2010c). Mesoporous silica materials have attracted considerable interest as suitable catalyst matrices due to their unique features. These characteristics include high surface area; tunable pore size; uniform pore distribution; high adsorption capacity; high thermal, chemical, and mechanical stabilities; and highly ordered pore network which facilitate the diffusion of reagents and products.

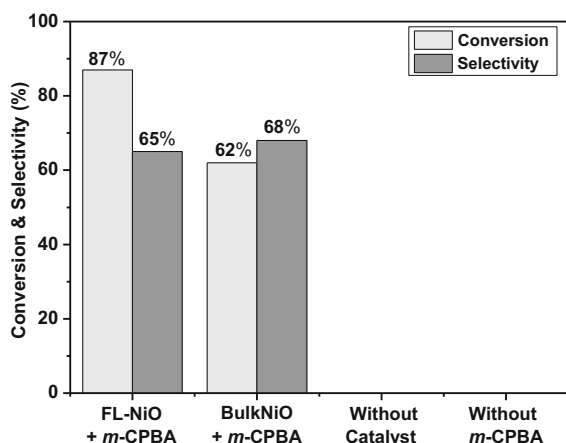


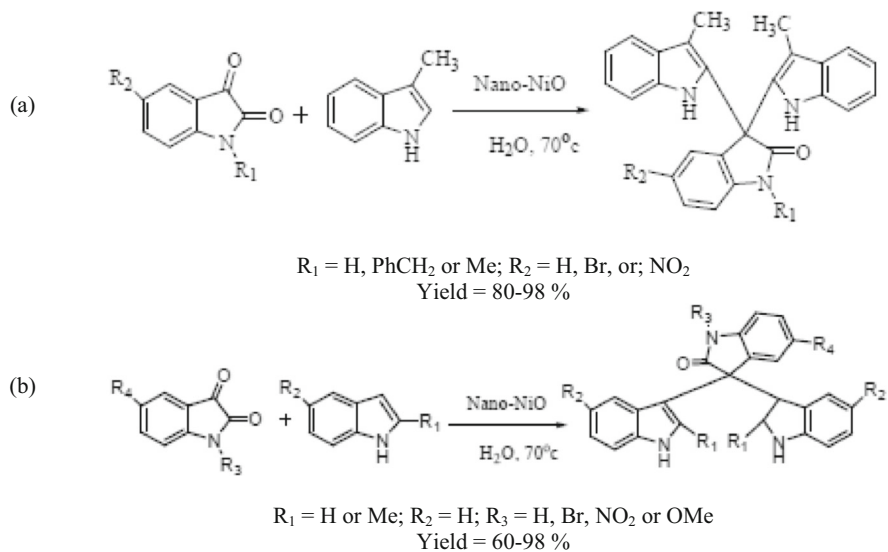
Fig. 11 The obtained conversion and selectivity of epoxidation of styrene catalysed by FL-NiO compared to BulkNiO and blank reactions. Conditions: catalyst: 10 mg, styrene: 0.06 mL, *m*-CPBA (1.5 eq): 156 mg, solvent: 3 mL of CH₃CN/CH₂Cl₂ (1:1 v/v), time: < 1 min, *T* = 22 °C, 1 atm

Synthesis methods of nickel nanoparticles

Unsupported nickel nanoparticles

Several methods have been used to prepare nickel NPs which can be classified into two principal categories: top–down methods and bottom–up methods (Pacioni et al. 2015; Swathy 2014; Horikoshi et al. 2013; Ahmed et al. 2016; Jamkhande et al. 2019). The top–down methods reduce the size of bulk material particles to NPs, whereas the bottom–up methods prepare NPs from atoms or molecules, using different mechanical, physical, and chemical techniques (Fig. 3) (Pacioni et al. 2015; Jamkhande et al. 2019).

Fig. 12 Synthesis of 2,2'-di(indolyl)oxindole (a) and 3,3'-di(indolyl)oxindole (b) derivatives. Reaction conditions: isatin compounds (1 mmol), indole compounds (2 mmol), nano-NiO (0.004 g) and water (2 mL) at 70 °C. The yield refers to pure isolated product



Top-down methods

Using these methods, bulk particles are reduced to NPs using different physical and chemical techniques such as mechanical milling, laser ablation, and thermal method (Meyers et al. 2006). Even though these methods are relatively easy to carry out, they are not suitable for synthesising NPs with determined shape and very small size. In addition, the top-down techniques can affect the physicochemical and surface of the obtained NPs

(Ahmed et al. 2016). Table 1 recapitulates the most used techniques in top-down methods with their advantages and disadvantages.

Bottom-up methods

The synthesis of Ni NPs using these methods is based on joining of atoms or small molecules. Table 2 recapitulates the most used techniques in this category with their advantages and disadvantages.

Fig. 13 Preparation of oxindole (a) and indoline (b) derivatives. Reaction conditions: dicarbonyl compounds (1 mmol), isatins (1 mmol), malononitrile (1 mmol), catalyst (0.0007 g), and H₂O (2 mL); reactions conducted at r.t. for 5 min

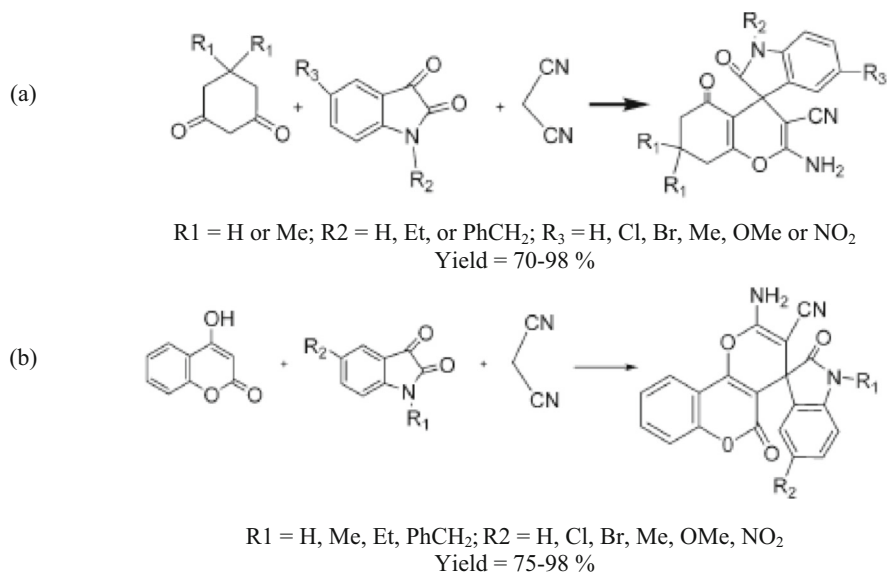


Fig. 14 XRD pattern of NiO nanoparticle

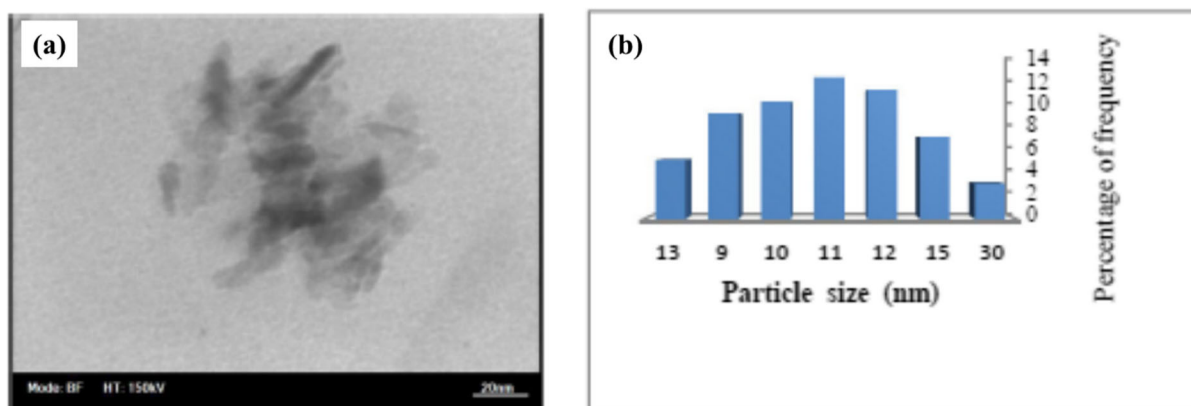
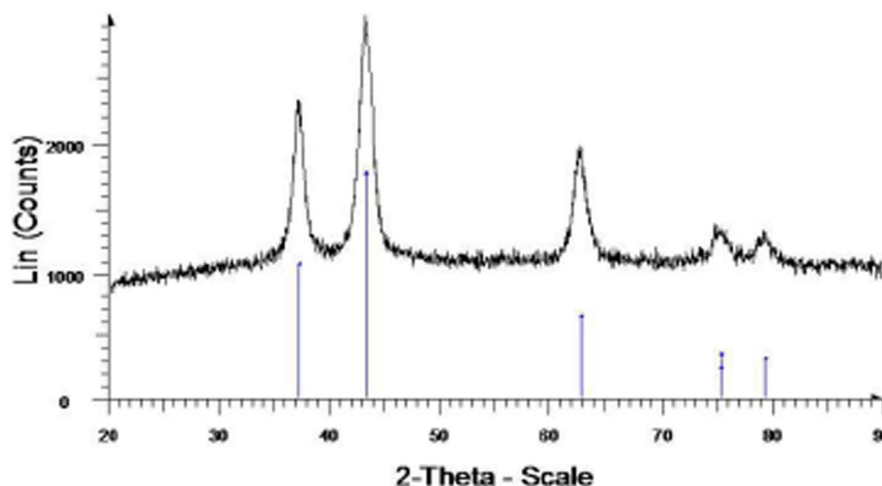


Fig. 15 (a) TEM pattern of NiO nanoparticle and (b) particle size distribution of NiO nanoparticle

Preparation of silica-supported nickel nanoparticles

Usually, silica-supported Ni NP-based catalysts are synthesized by introducing nickel precursors into the silica followed by calcination. The dispersion degree of nickel precursor in the silica before calcination will affect the particle size, degree of dispersion, and aggregation of

the obtained Ni NPs and will then affect the catalytic activity of the final nanocatalyst (Ashik et al. 2017). Generally, metal NP species would exhibit higher catalytic activity and stability if the active sites are considerable, quantized, confined, and accessible (Alshammari and Kalevaru 2016).

In the past decade, several techniques have been developed for the preparation of silica materials

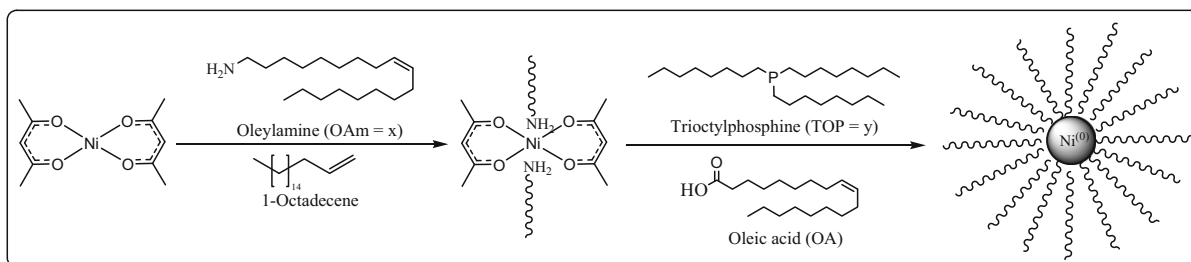


Fig. 16 Hot injection synthesis of monodispersed NPs

Table 3 Synthetic conditions and resulting size of Ni NPs

Samples	OAm ^a (x) [eq.]	TOP ^b (y) [eq.]	Size ^{c,d} [nm]
Ni_2.5×1.5y	2.5	1.5	1.3/8.0±1.4
Ni_5×1.5y	5	1.5	4.0/7.0±1.3
Ni_10×1.5y	10	1.5	5.6/10.6±1.9

^a Total number of equivalents of oleylamine (OAm) and 1-octadecene (21) kept constant by varying the amount of solvent

^b Trioctylphosphine

^c Determined by XRD

^d Determined by HAADF-STEM

supported Ni NPs. Among these techniques, the impregnation, ion exchange, sol–gel technique, microemulsion, co-precipitation, direct incorporation, and deposition of nickel precursors into the silica materials are the most commonly used methods (Solsona et al. 2016; Sasaki et al. 2018; Barhoum et al. 2017; Badari et al. 2015; Rudko et al. 2015; Ashik and Daud 2015). However, the use of these approaches is still limited by the NP size and aggregation, low dispersion, level of the incorporated Ni NPs into porous silica matrices, and the complicated, expensive, and time-consuming techniques.

The synthesis of Ni NPs with quantized size and high dispersion tended to be difficult. The study of the

catalytic activity of Ni NPs with quantized size was relatively scarce compared with other transition metal NPs.

In recent years, some traditional impregnation techniques and approaches have been developed to prepare highly active and well-dispersed supported nickel catalysts, such as using organic nickel precursor (Corma 1997), direct dispersion (Vadia et al. 2013), aqueous metal complexes (Ashik et al. 2017; Look and Clafin 2004), and surface modification (Ashik et al. 2017; Look and Clafin 2004). Despite this, the application of these techniques is still limited by the aggregation of Ni NPs, low dispersion, complicated preparation, and expensive metal precursors.

In addition, the carrier of the catalyst is another key factor for obtaining high catalytic activities. Mesoporous silica, as an important carrier, is well-known for its high surface area, high porosity, and oriented channels, which are ideal characteristics to enhance the catalyst activity (Kumar et al. 2016; Look and Clafin 2004; Rioux 2010; Rodríguez and Garcia 2007). Furthermore, due to the narrow size distribution of mesoporous silica channels, the growth of the metal particles would be well confined in these channels, and thus, quantized active sites would be produced (Wang et al. 2017; Penner 2014; Finiels et al. 2014). However, practical methods are still necessary to control the migration of Ni NPs from silica pores and channels and their aggregation, hence their deactivation. In addition, more efforts are still needed to control the dimension, geometry, and regularity of the silica channels and pores in a systematic and efficient methodology during the incorporation of these NPs into nanostructured mesoporous silica. Because if the interaction between metal particles and support is weak, metal species will migrate out of the silica pores and aggregate into bulk particles during the calcination step or during the catalysis process (Schubert and Hüsing 2005). Therefore, the force of the interaction between nickel and silica or the confinement of Ni NPs is necessary to stabilize the nickel species and to prevent their migration and aggregation during the calcining process (Lai et al. 2008; Ozin et al. 2009b).

Classical routes commonly used to date to prepare silica-supported Ni NPs with tailored properties are based on precipitation and impregnation techniques. Many efforts have been made to develop the colloidal methods to be able to tune the nickel-based catalyst properties, especially using sol immobilisation. The

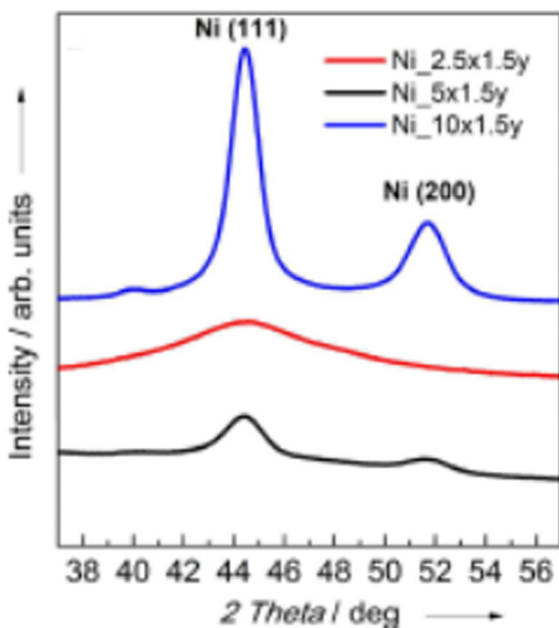
**Fig. 17** XRD pattern of Ni nanoparticles

Fig. 18 (a) and (b) are HR-HAADF-STEM images of Ni₅ × 1.5y. The arrow indicates the twinned lamellae of the NPs in (a) and smaller Ni NPs embedded in the organic shell in (b); (c) and (d) are HR-HAADF-STEM images of Ni₁₀ × 1.5y. In (c), the arrow indicates the fivefold axis of a multiply twinned decahedron. In (d), the arrow indicates the Ni atoms of smaller NPs embedded in the organic shell

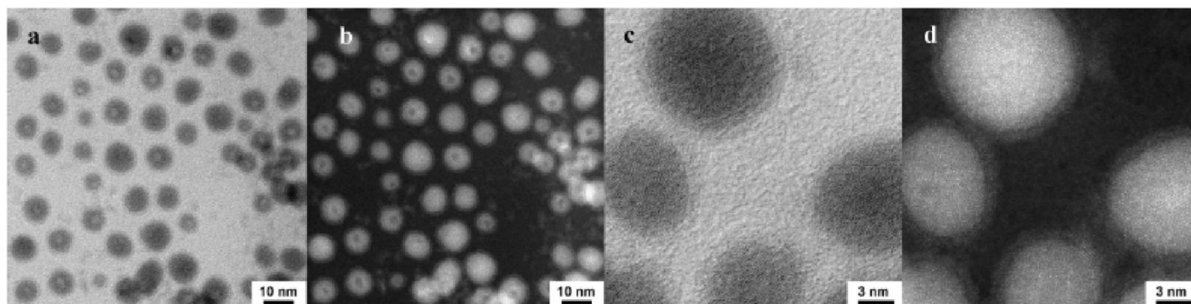
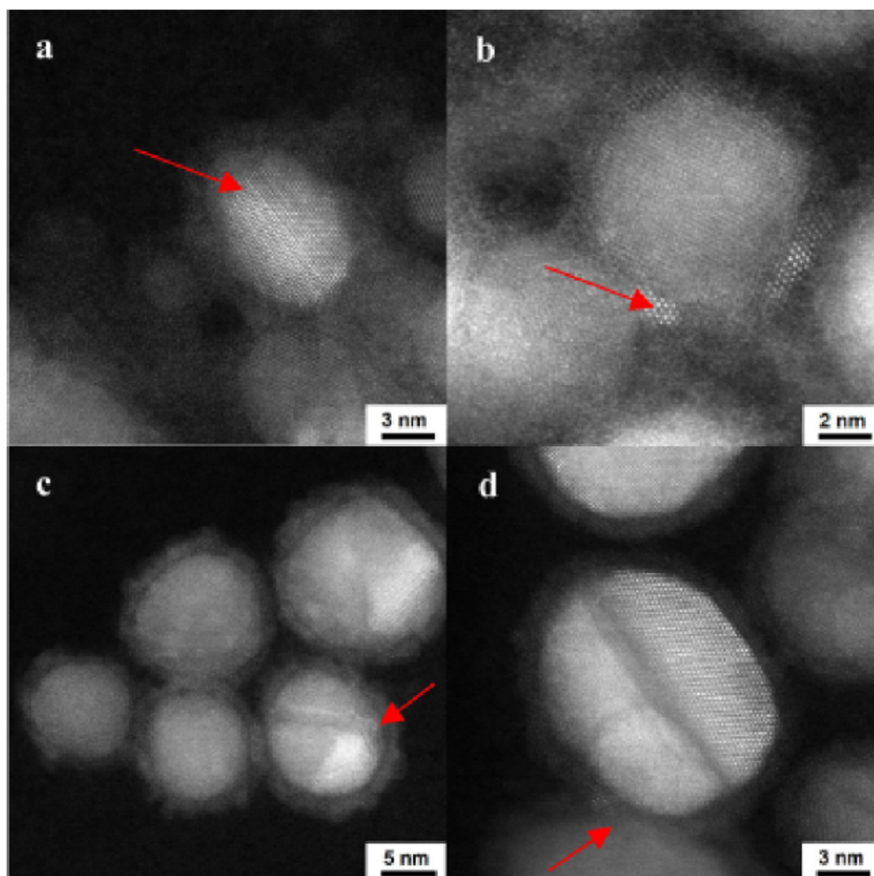


Fig. 19 (a) STEM images of Ni_{2.5} × 1.5y. LM BF-STEM (LM, low magnification; BF, bright field), (b) corresponding HAADF-STEM, (c) HR BF-STEM of a Ni NPs, (d) corresponding HAADF-STEM

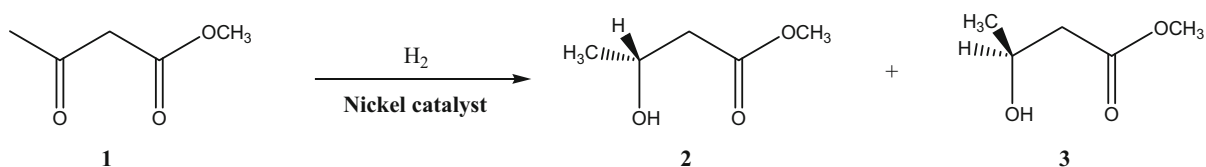


Fig. 20 Hydrogenation of methyl acetoacetate (1) and formation of two enantiomers, (*R*)- and (*S*)-methyl-3-hydroxybutyrate (2 and 3, respectively)

Table 4 Catalytic performance of Ni NPs in hydrogenation of methyl acetoacetate

Samples	Tot. MAA ^a conv. [%] ^c	Inst. (R)-MHB ^b selec. [%] ^d	Final ee [%] ^e
Ni_5×1.5y	69	48	−3
Ni_2.5×1.5y	36	48	−3
Ni_10×1.5y	74	46	−4

^a Methyl acetoacetate^b Methyl-3-hydroxybutyrate^c Conversion after 22 h of reaction^d Unless otherwise stated, selectivity at the same value (50%) of total MAA conversion^e Positive values indicate (*R*)-selectivity, negative (*S*)-selectivity

general procedures and advantages, as well as some drawbacks of these three principal methods, will be now discussed.

Impregnation method

Impregnation is a very commonly used procedure to synthesize nickel NPs with different sizes. This method

involves ‘wetting’ the catalyst support (here silica) with a solution of the nickel precursor, which is commonly a nickel salt. If the nickel precursor is dissolved into a volume of solvent equal to the silica total pore volume, a thick-paste like material is obtained; this point is called ‘incipient wetness point’. This technique is named as incipient wetness impregnation (IWI) (Frey and Hinrichsen 2012; He et al. 2015; Nakagawa et al. 2012). Then, the final material is obtained after the evaporation of the solvent followed by a calcination process, to transform the nickel precursor to nickel oxide NPs (NiO). The final material can be transformed to reduced form (Ni NPs), if required.

However, controlling the size and dispersion of NiO NPs using this method is still challenging. The size of the obtained NiO NPs can be affected by four principal factors: the silica surface area, nickel loading, solvent nature, and annealing conditions. A high surface area of the silica and low nickel loading promote the formation of smaller NiO NPs with high dispersion (Yao et al. 2010). In addition, high thermal treatment is required to remove chlorine residues, (Zhao et al. 2020) which thereafter could lead to particles agglomeration, in

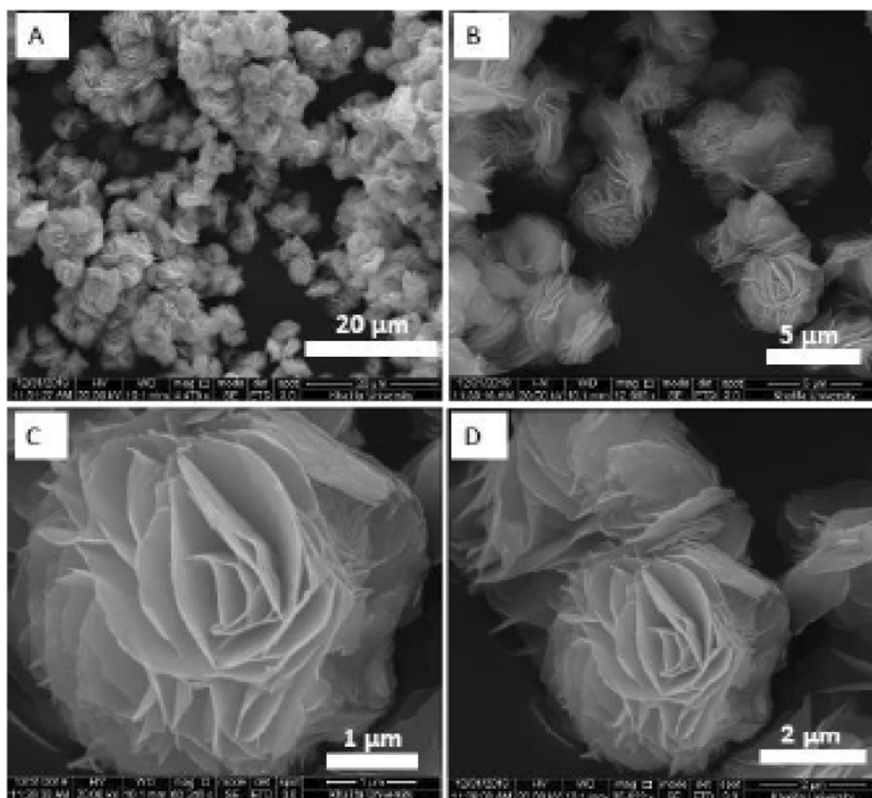
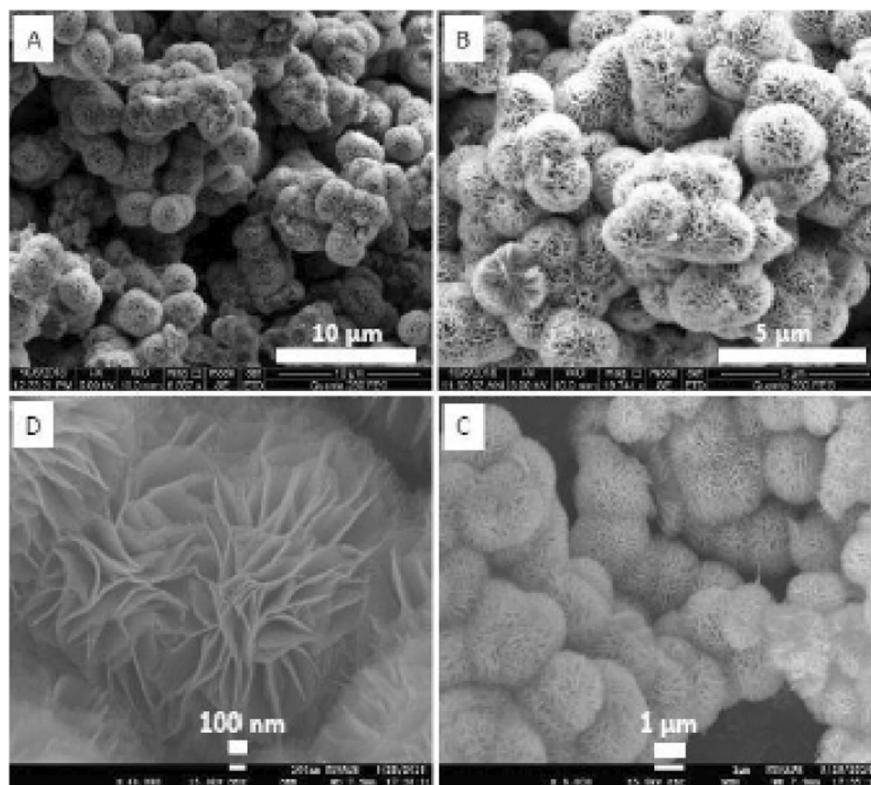
Fig. 21 SEM pictures of NiO microspheres prepared without CTAB

Fig. 22 SEM pictures of NiO microspheres prepared with CTAB



particular in case of high nickel loading (Spagnolo et al. 2016).

Precipitation methods

The co-precipitation is the most commonly used method for the preparation of mixed metal oxides NPs. This method is based on a simultaneous precipitation of both metal and support precursors, in an alkaline media, such as aqueous solutions of NaCO_3 or K_2CO_3 . Generally, the co-precipitation process provides strong metal/support interactions.

The deposition–precipitation (DP) method is similar to co-precipitation. However, DP technique involves a controlled precipitation of highly soluble metal precursor (e.g. nickel nitrate or acetate) inside the silica. The precipitation of the metal precursor can be achieved either by changing the solution pH or the concentration of a complexation agent or by adding a precipitation or reducing agent (Bianchi et al. 2005). Two main factors have to be ensured to avoid a spontaneous precipitation of the metal precursor in solution, namely strong metal–support interaction and appropriate metal precursor concentration. In general, the silica surface acts as a

nucleation agent for the precipitation of the metal precursor. The desired catalyst is obtained after subsequent calcination steps (Patil et al. 2012).

Colloidal methods

Colloidal methods are three-dimensional syntheses which use stabilising agents (protective agent) to prevent the metal NP aggregation via electrostatic repulsion or steric inhibition. Different molecules can play the role of stabilising agent, including surfactants, polymers, and donor ligands.

These methods involve many steps: (i) preparation of a colloidal metal by dissolving the required metal precursor (commonly a salt) in a suitable solvent using a surfactant as protective agent (e.g. cetyltrimethylammonium bromide (CTAB)), (ii) deposition of the metal colloids into the selected support, and (iii) chemical reduction of the metal salt to zero valent mixture metal (Mehrabadi et al. 2017). Metal colloids can be carried out either in organic or aqueous medium, depending on the nature of the surfactant used.

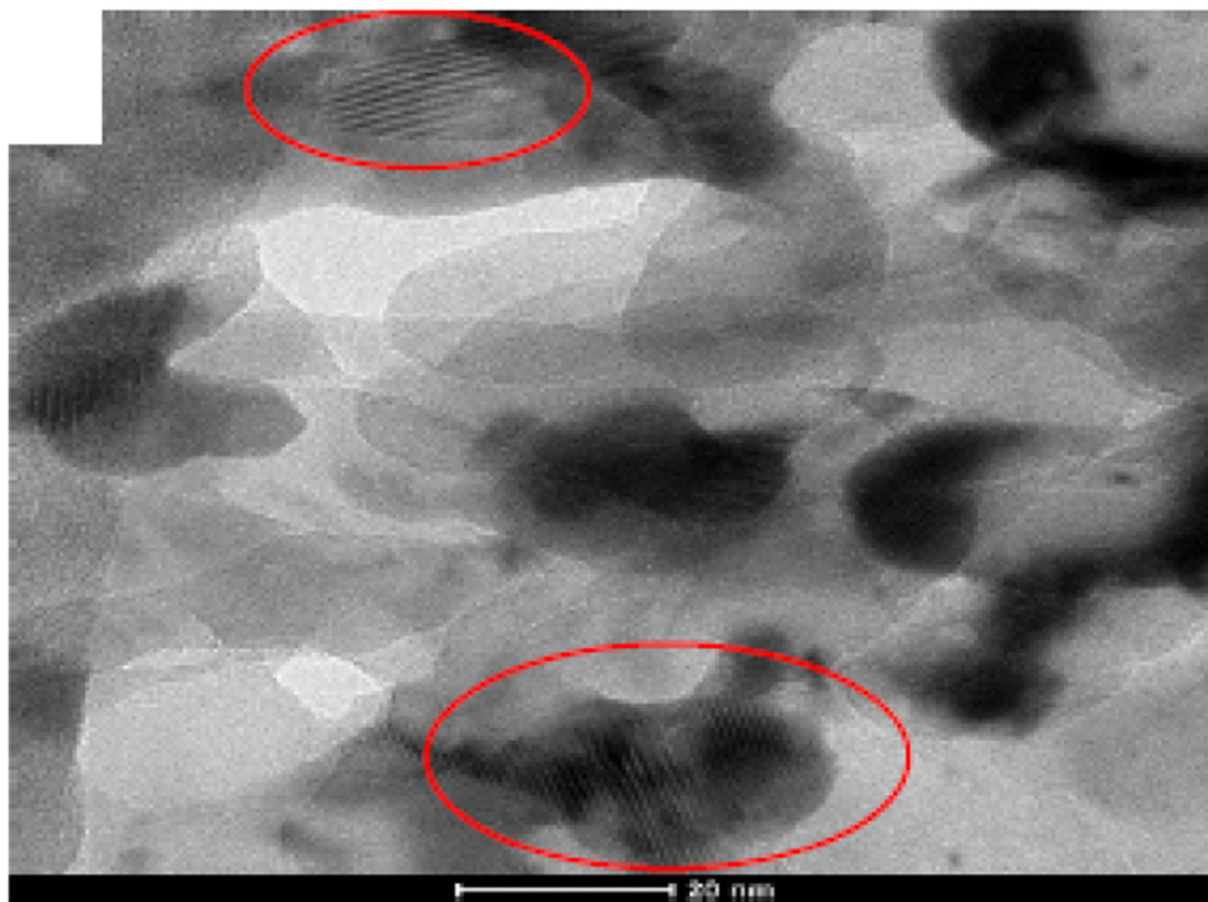


Fig. 23 TEM pictures of the obtained NiO nanoflakes

This method can produce very small nickel NP sizes. The surfactant can be removed either by solvent extraction in diluted acidic conditions (e.g. HCl, 2 M in ethanol) or by using high-temperature treatment (e.g. calcination). It is suitable to develop an alternative route to synthesize highly dispersed fine metal NPs without using surfactant or any protection agents, hence decreasing the level of complexity, avoiding final catalyst contamination and protecting the environment.

The sol immobilisation process is an extension of the colloidal methods and involves immobilizing the colloidal metal into a support material by changing the pH. The metal–support interaction can be enabled by reducing the pH under the isoelectric point of the support. Actually, the properties of the metal NPs can be tuned before their immobilisation by changing different reaction conditions such as reducing agent, metal concentration, and metal/stabilizer ratio (Kennedy et al. 2015).

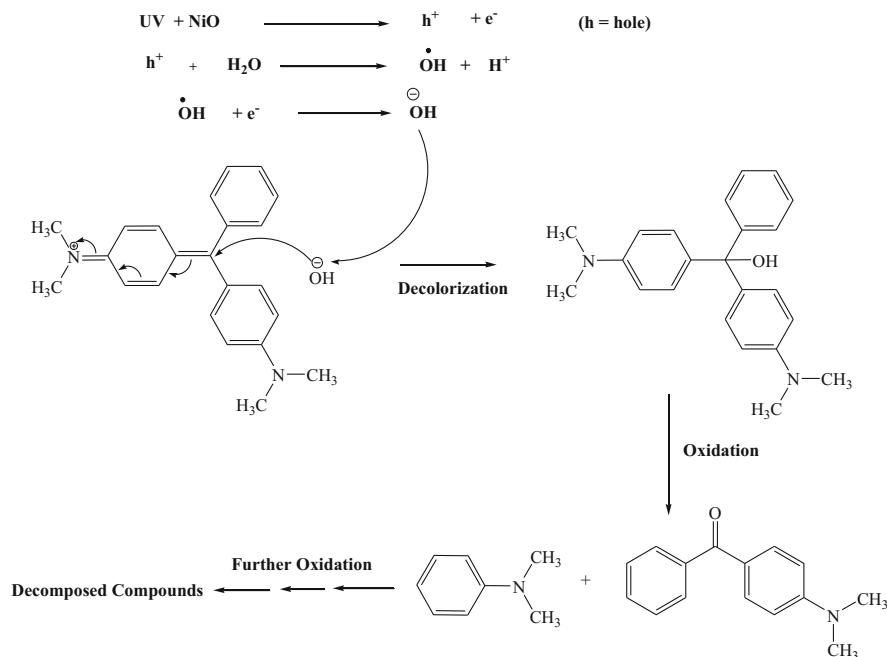
The nature of the reducing agent can affect the metal NP properties. A panoply of reducing agents has been used for the preparation of metal NP catalysts, such as hydrogen, hydrazine, boron hydrides, and alcohols (Jia and Schüth 2011).

The utilisation of polymers as protecting agents is preferable as they are able to tailor the metal NP properties and also enhance their long-term stability during catalysis process (Yoshida et al. 2005). Polymers can bind selectively to specific crystal planes, leading to NPs with controlled shape and surface site (Chen et al. 2015; Zhou et al. 2002).

Recent applications of unsupported nickel nanoparticles in catalysis

Unsupported catalysts occupy the large section of industrial catalysis. This includes metals, metals alloys,

Fig. 24 The proposed photocatalytic mechanism of MG dye decolourisation over the flower-like NiO NPs



metal oxides, metal sulphides, zeolites, etc. Unsupported catalysts have much lower surface areas, typically in the range of 1 to 100 m²/g. Among the most important metal oxides, NiO NPs have been prepared by different methods and techniques and employed as a catalyst for many chemical transformations.

Different approaches are intensively investigated, and important progress has been made in the synthesis of NiO NPs with different morphologies, sizes, shapes, and crystalline structures. The most employed methods

for the synthesis of unsupported NiO NPs are discussed above. The common aim of all these methods and techniques is to obtain well-defined and reproducible nanoparticles by employing a simple, scalable, and low-cost process. Therefore, NiO NPs have been prepared in different morphological structures, such as nanoflakes, nanoflowers, nanorods, nanosheets, nanospheres, nanoballs, nanotubes, and nanowires (Paulose et al. 2017).

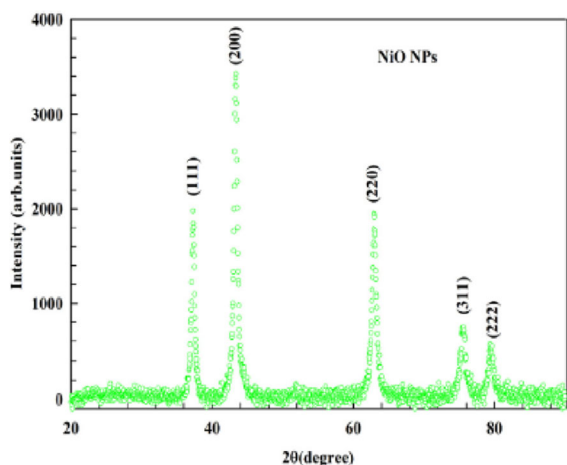


Fig. 25 XRD patterns obtained for NiO NPs prepared with a bio-synthesis method using the extract from *Persea americana* seeds

Heterogeneous catalysis

Only a few articles in the literature reported the investigation of Ni NPs in heterogeneous catalysis. Abboud et al. (Abboud 2020) reported recently the synthesis of highly ordered mesoporous flower-like NiO NPs and their utilisation as catalyst for the epoxidation reaction of cyclohexene to produce cyclohexene oxide. NiO NPs were prepared by hydrothermal-assisted chemical precipitation method, using nickel acetate tetrahydrate as a metal source, ammonium hydroxide (NH₄OH) as a base, diethanolamine (DEA) as complexing agent, and CTAB as a structure directing agent. The principal steps involved in this synthesis are described in Fig. 4 below.

The obtained material was characterized by SEM TEM and EDX. The SEM images (Fig. 5) clearly showed that the prepared NiO consists of fairly flower-

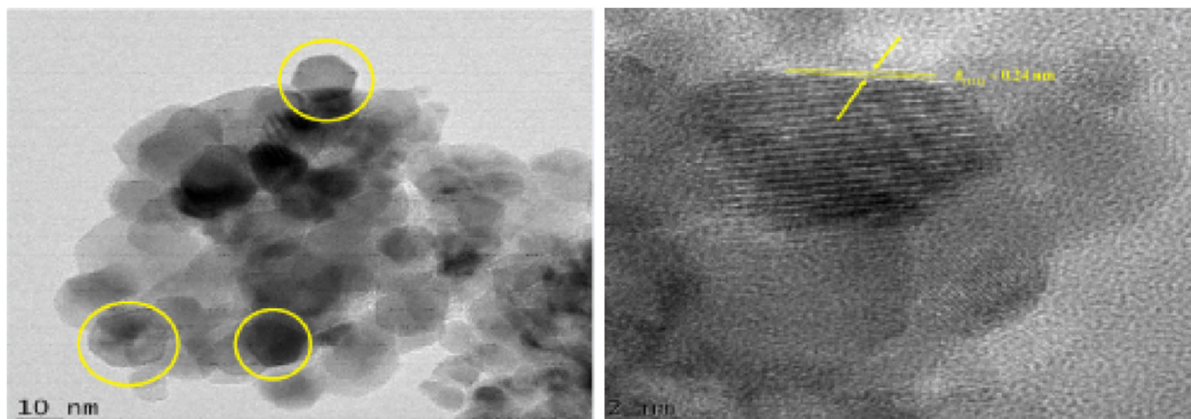


Fig. 26 High-resolution TEM images of the biosynthesized NiO NPs annealed at 500 °C

like microspheres, similar to peony flowers, with a uniform porous structure and size distribution, and ripple-like pores.

Powder X-ray diffraction (XRD) was used to identify the structure of NiO NPs (Fig. 6). The XRD pattern shows the principal peaks observed at $2\theta = 37.311, 43.411, 62.871, 75.531,$ and 79.461 , assigned to the (111), (200), (220), (311), and (110) planes, respectively, confirming the

formation of highly pure NiO NPs (Behnajady and Bimeghdar 2014).

The surface structure of the nanoflakes was investigated by TEM. The obtained images are presented in Fig. 7, which show very thin and aggregated nanoflakes in random directions (Fig. 7A), with different shapes, and with diameters ranging from 10 to 100 nm (Fig. 7B). The TEM images clearly illustrate the

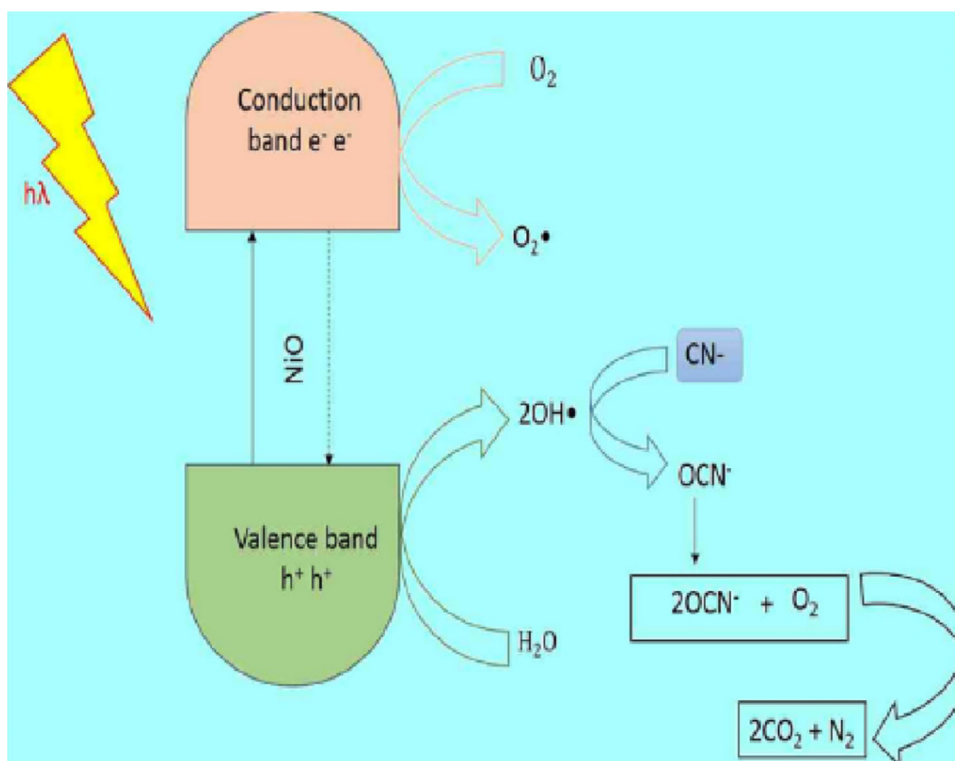


Fig. 27 Degradation mechanism proposed for photo-oxidation of FCN on the surfaces of NiO NPs

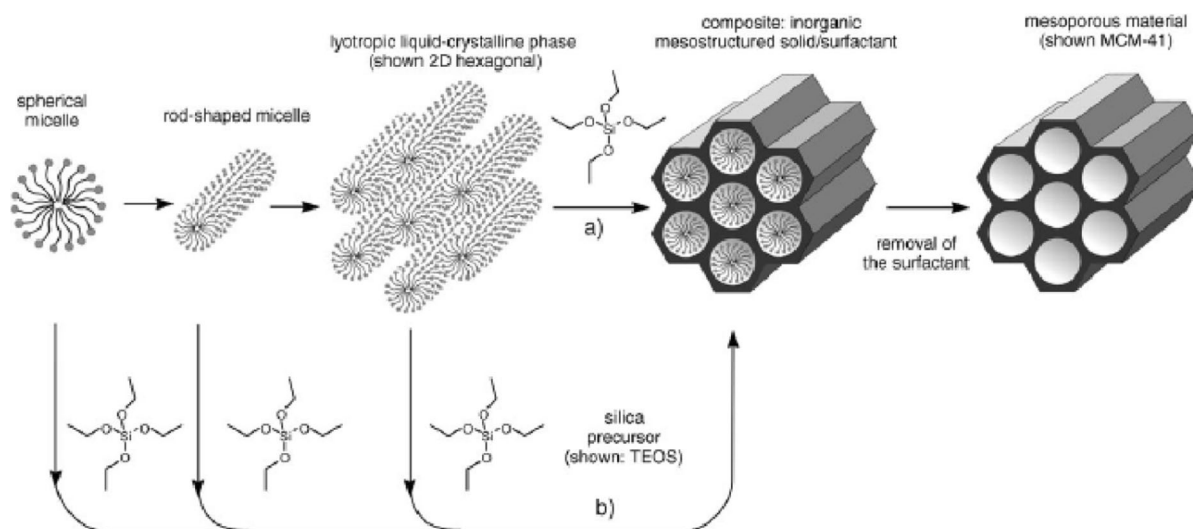


Fig. 28 Formation of mesoporous materials by structure-directing agents: (a) true liquid–crystal template mechanism, (b) cooperative liquid crystal template mechanism (Jadhav et al. 2015)

nanostructure inside of the nanoflakes in the form of uniform and highly ordered channels (see the red circles in Fig. 7A).

The prepared flower-like NiO NPs were used as a catalyst for the epoxidation reaction of cyclohexene to produce cyclohexene oxide. The *meta*-chloro peroxybenzoic acid (*m*-CPBA) was used as an oxidant and $\text{CH}_2\text{Cl}_2/\text{CH}_3\text{CN}$ as a solvent at ambient conditions (Fig. 8). The obtained results shown an instant reaction with high conversion of cyclohexene of 91%, and cyclohexene oxide selectivity of 53%, compared to 65

and 58% for bulk NiO particles (prepared by calcination of $\text{Ni}(\text{NO}_3)_2 \cdot 4\text{H}_2\text{O}$ at 500 °C for 4 h), respectively (Fig. 9). The reusability of mesoporous flower-like NiO NPs was also studied. After four successive runs, the conversion of cyclohexene was decreased to 63% with almost the same selectivity (53%). This decrease in the catalytic activity of NiO NPs was attributed to the aggregation and partial dissolution of NiO NPs in reaction mixture.

The flower-like NiO NP prepared with CTAB was also used by Abboud et al. as catalyst in the epoxidation

Table 5 SBA-15 supported NiO NPs reported in the literature

Catalyst	Nickel precursor	Synthesis method	Particle size (nm)	Application	Ref
NiO/Al-SBA-15	$\text{Ni}(\text{NO}_3)_2 \cdot 6\text{H}_2\text{O}$	Wet impregnation	9–10	Solvent-free deoxygenation of palm fatty acid distillate	Baharudin et al. 2019)
NiO/SBA-15	$\text{Ni}(\text{NO}_3)_2 \cdot 6\text{H}_2\text{O}$	Wet impregnation	8–20	Carbon dioxide reforming of methane	Yang et al. 2017)
NiO/Al-SBA-15	Molecular Ni_4O_4 clusters	Incipient wetness impregnation	<20	Dry reforming of methane	Baktash et al. 2015)
NiO/SBA-15	$\text{Ni}(\text{NO}_3)_2 \cdot 6\text{H}_2\text{O}$	Direct wet impregnation ^a Post synthesis impregnation ^b	-	Conversion of producer gas	Lu et al. 2014)
NiO/SBA-15	$\text{Ni}(\text{NO}_3)_2 \cdot 6\text{H}_2\text{O}$	Sol–gel coating	5–15	Dry reforming of methane	Ahmed et al. 2012)
NiO/SBA-15	$\text{Ni}(\text{OCOCH}_3)_2 \cdot 4\text{H}_2\text{O}$	Post-synthesis grafting method	9±4	Carbon dioxide reforming of methane	Liu et al. 2009)

^a Nickel precursor was added during the synthesis of SBA-15

^b Nickel precursor was added to pre-prepared SBA-15

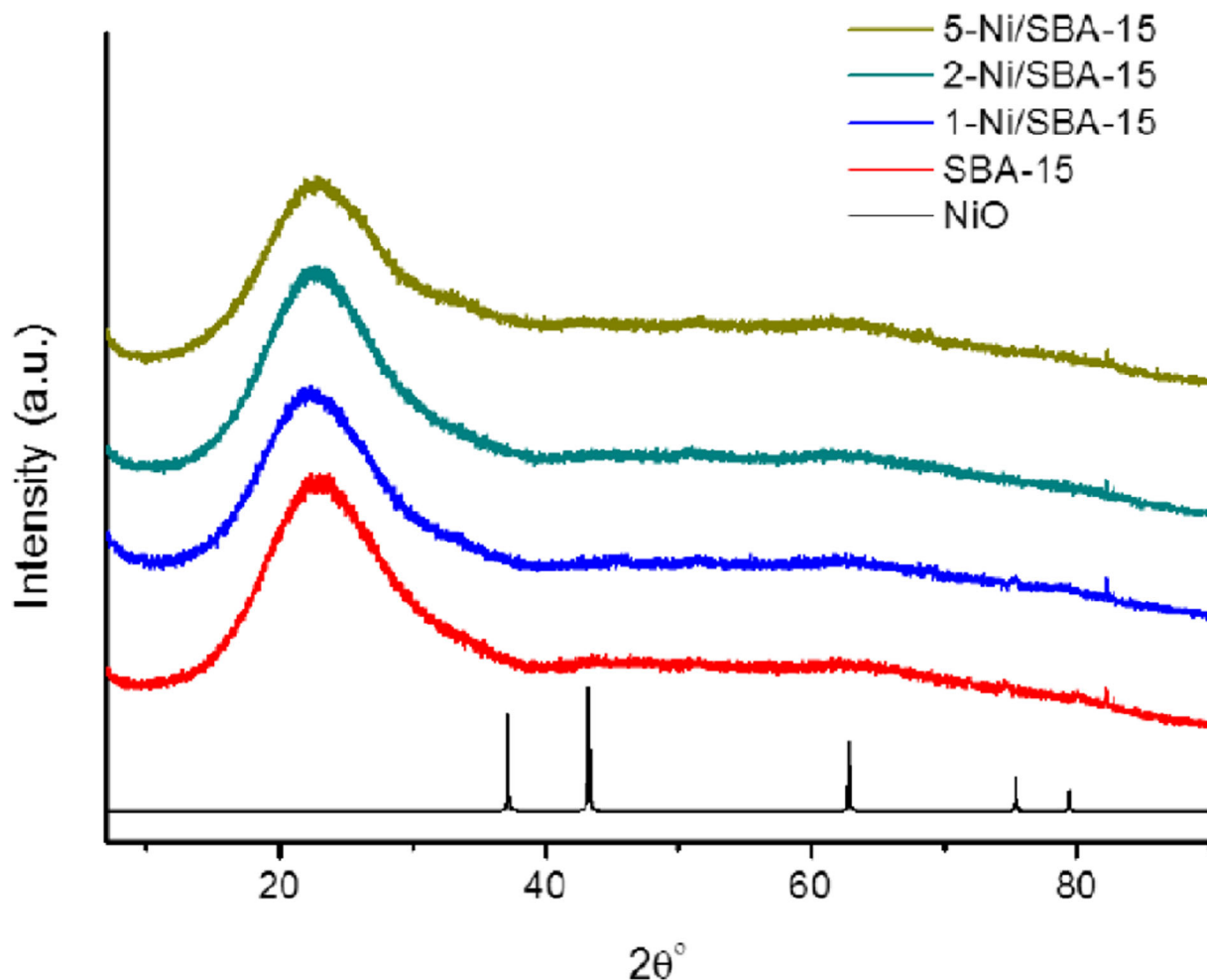


Fig. 29 Wide-angle XRD of Ni/SBA-15

Table 6 Characterisation and test results of the Ni4/SBA-15 and Ni/SBA-15 catalysts

Samples	Ni ^a [wt%]	Activity ^b [mol _{CH₄} /mol _{Ni} /min]		
		500 °C	550 °C	600 °C
1-Ni4/SBA-15	0.52	3.2	6.0	13.9
2-Ni4/SBA-15	0.81	3.5	5.5	9.7
5-Ni4/SBA-15	1.67	3.1	3.8	5.3
1-Ni/SBA-15	0.51	3.9	3.9	-
2-Ni/SBA-15	0.97	3.0	5.0	8.3
5-Ni/SBA-15	2.53	1.4	2.6	3.4

^a Metal content from ICP measurement

^b Reaction rate based on mole CH₄ converted per mole Ni per time on stream

reaction of styrene in ambient conditions, using *m*-CPBA (1.5 eq) as an oxidant and in the similar conditions used for the epoxidation of cyclohexene (Fig. 10) (Sahlabji et al. 2020). NiO NP catalyst also showed an immediate (less 1 min) reaction with high conversion of 87% and selectivity of 65% (Fig. 11), with high turnover frequency (TOF) of 243/s. Moreover, this catalyst is easily separable and recyclable up to four runs with slight decrease in the catalytic activity.

Unsupported NiO NPs were prepared and used by Nasserri and co-workers as green, inexpensive, and efficient heterogeneous nanocatalyst for the synthesized of diindolyloxindole (Fig. 12) and spirooxindoles (Fig. 13) derivatives in water, which are an important class of potentially bioactive compounds (Nasserri et al. 2015a, 2015b). The desired products were obtained with high yields in

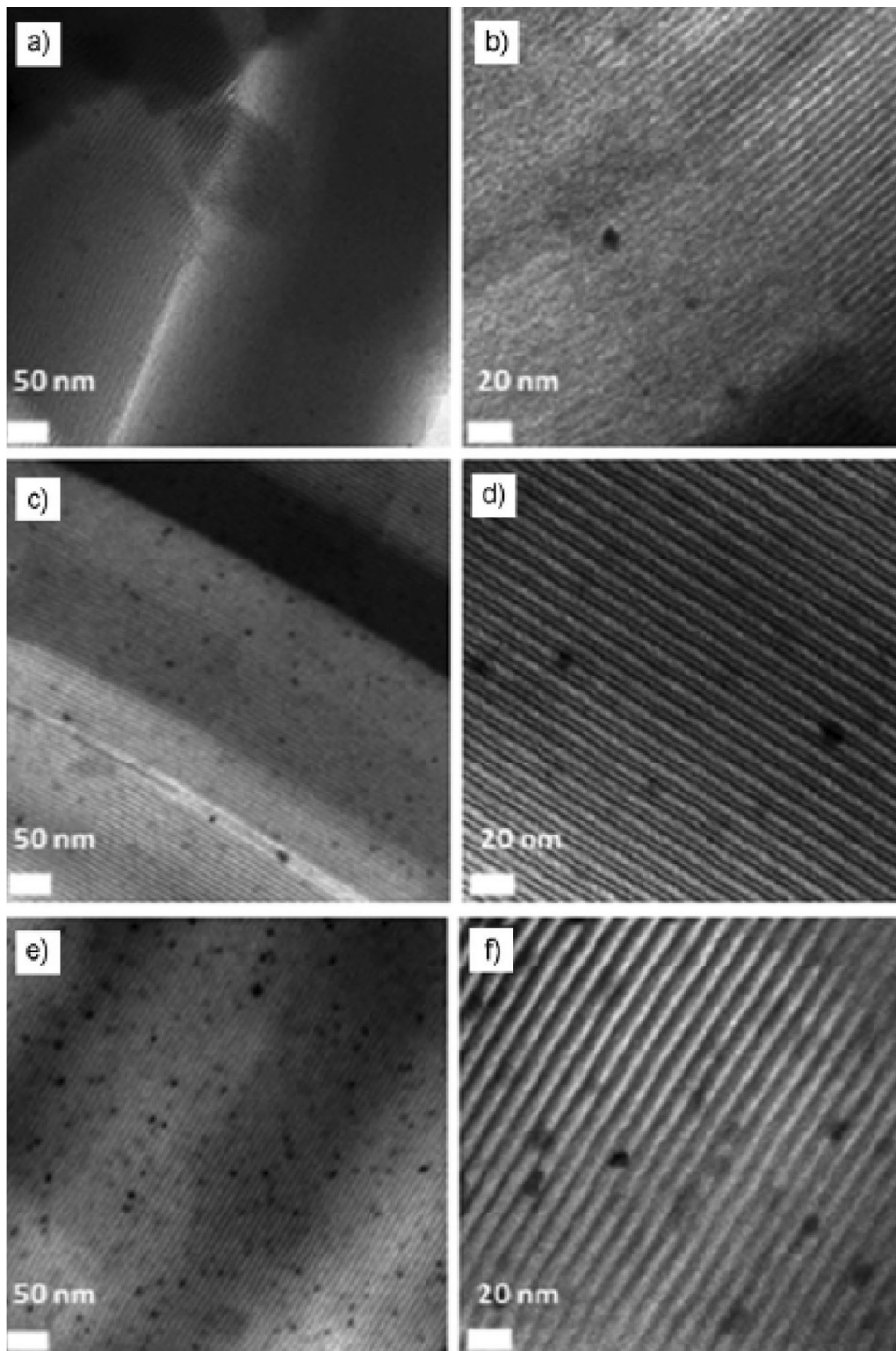


Fig. 30 TEM images of Ni/SBA-15. a, b) 1-Ni4/SBA-15, c, d) 2-Ni4/SBA-15, and e, f) 5-Ni4/SBA-15 (Baktash et al. 2015)

mild conditions compared to other catalysts such as other transition metal oxides including bulk NiO particles.

The obtained NiO NPs in this work were prepared by chemical reduction method in water, using urea as a reducing agent. The structure of the prepared material

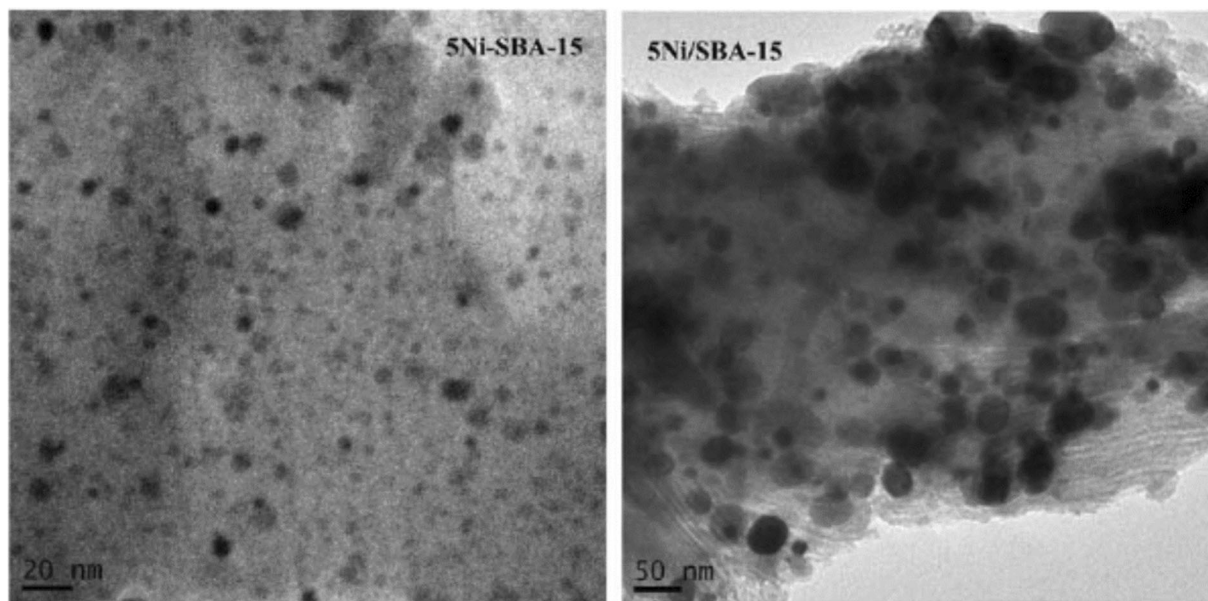


Fig. 31 TEM images of the spent catalysts. 5Ni-SBA-15 prepared by post-synthesis grafting, 5Ni/SBA-15 prepared by impregnation (Liu et al. 2009)

was confirmed by XRD (Fig. 14). XRD patterns of the products were obtained after the calcination of the precursor at 400 °C.

The obtained material was investigated by TEM. The average size of the obtained particles was around 11 nm (Fig. 15).

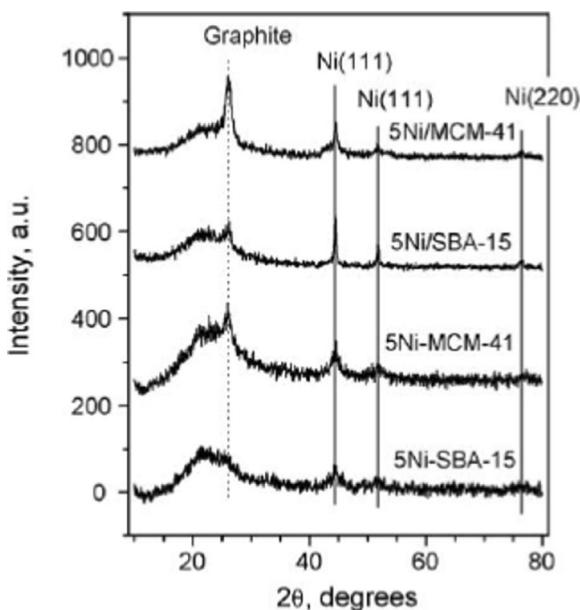


Fig. 32 XRD patterns of spent catalysts

Recently, Arrigo et al. (Arrigo et al. 2020) have investigated the influence of the preparation condition on the structure of Ni NPs, using hot injection colloidal method, with different amounts of oleylamine (OAm) and trioctylphosphine (TOP), which were used as reducing and protective agents, respectively (Fig. 16). It was found that changing the amount of OAm and TOP affected both the size of the NPs and the Ni electronic structure (Table 3).

The successful formation of metallic Ni NPs was confirmed by XRD (Fig. 17).

The obtained Ni₅ × 1.5y NPs were characterized by high-resolution high angle annular dark field scanning transmission electron microscopy (HA-HAADF-STEM) (Fig. 18a and b). This figure shows oval NPs with a twinned cuboctahedron (Fig. 18a) formed by many parallel twin lamellae. Ni NPs are embedded in an organic shell (Fig. 18b). Figure 19 shows the core-shell form of Ni_{2.5} × 1.5y.

The catalytic activity of the obtained material was evaluated in selective asymmetric hydrogenation of methyl acetoacetate (MAA) to chiral methyl-3-hydroxy butyrate (Fig. 20). It was found that (*R*)-selectivity was higher on the oxidized surface of Ni NPs and at low conversion, without any impact of unsupported NP size on the selectivity (Table 4).

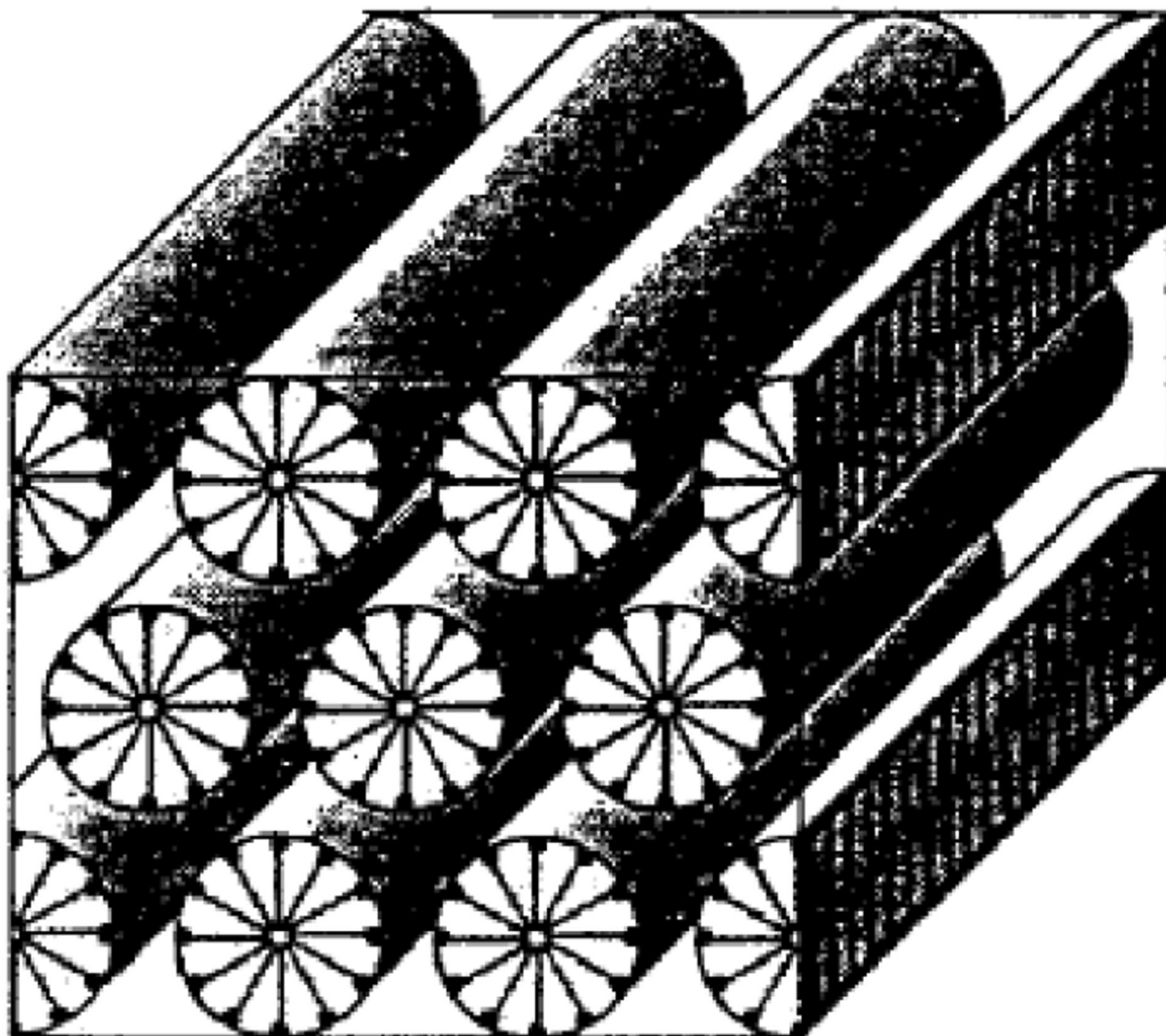


Fig. 33 Structure of MCM-41 (Schumacher et al. 2000)

Heterogeneous photocatalysis

Abboud et al. (Abboud et al. 2020) reported recently the synthesis of highly ordered mesoporous flower-like NiO NPs and their utilisation as a heterogeneous photocatalyst for the decolourisation of methyl green (MG) dye, under UV light in aqueous solution. NiO NPs were prepared by hydrothermal-assisted chemical precipitation method, using nickel acetate tetrahydrate as a metal source, ammonium hydroxide (NH_4OH) as a base, diethanolamine (DEA) as complexing agent, and cetyltrimethylammonium bromide (CTAB) as a structure directing agent. $\text{Ni}(\text{OH})_2$ precursor was synthesized

with and without CTAB to investigate its effect on Ni NPs shape and size.

Figures 21 and 22 show the SEM micrographs of flower-like NiO NPs obtained with and without CTAB, respectively. The characterisation results revealed that both CTAB and DEA were involved in the synthesis process. The flower size of the obtained NiO microspheres with CTAB was $\sim 2 \mu\text{m}$ with nanoflakes size $\sim 10\text{--}100 \text{ nm}$. The size of flower-like NiO microspheres prepared without CTAB was increased to $\sim 5 \mu\text{m}$ without any significant change in nanoflakes size.

The structure and the high purity of NiO NPs were confirmed by powder X-ray diffraction (see Fig. 6

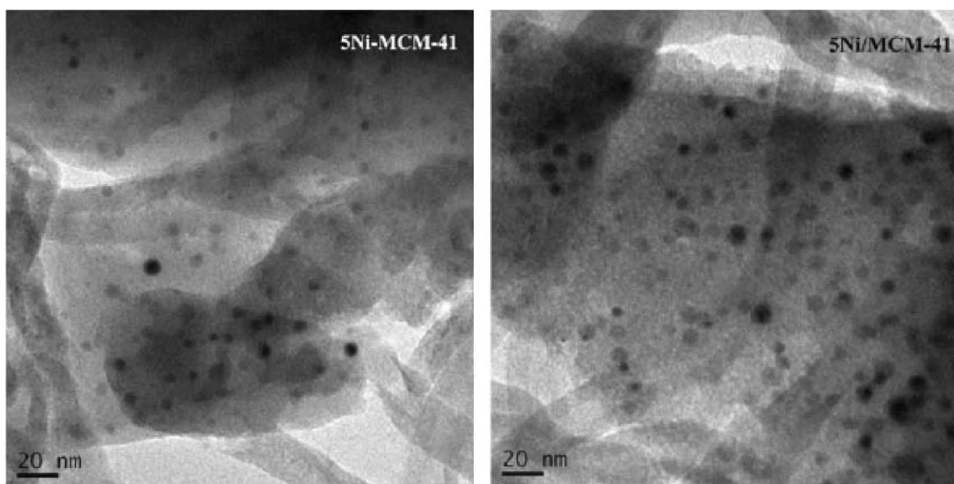


Fig. 34 TEM images of the spent catalysts. 5Ni-MCM-41 prepared by post-synthesis grafting, 5Ni/MCM-41 prepared by impregnation (Liu et al. 2009)

above). The investigation of these flower-like NiO NPs in nanoscale using TEM revealed the high order and uniform 2D nanostructure of the NiO nanoflakes (Fig. 23). In addition, BET results indicated the mesoporosity of the obtained material with a surface area of 21 m²/g and pore diameter of ~ 6 nm.

The photocatalytic activity of the prepared mesoporous flower-like NiO NPs was evaluated in the decolourisation of methyl green (MG) dye in water

under UV light illumination (Fig. 24). This nanocatalyst exhibited an excellent dispersion in the dye’s solution, and a good photocatalytic degradation of MG, with a rate constant about 10 times higher than that of the bulk NiO counterpart.

Bashir et al. recently prepared NiO NPs with cubic-type structure, using nickel nitrate hexahydrate, as a nickel precursor, dissolved in an extract of *Persea americana* seeds as an ecofriendly biosynthesis method

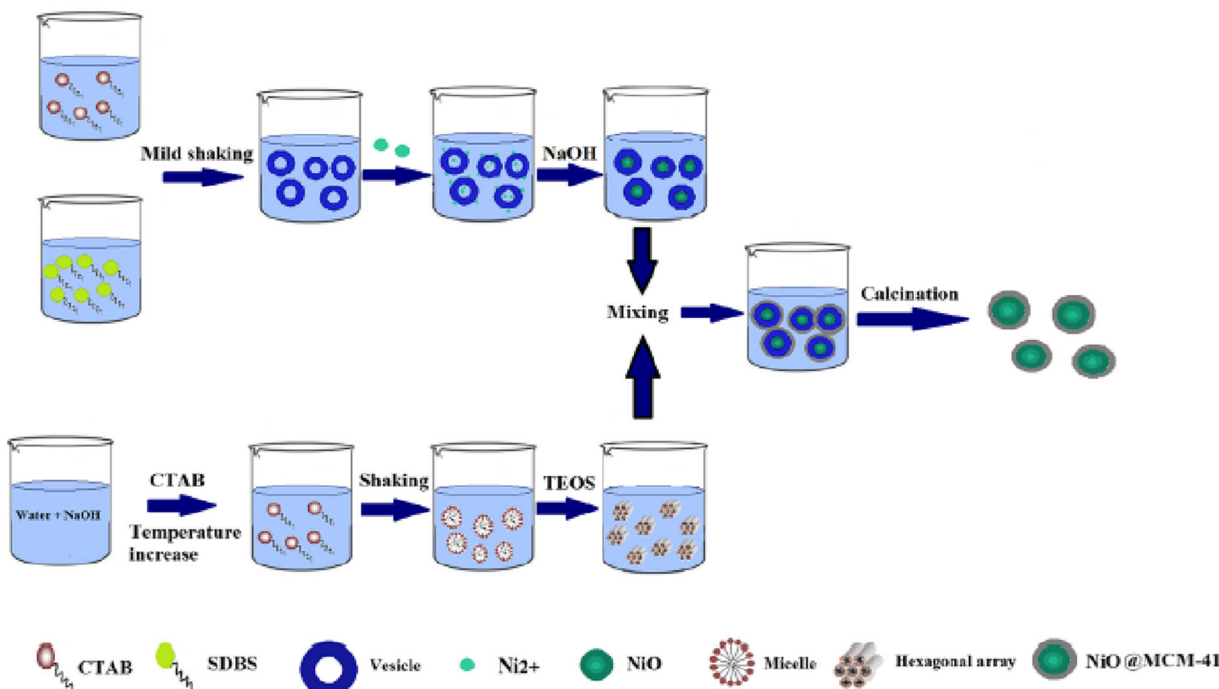


Fig. 35 Schematic diagram of the formation mechanism of the NiO@MCM-41 nanocomposite (Roosta et al. 2018)

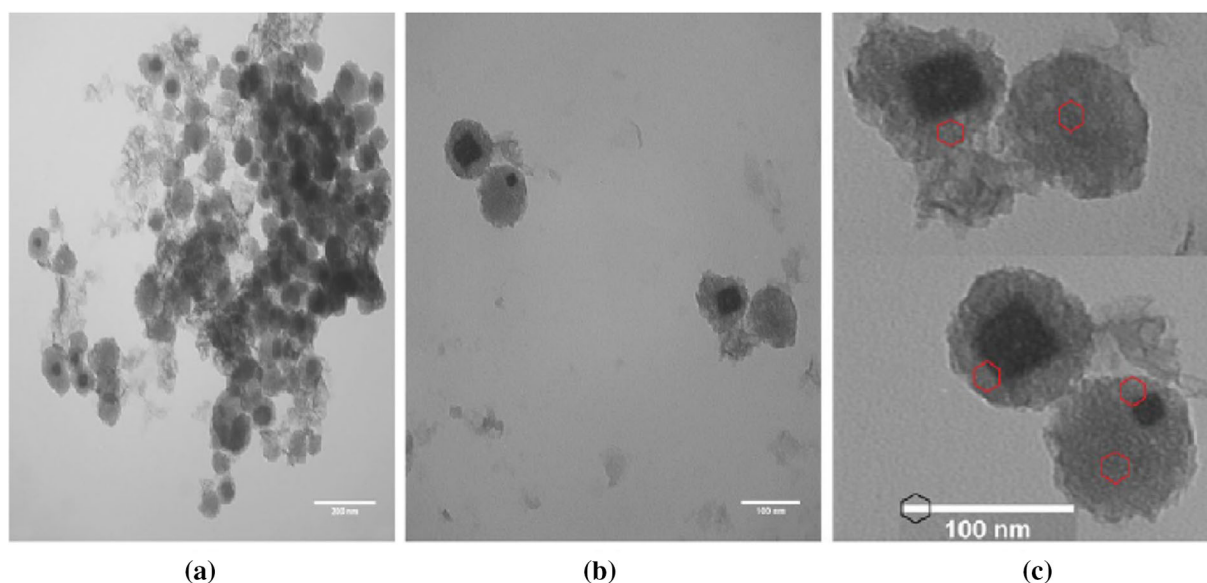


Fig. 36 TEM images of NiO@MCM-41 nanocrystals, (a) zoomed out, (b) zoomed in; (c) image (b) was enlarged, cropped, and recombined, and the hexagonal order of pores was made distinguishable via red polygons. (Colour figure online) (Roosta et al. 2018)

(Bashir et al. 2019). The NiO NP type structure was confirmed by XRD (Fig. 25).

TEM images showed rhombohedral and spherical shapes of NiO NPs with low agglomeration, and particle size around 11 nm (Fig. 26). The obtained NiO NPs were used as a catalyst for the photodegradation of free cyanide (Fig. 27). The obtained material exhibited a good photocatalytic activity with a maximum photocatalytic oxidation efficiency of 84% after 30 min.

However, unsupported Ni NPs still suffer from different drawbacks such as deactivation by aggregation, low durability, low dispersibility, and electron and hole recombination. Characteristics such as optical and catalytic activity may be lost if the dispersion of unsupported Ni NPs is not adequately modulated.

Mesoporous silica-supported nickel nanoparticles

Introduction

Several efforts have been deployed to overcome the unwanted effects of unsupported Ni NPs by either in situ synthesis or incorporating them into a solid matrix, like silica, carbon, or polymers. Among the different solid supports that have been used to encapsulate, these NP catalysts are the porous silica materials. They have been considered as excellent transparent solid supports,

because of their high surface area, thermal stability, chemical inertia, transmittance to radiation, high absorption capacity, and facilitating the interface reaction with organic compounds for photocatalytic degradation (Barhoum et al. 2017). Therefore, a porous silica framework facilitates the use of Ni NPs for the desired purposes while avoiding the drawbacks mentioned above.

Since Mobil Oil Corporation scientists discovered the Mobil Crystalline Materials (MCMs), such as MCM-41 and SBA-15 in 1992 and 1998, respectively, these mesoporous silica materials (MSMs) have attracted much attention in a wide variety of applications including catalysis, adsorption, separation, drug delivery, and sensing (Amin 2020). The importance of these materials is due to their important intrinsic properties such as tunable porosity and morphology, large internal surface area, narrow and highly uniform pore size distribution, and three-dimensional space required to realize the doping and confinement of different functional components, in addition to their high thermal and chemical stability. MSM also shows a high adsorption capacity and an ordered porous 3-D network that make them have a high diffusion of substrates and reaction products. All these properties open up a high application potential of those materials in the field of catalysis (Amin 2020; Weiping and Lide 1997; Lai 2013; Dixit et al. 2013; Luque et al. 2012).

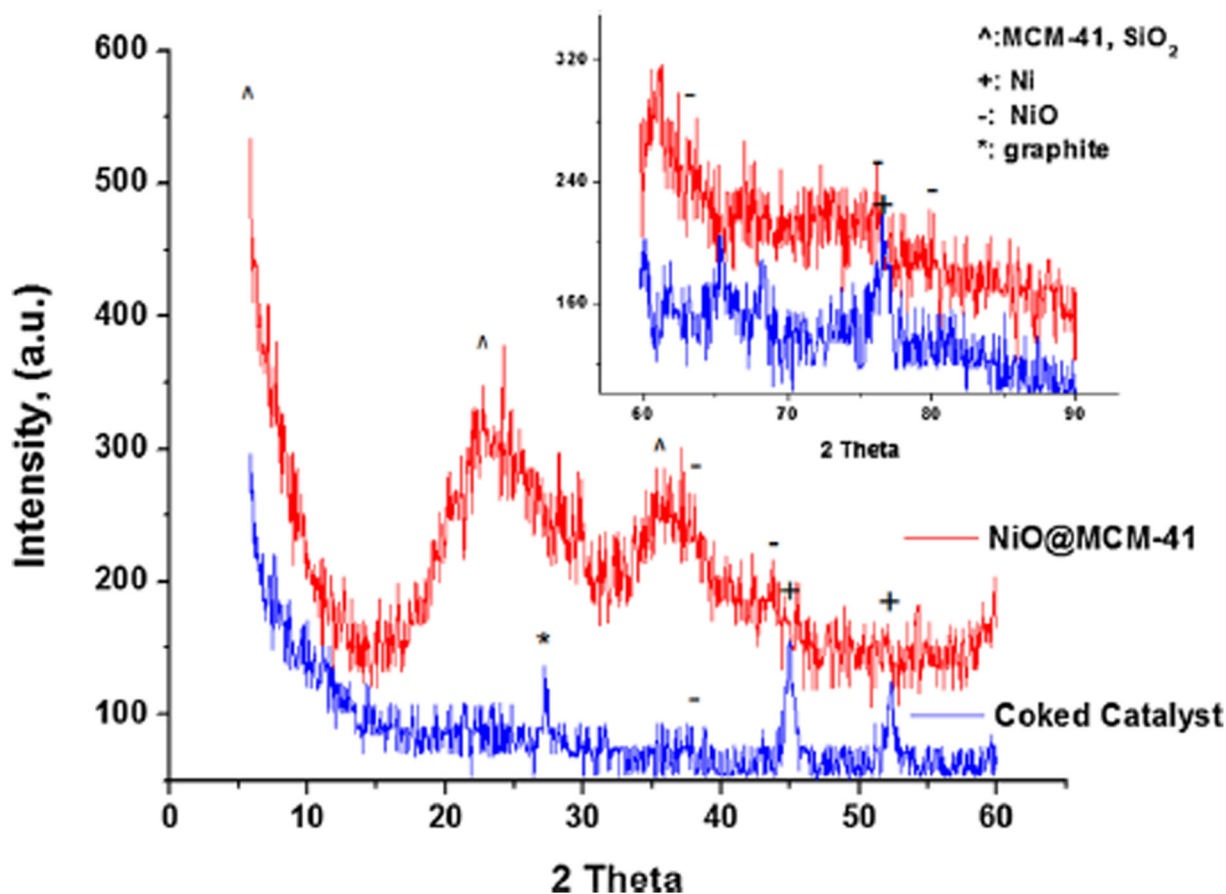


Fig. 37 Wide-angle X-ray diffraction pattern of the nanocomposite and the used catalyst. Diffraction data of inset figure were recorded in a different analysis

The successful incorporation of Ni NPs in mesoporous silica with stable and quantified NP size will increase the surface area to volume ratio and consequently increase the number of active sites of Ni NPs per area unit, inhibit the particles aggregation, improve the reusability of the obtained nanocatalyst, and consequently improve its catalytic performance.

Here we are going to discuss some recent applications in heterogeneous catalysis of Ni NPs supported on different types of MSMs, such as SBA-15, MCM-41, MCM-48, TUD-1, and other MSMs.

Nickel NPs supported into SBA-15

SAB-15 is one of the most used MSMs as a support in heterogeneous catalysis. SAB-15 is characterized by high specific surface area (400–900 m²/g), tunable uniform hexagonal pore-network that have high hydrothermal and mechanical stability, with narrow pore size

distribution, pore diameter ranges from 5 to 15 nm, pore volume up to 1.1 cm³/g, and relatively thick walls that range between 3.1 and 6.4 nm, with a circular pore shape.

SAB-15 has been prepared in acidic medium, using the triblock copolymer (EO₂₀PO₇₀EO₂₀) Pluronic 123 (P123) as a structure directing agent, and tetraethyl orthosilicate (TEOS) as a silica source, following the mechanism described in Fig. 28 below (Jadhav et al. 2015).

Ni NPs have been incorporated in SBA-15 using different methods and applied as catalysts for various chemical transformations. The most techniques used to incorporate Ni NPs into SBA-15 are wet impregnation using nickel nitrate hexahydrate as nickel precursor (Table 5). The nickel particle size of the obtained materials was between 5 and 20 nm. The most Ni@SBA-15 catalysts prepared are used for reforming of methane.

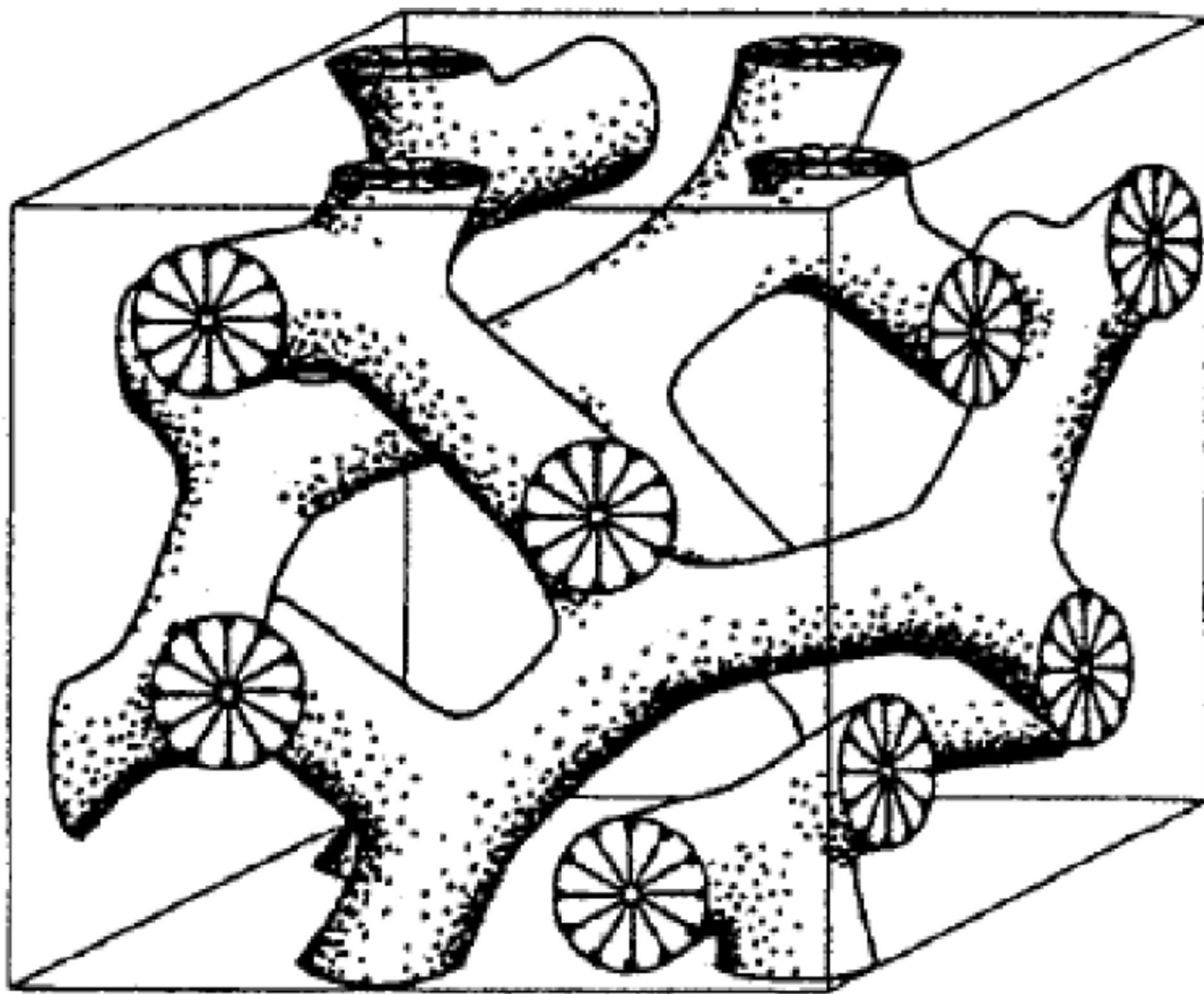


Fig. 38 Structure of MCM-48 (Schumacher et al. 2000)

Thomas et al. (Baktash et al. 2015) used incipient wetness impregnation method to prepare NiO NPs supported on SBA-15 using molecular Ni_4O_4 clusters as nickel precursor.

The XRD patterns of Ni/SBA-15 samples after calcination (before reduction) are presented in Fig. 29. The characteristic reflexes for NiO at $2\theta = 37.2, 43.1,$ and 62.88 , corresponding to the (111), (200), and (220) planes of cubic NiO, respectively, were not observed for all Ni/SBA-15 samples. The observed reflexes are very weak and broad, which points to the formation of very small and highly dispersed Ni species.

The presence of nickel and the actual metal contents of the samples were determined after the calcination step by inductively coupled plasma (ICP), and the obtained results are presented in Table 6.

The TEM images revealed the formation of NiO NPs with particle size < 20 nm (Fig. 30). Authors claimed that the utilisation of these clusters may have a significant effect on the dispersion of NiO NPs through the SBA-15 framework compared to other traditional precursors such as nickel nitrate. The obtained nanocatalyst was reduced to Ni(0) and used for dry reforming of methane.

Liu and co-workers (Liu et al. 2009) reported the synthesis of SBA-15 supported Ni catalysts using a post-synthesis grafting method and nickel acetylacetonate as nickel precursor. In this method, the appropriate amount of nickel acetylacetonate complex was added dropwise to a suspension of SBA-15 in toluene. After refluxing the mixture overnight, filtration, and washing, the obtained SBA-15 grafted nickel acetylacetonate

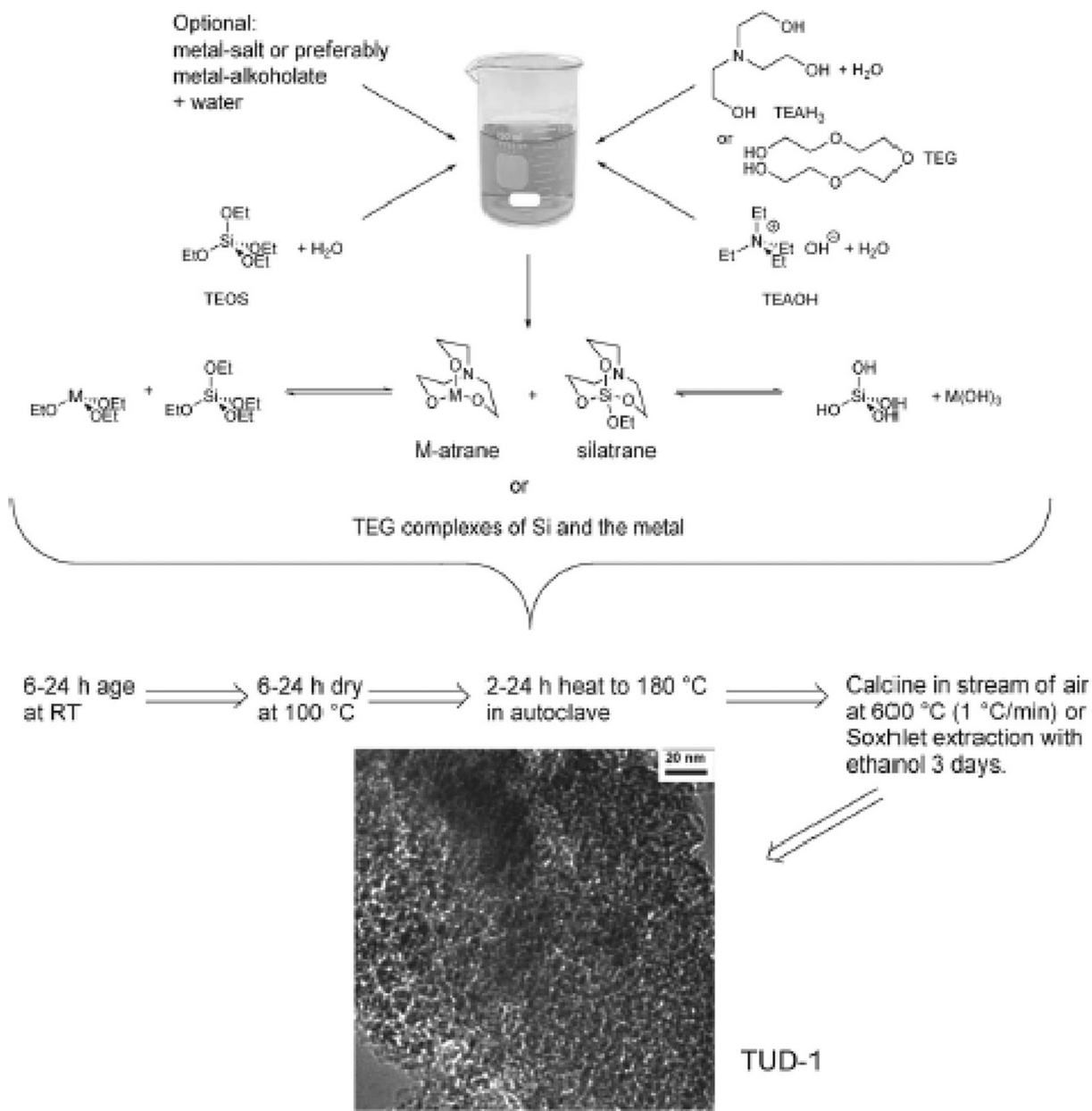


Fig. 39 The synthesis of mesoporous TUD-1 and M-TUD-1 is straightforward (Telalović et al. 2010)

powder was calcined at 540 °C to obtain the desired catalyst. The Ni particle size of the material obtained by post-synthesis grafting method was 9 ± 4 nm compared to 31 ± 12 nm for the material prepared by conventional impregnation method (Fig. 31). The existence of nickel particles with large size, especially for the catalysts prepared via impregnation, could be attributed to a remarkable sintering of Ni particles occurring during the stability test.

The catalytic activity of the obtained catalysts was evaluated in CO₂ reforming of methane. The highest catalytic performance and stability and high Ni NP dispersion through silica matrix were observed over a 5-wt% Ni loading prepared by post-synthesis grafting method.

The structure of fresh Ni NPs in these materials was not confirmed by XRD or EDX. Only low-angle XRD was performed to demonstrate that the structural

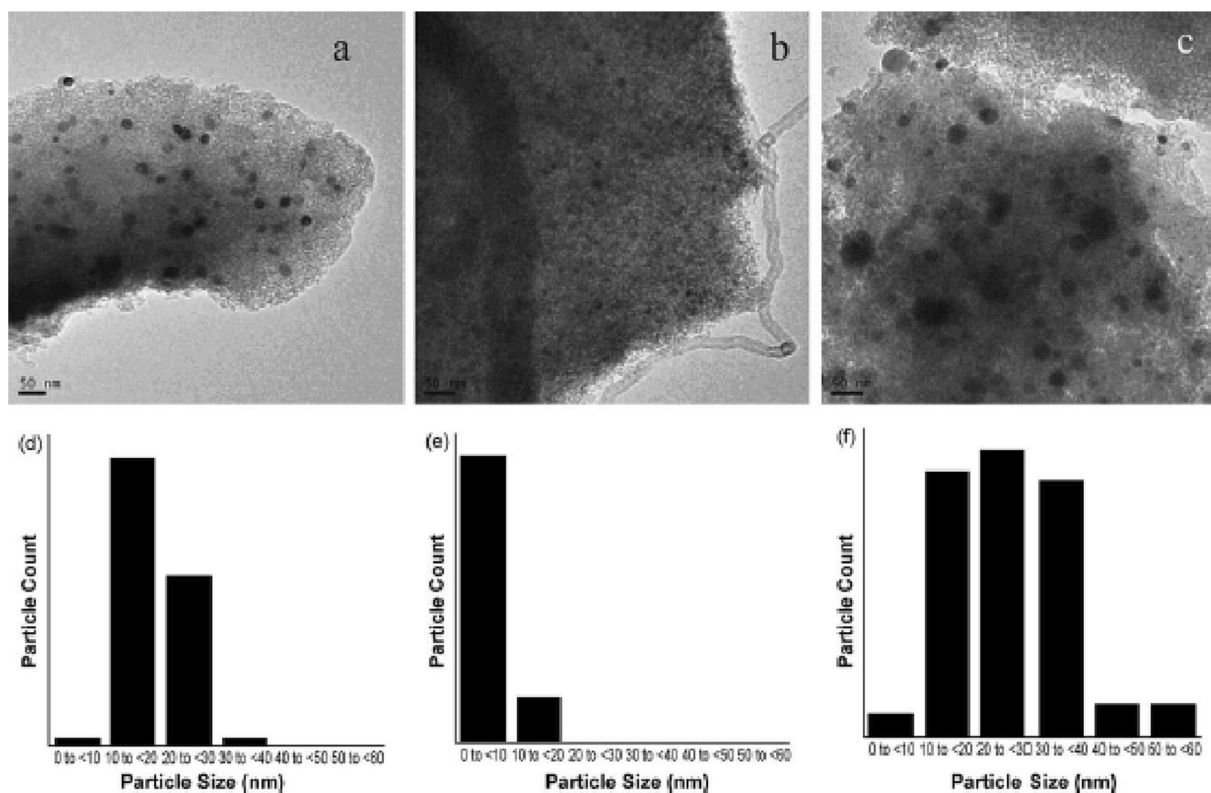


Fig. 40 TEM results for spent catalysts: (1) TEM images for (a) spent Ni-DHT, (b) spent Ni-GRF, and (c) spent Ni-IMP, respectively; (2) nickel particle size distributions for (d) spent Ni-DHT, (e) spent Ni-GRF, and (f) spent Ni-IMP, respectively (Quek et al. 2010)

integrity was retained after the incorporation of Ni and the calcination process. However, XRD was performed to the spent catalysts to determine its crystalline phases after reaction. As shown in Fig. 32, the diffraction peaks of Ni particles can be seen over all the spent catalysts.

Nickel NPs supported in MCM-41

MCM-41 is one of the most widely investigated ordered mesoporous silica materials due to its valuable physical properties. MCM-41 is characterized by highly ordered hexagonal one-dimensional and unidirectional pores system (Fig. 33) (Schumacher et al. 2000) and narrow pore size distribution, with pore size that ranges from 3 to 7 nm, pore volume nearly 1.0 cm³/g, and high surface area up to 1000 m²/g, with wall thickness up to 1.8 nm. In addition, MCM-41 presents good thermal and chemical stability, uniform channels 2–10 nm in diameter, and no toxicity of both template and silicon source.

MCM-14 materials have been synthesized in an alkaline condition using cetyltrimethylammonium

bromide (CTAB) as structure directing agent, and TEOS as silica source, following the same mechanism described for the synthesis of SBA-15 (Fig. 28). The main differences between the structure of MCM-41 and SBA-15 are primarily in pore geometry, pore shape, and the wall thicknesses.

However, only few publications reported the incorporation of Ni NPs in MCM-41 and the obtained nanocatalysts mainly applied for CO₂ reforming of methane.

Liu et al. (Liu et al. 2009) also reported the preparation of Ni-MCM-41 catalyst and its evaluation in CO₂ reforming of methane. This material was prepared using the same method described for Ni-SBA-15 which is the post-synthesis grafting method, using nickel acetylacetonate as nickel precursor. The Ni NP size of Ni-MCM-41 was 7.6 ± 1.8 nm, compared to 12.1 ± 3.2 nm for Ni/MCM-41 which was prepared using conventional impregnation technique. The Ni NP size obtained with MCM-41 was smaller than that observed in SBA-15 (Fig. 34). However, Ni-SBA-15 obtained by grafting

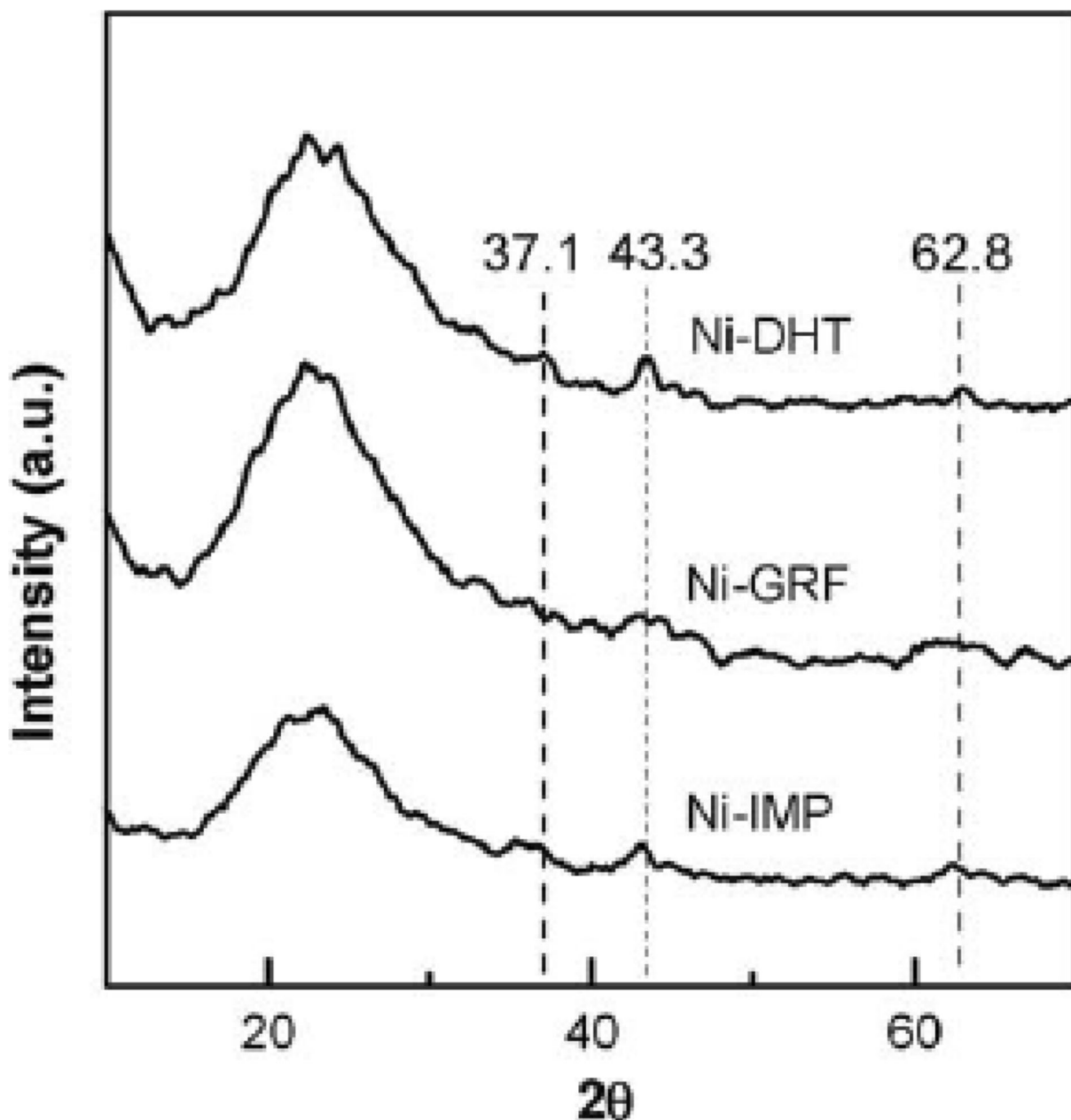


Fig. 41 High-angle XRD patterns of Ni-containing TUD-1 catalysts

method exhibited an excellent catalytic activity and high stability over Ni-MCM-41, due to its high inhibition on nickel sintering and carbon formation.

As mentioned above for SBA-15, only low-angle XRD was performed to demonstrate the preservation of the mesoporosity of the material after the incorporation of Ni and the calcination process. Wide-angle XRD was performed only to the spent catalysts to determine its crystalline phases. The average sizes of Ni particles

calculated by Scherrer equation revealed the following sequence: 5Ni-MCM-41 (7.3 nm) < 5Ni-SBA-15 (8.4 nm) < 5Ni/MCM-41 (14.0 nm) < 5Ni/SBA-15 (19.4 nm).

In another work, Roosta et al. reported the synthesis of NiO@MCM-41 catalyst in the form of core-shell nanocomposite and its catalytic evaluation in CO₂ reforming of methane (Roosta et al. 2018). NiO@MCM-41 nanocomposite was prepared by two-

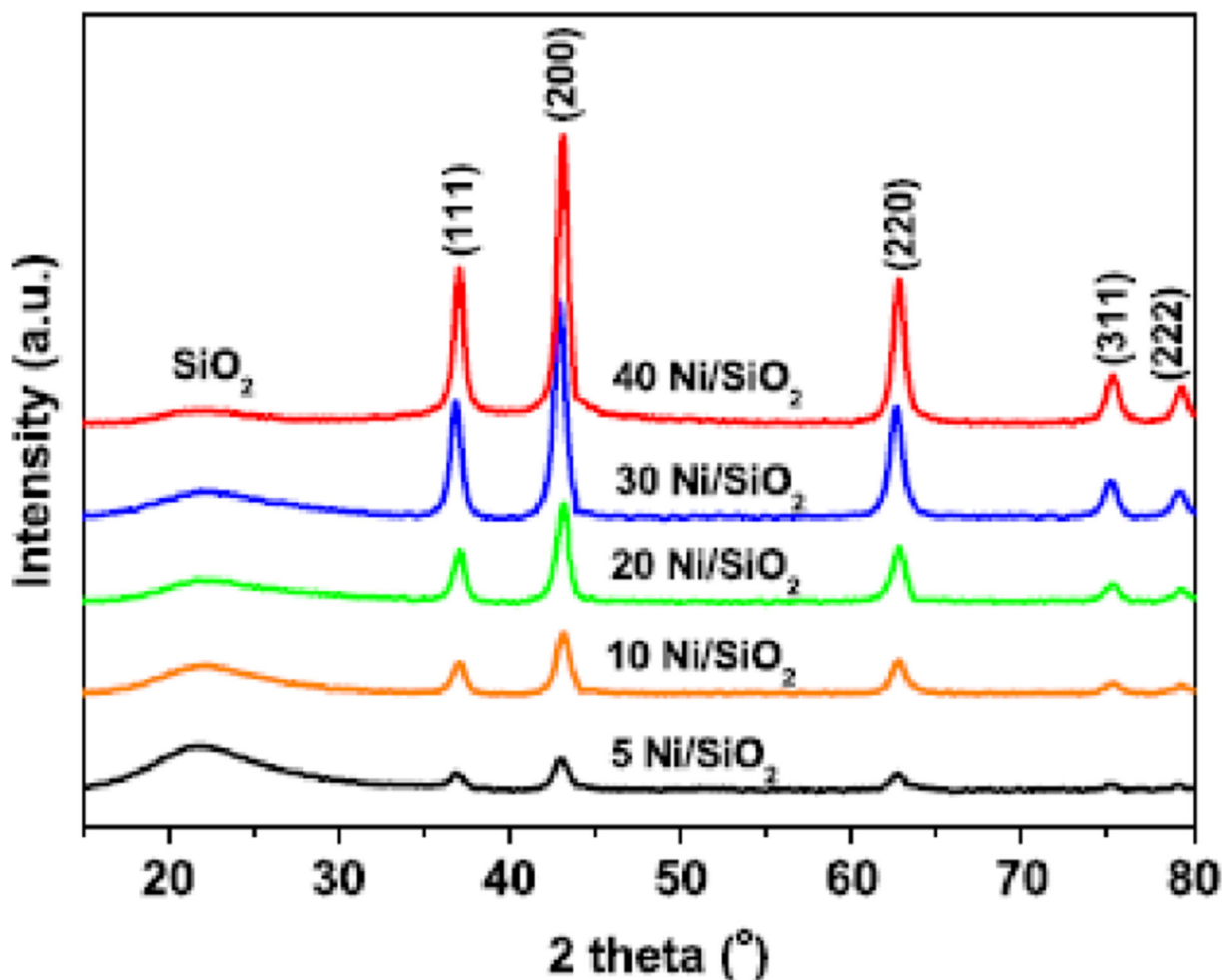


Fig. 42 Powder XRD patterns of Ni/SiO₂ catalysts

step soft templated nanocasting method, using vesicles as soft template (Fig. 35). First, stable vesicles were formed by a mixture of two surfactants, CTAB and SDBS, with a ratio of CTAB/SDBS 1:2. Then, nickel nitrate was inserted inside the vesicles. The obtained Ni@vesicles were covered by MCM-41 gel. After the calcination step, the NiO@MCM-41 core-shell nanocomposite was obtained.

The TEM images (Fig. 36) of the obtained core-shell nanocomposite showed a particle's average diameter of 70–80 nm, with a spherical shape. CO₂ reforming of methane conversion over the prepared core-shell nanocatalyst led to CO₂ and H₂ conversion of 48% and 42%, respectively.

XRD analyses were performed before and after the reaction to evaluate the present crystalline phases in the catalyst (Fig. 37). NiO lattice reflection appeared at 2θ

= 38, 43.8, 63.2, 76.2, and 79.8 (Zhang et al. 2017), and FCC Ni lattice reflection appeared at 2θ = 45, 52.2, and 76.7 (Zhang and Li 2015). The absence and presence of reflection attributed to the metallic nickel (Ni) in the spent catalyst confirmed the reduction of NiO to Ni in the core of NPs. The presence of distinct reflections of Ni lattice of spent catalyst indicated the stable condition of the metallic phase of the core region of NPs after the reaction.

Nickel supported in MCM-48

MCM-48 is an important member of the M41S family (e.g. MCM-41, MCM-48, MCM-50). (Kresge et al. 1992). It is characterized by 3-D cubic structure, with two non-intersecting gyroidal pores (Fig. 38) (Schumacher et al. 2000). MCM-48 is characterized by

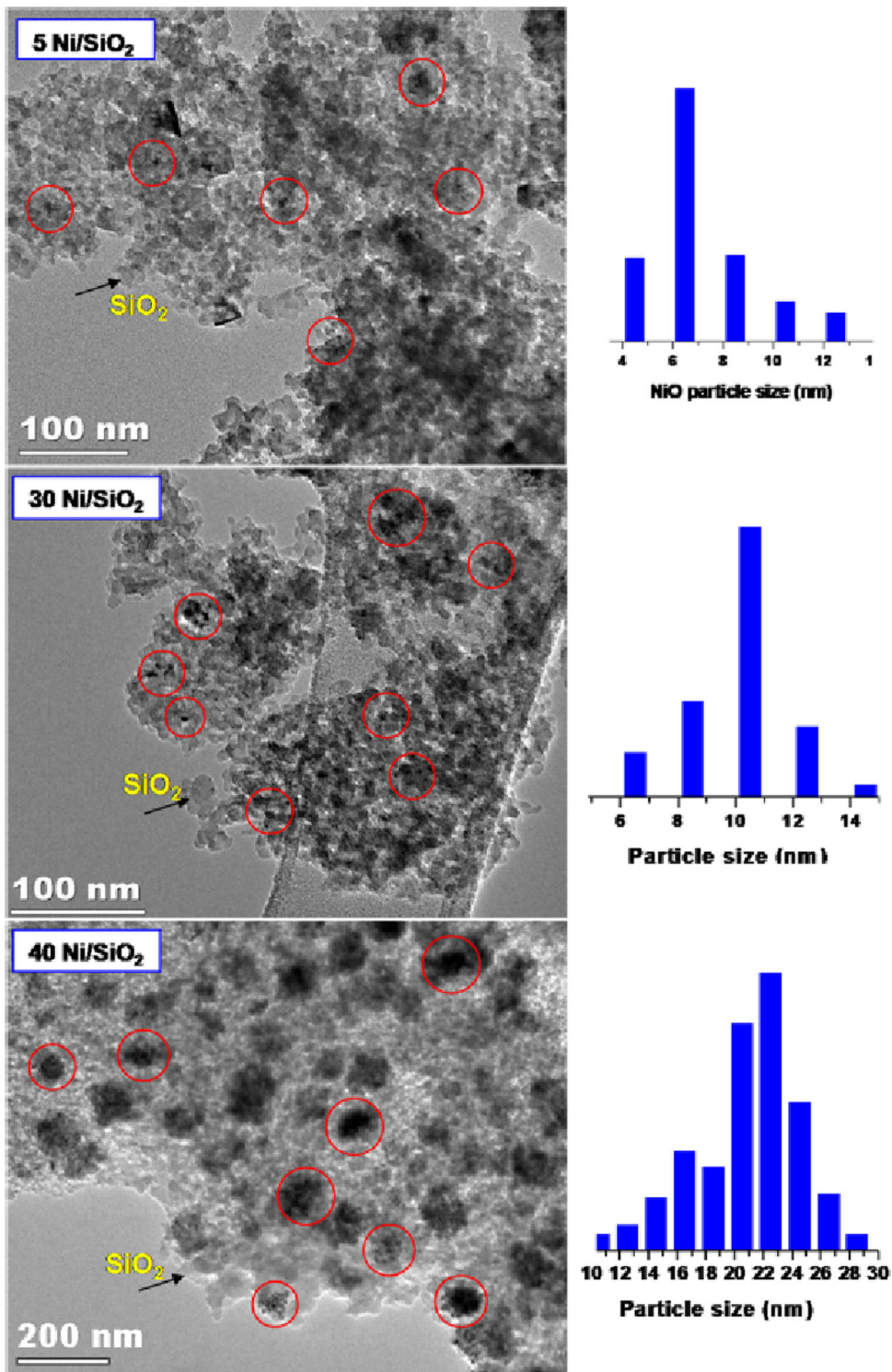


Fig. 43 TEM images and the corresponding particle size distribution of 5% Ni/SiO₂, 30% Ni/SiO₂, and 40% Ni/SiO₂ catalysts (Mallesham et al. 2018)

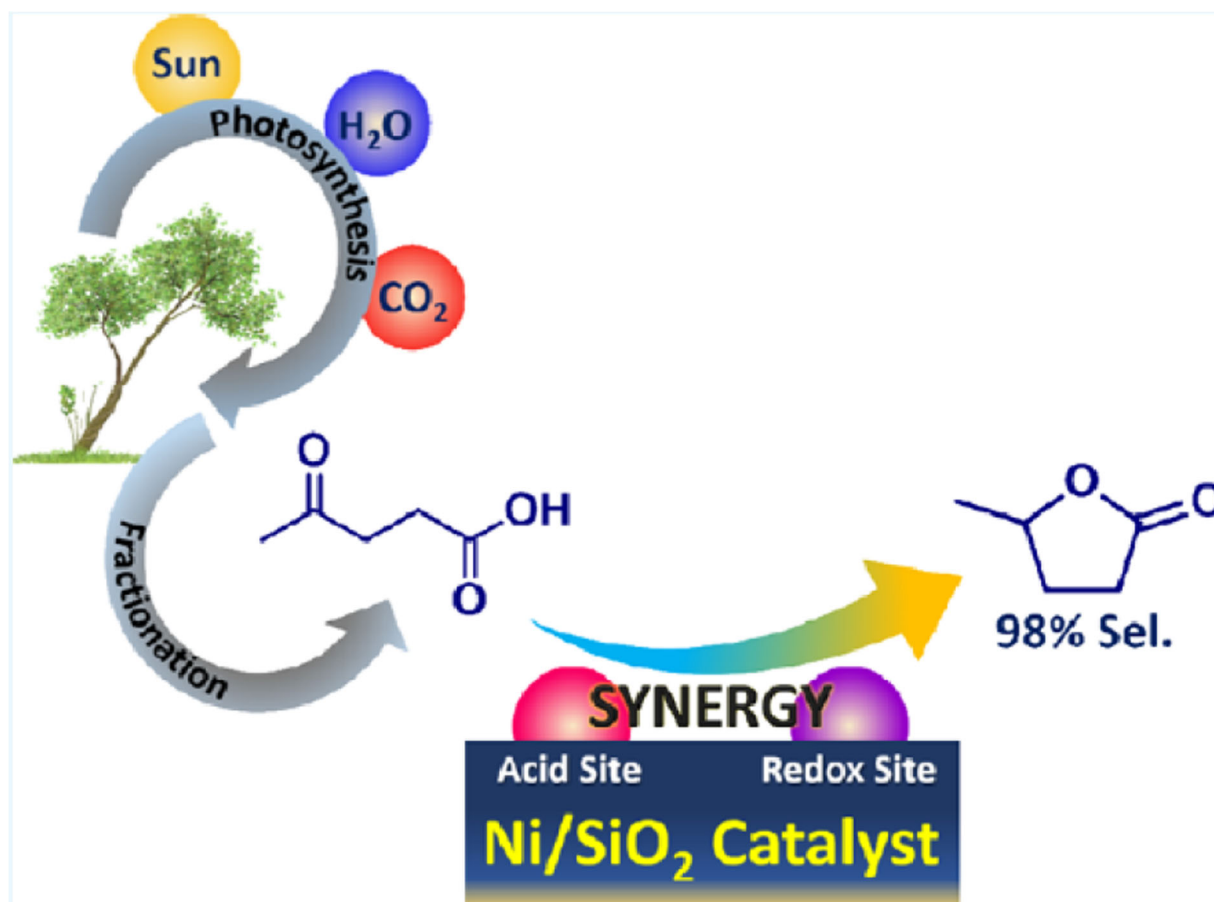


Fig. 44 Conversion of levulinic acid to γ -valerolactone over Ni/SiO₂ (Mallesham et al. 2018)

a high surface area up to 1000 m²/g, pore size ranges from 2 to 4 nm, and pore volume up to 0.8, with wall thickness around 1.5 nm. Compared to MCM-41, MCM-48 is more resistant to pore blocking because it provides fast diffusion of molecules through its 3-D pore network, which is very suitable in catalysis. Although MCM-48 has, doubtlessly, a high potential as a catalytic support and selective adsorbent, it has not received enough attention compared to MCM-41. This is probably due to the difficulty of synthesising it.

Indeed, the classic structure directing agents (SDAs) that have been used in the preparation of the M41S family are the alkyltrimethylammonium halides. These surfactants form preferentially a hexagonal or lamellar structure in solution, which makes the preparation of MCM-48 (cubic structure) with high quality is very sensitive to a narrow margin of error, with very poor reproducibility. The synthesis of MCM-41 can be

affected by different synthesis parameters, such as the type of surfactant, temperature, solution composition, even stirring speed, and type of washing solvent (Mokri et al. 2019).

Only a few publications reported the incorporation of nickel particles into MCM-48 for utilisation in catalysis. Shaban et al. reported recently the preparation of MCM-48 supported NiO NPs by wet impregnation method, using nickel chloride hexahydrate as metal precursor in water, with MCM-48/nickel precursor ratio of 1:1 (w/w) (Shaban et al. 2020). Unfortunately, the NiO particle size and their dispersion in the MCM-48 framework were not investigated in this work, using neither TEM nor XRD. Authors claim that the incorporation of NiO in MCM-48 led to a considerable reduction in NiO band gap energy to 2.4 eV. The obtained material was used as a catalyst for the photodegradation of Congo red dye. It has been reported that the adsorption capacity and the

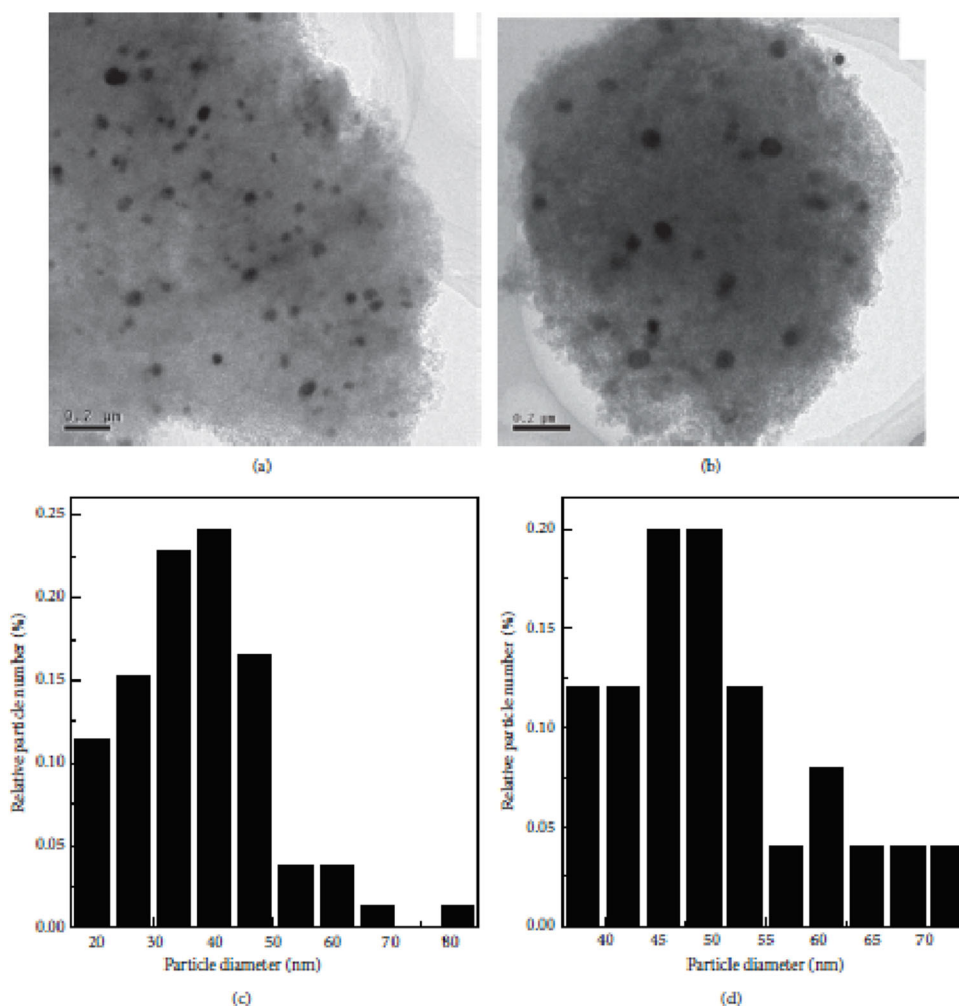


Fig. 45 TEM images of (a) reduced 3NiSN and (b) deactivated 3NiSN, and histogram of the particle size distribution obtained from sampling of nanoparticles from TEM data (c) for reduced 3NiSN and (d) for deactivated 3NiSN (He et al. 2015)

photocatalytic activity were enhanced in the composite NiO/MCM-48 compared to that in both NiO and MCM-48.

In another work, Hinrichsen and co-workers reported the synthesis of MCM-48 and its functionalisation with nickel and aluminium, using two different methods, which are incipient wetness impregnation (IWI) and template ion exchange (TIE) (Frey and Hinrichsen 2012). The characterisation results showed that the structure of MCM-48 was preserved after the functionalisation step using the IWI method, whereas the MCM-48 was partly affected by the TIE method. Here, also, the NiO particle size and their dispersion in MCM-48 were not studied using TEM and/or XRD.

The obtained materials were used to catalyse the conversion of ethene to propene. The highest

conversion and selectivity obtained with the optimal nickel and aluminium loadings, prepared by both methods, were 40% and 56%, respectively.

Ni nickel supported in TUD-1

TUD-1 is a mesoporous silicate material, first prepared by Jansen et al. in 2001 at Technische Universiteit Delft (TUD) (Jansen et al. 2001). Unlike most other mesoporous silica materials, TUD-1 is relatively simple to synthesize (Telalović et al. 2010). It has three-dimensional and irregular sponge-like porous structure, with high surface area ($> 1200 \text{ m}^2/\text{g}$), pores of varying diameter (2.5–20 nm), and wall thickness ranges from 2.5 to 4 nm. These properties allow fast diffusion through

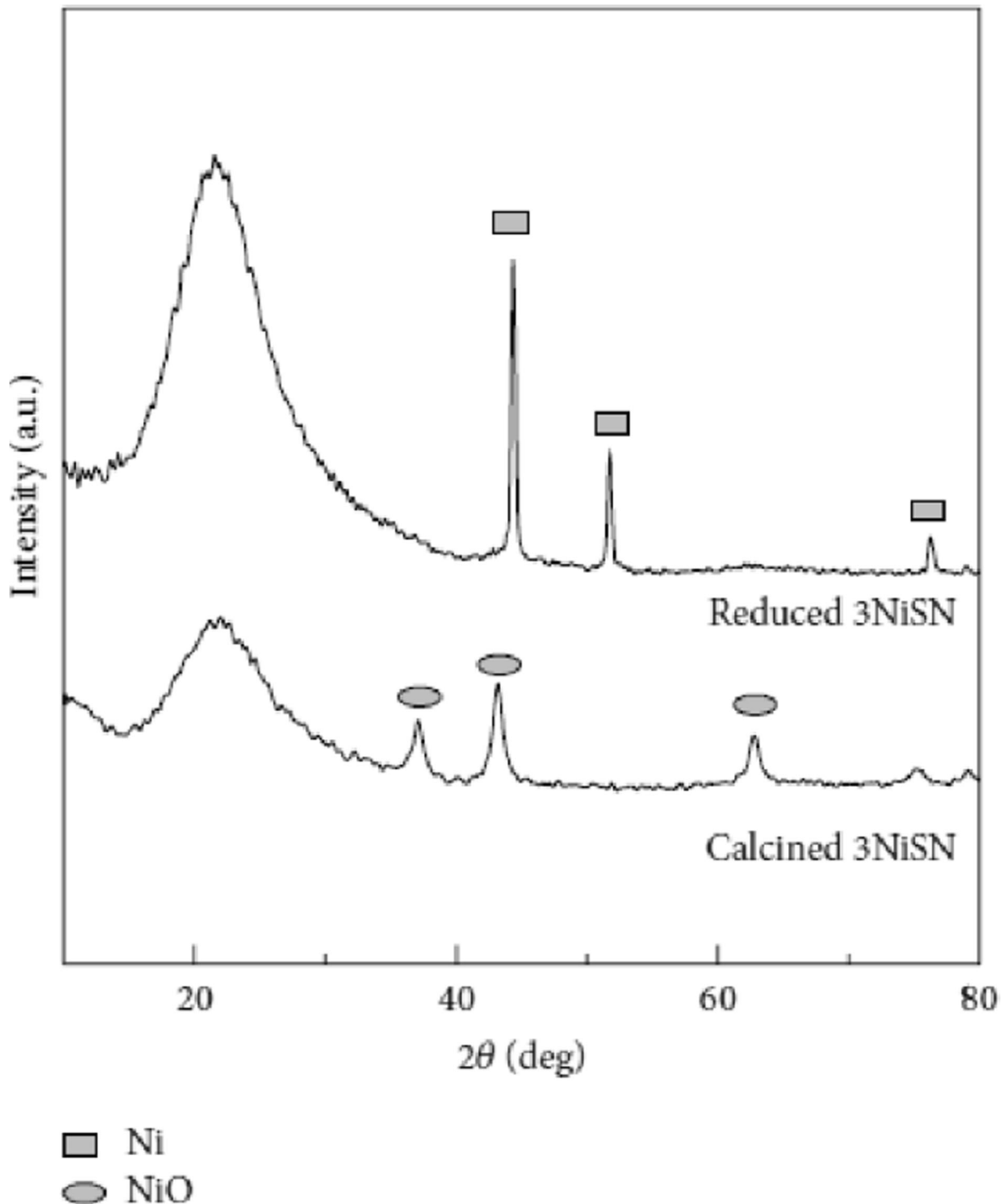


Fig. 46 XRD patterns of 3NiSN before and after reduction in H₂ for 4 h

TUD-1 pore network, making it an efficient and promising catalyst support in heterogeneous catalysis.

The synthesis of TUD-1 is based on the sol-gel process, using TEOS as silicon source. Unlike the

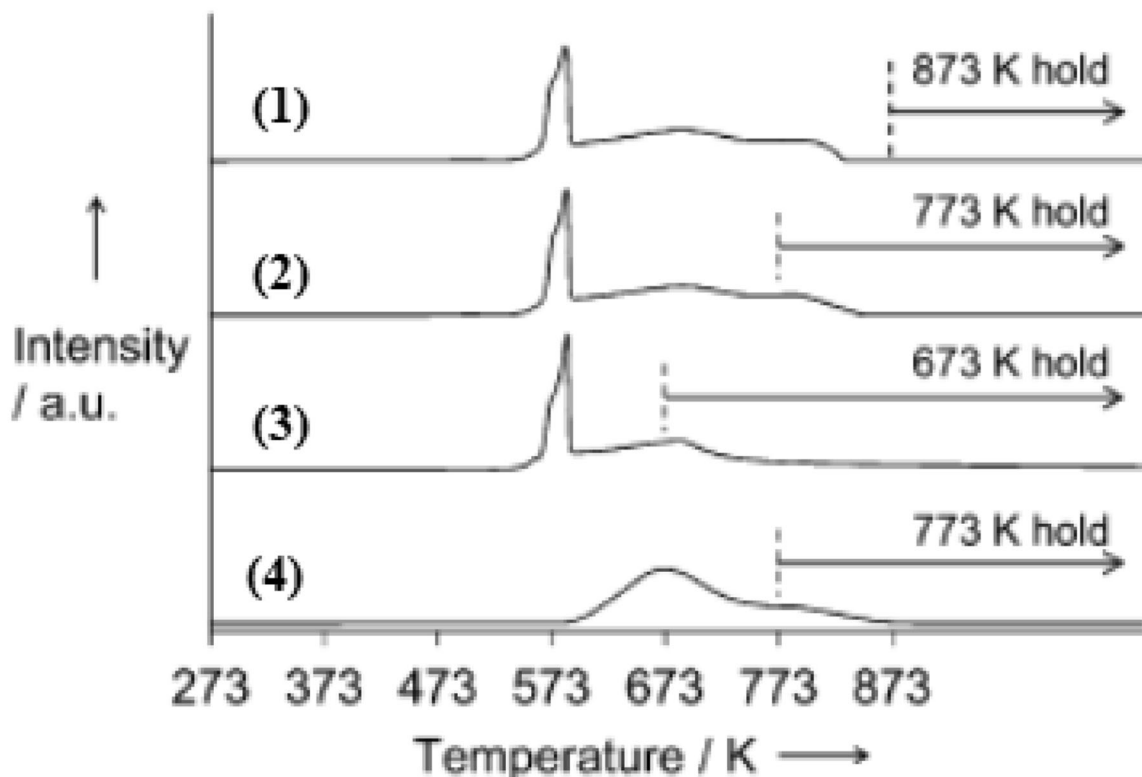
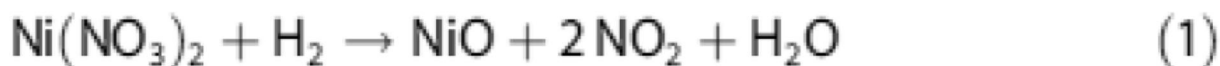


Fig. 47 TPR profiles of $\text{Ni}(\text{NO}_3)_2/\text{SiO}_2$. (1–3): without calcination and (4) after calcination at 773 K. Conditions: heating rate = 10 K/min, 5% H_2/Ar atmosphere

synthesis of many other mesoporous silica materials, no surfactant is needed to build the TUD-1 regular pore system. Instead, either tetraethylene glycol (TEG) or triethanolamine (TEAH_3) is used to chelate the silica and to obtain a porous structure. This synthesis method can be modified to introduce another metal (M) to the TUD-1 framework, to obtain a modified material (M-TUD-1) with different catalytic activities. Figure 39 illustrates the synthesis of TUD-1 and M-TUD-1 (M: metal).

Combination of two different metals into TUD-1 can induce a synergy between Brønsted and Lewis in the obtained catalyst. In addition to efficient applications in

acid, photocatalysis, and redox, TUD-1 demonstrated to be an outstanding carrier for many catalysts (Telalović et al. 2010; Gorsd et al. 2018; Tanglumert et al. 2011).

However, only fewer publications reported the synthesis and catalytic activity evaluation of TUD-1 supported nickel NPs.

Yang et al. reported the synthesis of nickel containing TUD-1 nanocatalyst using three different methods, direct synthesis (Ni-DHT), grafting (Ni-GRF), and impregnation (Ni-IMP) method, and the obtained materials were used to catalyse CO_2 reforming of methane. (Quek et al. 2010).

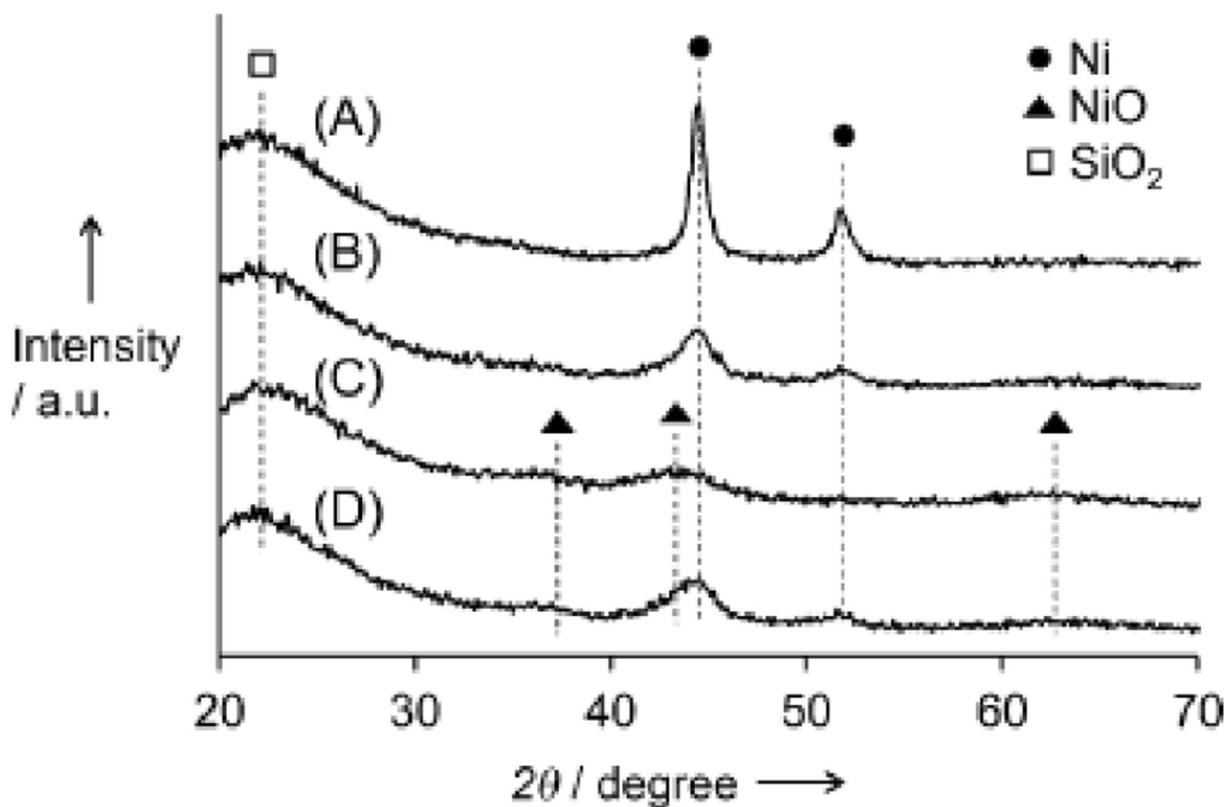


Fig. 48 XRD patterns of the catalysts under air. (A) Ni/SiO₂-cal-773, (B) Ni/SiO₂-873, (C) Ni/SiO₂-773, and (D) Ni/SiO₂-673

Results showed that a small amount of aggregates was formed in the materials prepared by Ni-DHT and Ni-GRF, with high dispersion, compared to that prepared by Ni-IMP (Fig. 40). The smallest particle size was obtained by Ni-DHT. Although the catalyst prepared by the later method exhibited the highest catalytic activity. However, the grafted catalyst showed high stability and long-term activity. This is probably due to more easily accessible Ni-active sites in the grafted catalyst. Hence, the Ni-TUD-1 catalyst prepared by grafting method can be nominated as a better candidate for CO₂ reforming of methane.

The formation of crystalline NiO after calcination was confirmed by normal angle XRD (Fig. 41). Weak peak intensity was attributed to the high dispersion of NiO particles through the TUD-1 framework. The nickel content in all samples was measured by ICP test.

Nickel nanoparticles supported in other types of silica

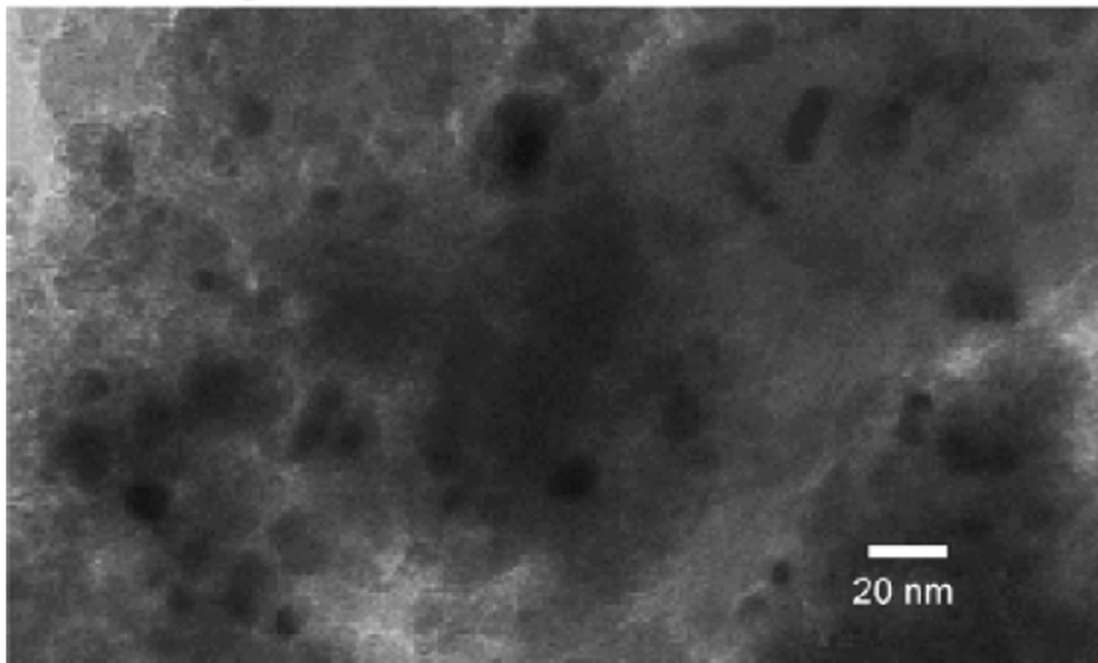
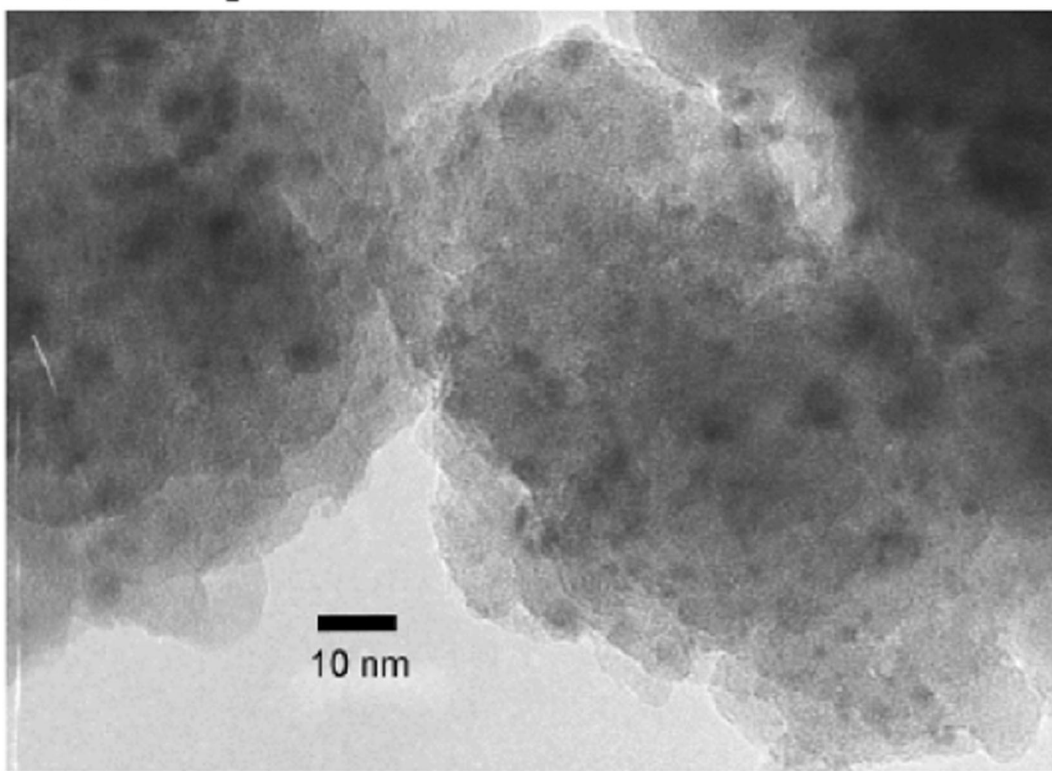
Several works reported the incorporation of nickel NPs in other silica materials and their application in catalysis.

Reddy et al. (Mallesham et al. 2018) reported the preparation of silica-supported Ni NPs with different Ni loadings (5, 10, 20, 30, and 40%), using impregnation method. This catalyst was prepared by dispersing a colloidal SiO₂ in water followed by the addition of an aqueous solution of Ni(NO₃)₂·6H₂O. The obtained materials were calcined under air at 500 °C for 5 h.

The structure of NiO particles in all Ni/SiO₂ catalysts (with different Ni loading, from 5 to 40%) was confirmed by XRD (Fig. 42).

TEM images revealed the formation of uniformly dispersed NiO NPs on SiO₂ matrix (Fig. 43). The average particle size was around 9 nm for all samples with loadings up to 30%. However, the particle size was drastically increased to more than 21 nm at 40% Ni loading.

The high dispersion of NiO NPs has improved a synergistic metal–silica interaction, in particular for the 30% Ni loading sample, leading to enhanced acidic and redox properties. The prepared 30% Ni/SiO₂ material exhibited the best catalytic performance, with 98% selectivity to γ -valerolactone at total conversion of levulinic acid for 2 h (Fig. 44).

(A) Ni/SiO₂-cal-773(B) Ni/SiO₂-873**Fig. 49** TEM images of the reduced catalysts at (A) 773 K and (B) 873 K (Nakagawa et al. 2012)

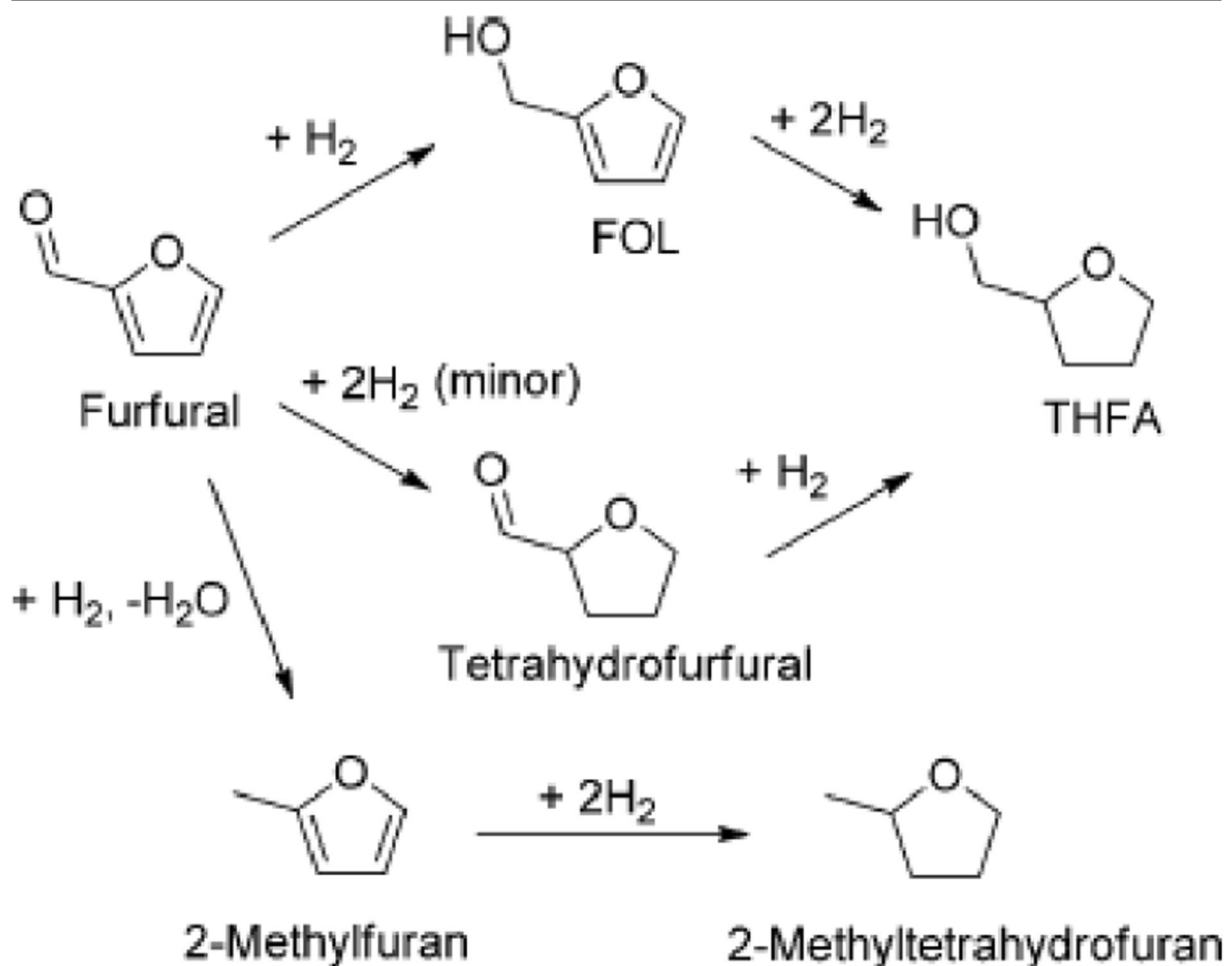


Fig. 50 Reaction pathways for the hydrogenation or hydrogenolysis of furfural (Nakagawa et al. 2012)

Luo et al. (He et al. 2015) reported the preparation of silica-supported NiO NPs using incipient wetness impregnation (IWI) method, with a commercial silica ($S_{\text{BET}} = 498.8 \text{ m}^2/\text{g}$, Nanjing Tianyi Inorganic Chemical Factory) and nickel nitrate as a precursor. The as-made material was calcined at 380 °C then NiO reduced to Ni after treatment by H₂ at 700 °C. The Ni/SiO₂ catalyst was designated as 3NiSN. Ni NPs were highly dispersed in the silica framework, with particle size around 38 nm (Fig. 45). However, Ni NPs were weakly interacted with the support, with obvious particles sintering problems. Consequently, a rapid deactivation of the catalyst was observed during the combination process of CO₂ reforming and partial oxidation of methane (CRPOM) to produce syngas.

XRD analyses were carried out to understand the crystalline structure of 3NiSN catalysts, and the results

are presented in Fig. 46. The results showed only the FCC NiO phase, with typical reflections of the (111), (200), and (220) planes at $2\theta = 37^\circ$, 43° , and 63° , respectively. After reduction under H₂ for 4 h, the peaks attributed to NiO disappeared, and three other peaks around $2\theta = 44^\circ$, 52° , and 76° for Ni (111), Ni (200), and Ni (220) planes, respectively, were observed, indicating the successful transformation of NiO to metallic Ni.

Tomishige et al. (Nakagawa et al. 2012) reported the synthesis of silica-supported Ni NPs by reduction of nickel nitrate using H₂ (Eq. 1). The nickel nitrate in water was first impregnated in a commercial silica (Fuji Silysia G-6; BET surface area 523 m²/g) using incipient wetness impregnation (IWI) method; then, the obtained as-made material was reduced to Ni NPs after treatment

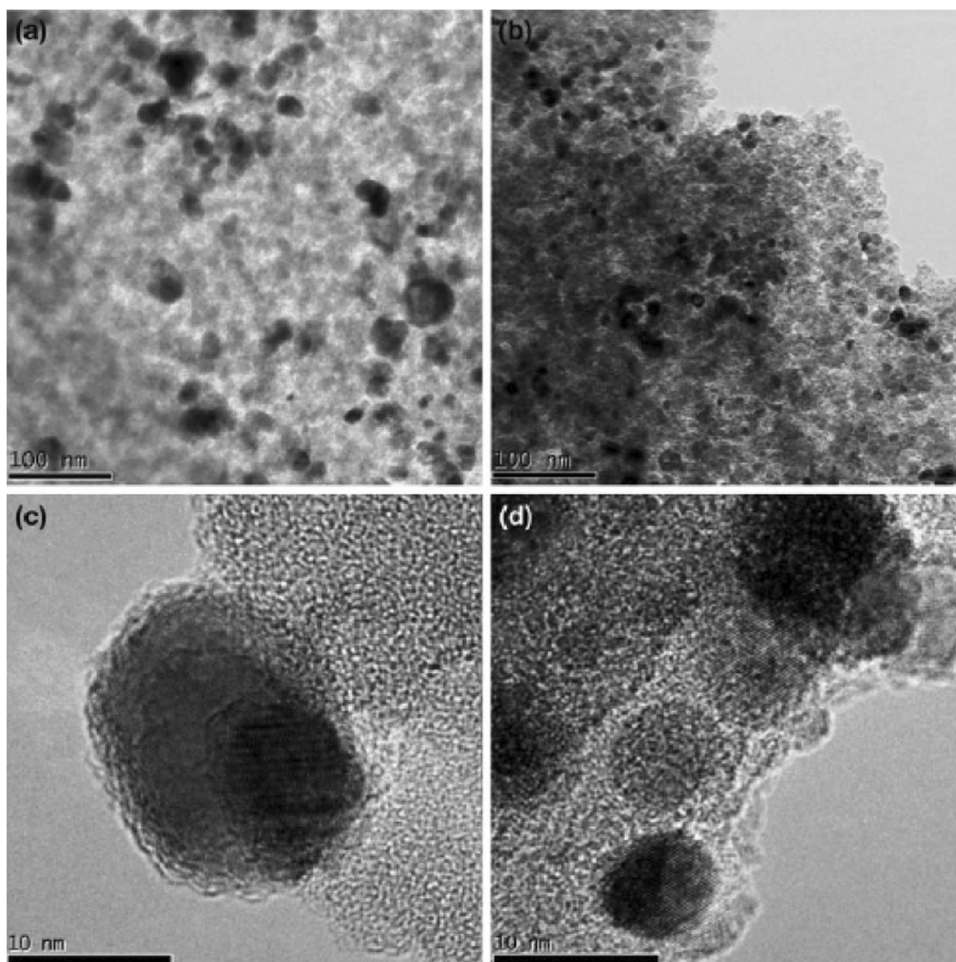
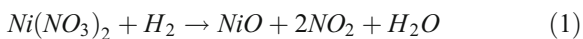


Fig. 51 TEM images of samples after reduction at 500 °C for 2 h. (a, c) Ni/SiO₂-C without treatment with plasma; (b, d) Ni/SiO₂-P treated with plasma (Shi and Liu 2009)

by flowing H₂ at different temperatures (670–870 K) (Fig. 47) in glass tube reactor.



The structure of Ni species in the reduced catalysts was identified by powder XRD, and the obtained results are shown in Fig. 48.

For the samples reduced at high temperature, Ni/SiO₂-873 (Fig. 47—curve 1 and Fig. 48B) and Ni/SiO₂-cal-773 (Fig. 47—curve 4 and Fig. 48A), only peaks attributed to Ni metal were present. However, in the case of Ni/SiO₂-773 (Fig. 47—curve 2 and Fig. 48C) and Ni/SiO₂-673 (Fig. 47—curve 3 and Fig. 48D), both Ni metal and NiO particles were present.

The obtained Ni NP size was less than 4 nm with low dispersion as shown in TEM images (Fig. 49). The catalytic activity of the prepared catalyst was evaluated in the hydrogenation of furfural to 2-methyltetrahydrofuran (Fig. 50). The product was obtained with a maximum yield of 94%. It was found that low turnover frequency (TOF) was obtained with large Ni particle size.

In another work, Shi and Liu (Shi and Liu 2009) reported the synthesis of 10 wt% NiO NPs supported on silica, by conventional incipient impregnation method, using commercial SiO₂ powder, and nickel nitrate hexahydrate as precursor in water at room temperature. After stirring (12 h) and drying (100 °C/12 h), the obtained material was treated with a glow discharge plasma for 1 h and denoted by Ni/SiO₂-P. Another part of the sample was calcined at 500 °C without plasma

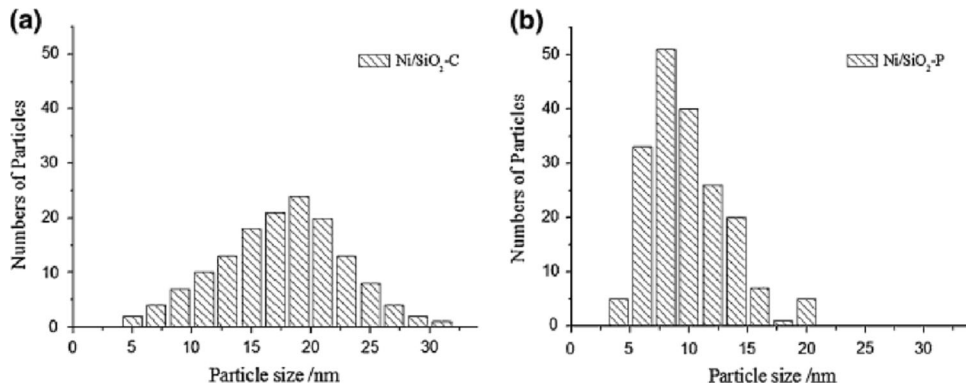


Fig. 52 Size distributions after reduction at 500 °C for 2 h. (a) Ni/SiO₂-C without treatment with plasma; (b) Ni/SiO₂-P treated with plasma (Shi and Liu 2009)

treatment. This thermal treated sample was denoted by Ni/SiO₂-C.

After calcination (500 °C/4 h) and reduction process (H₂, 500 °C/2 h), the obtained silica-supported Ni NPs

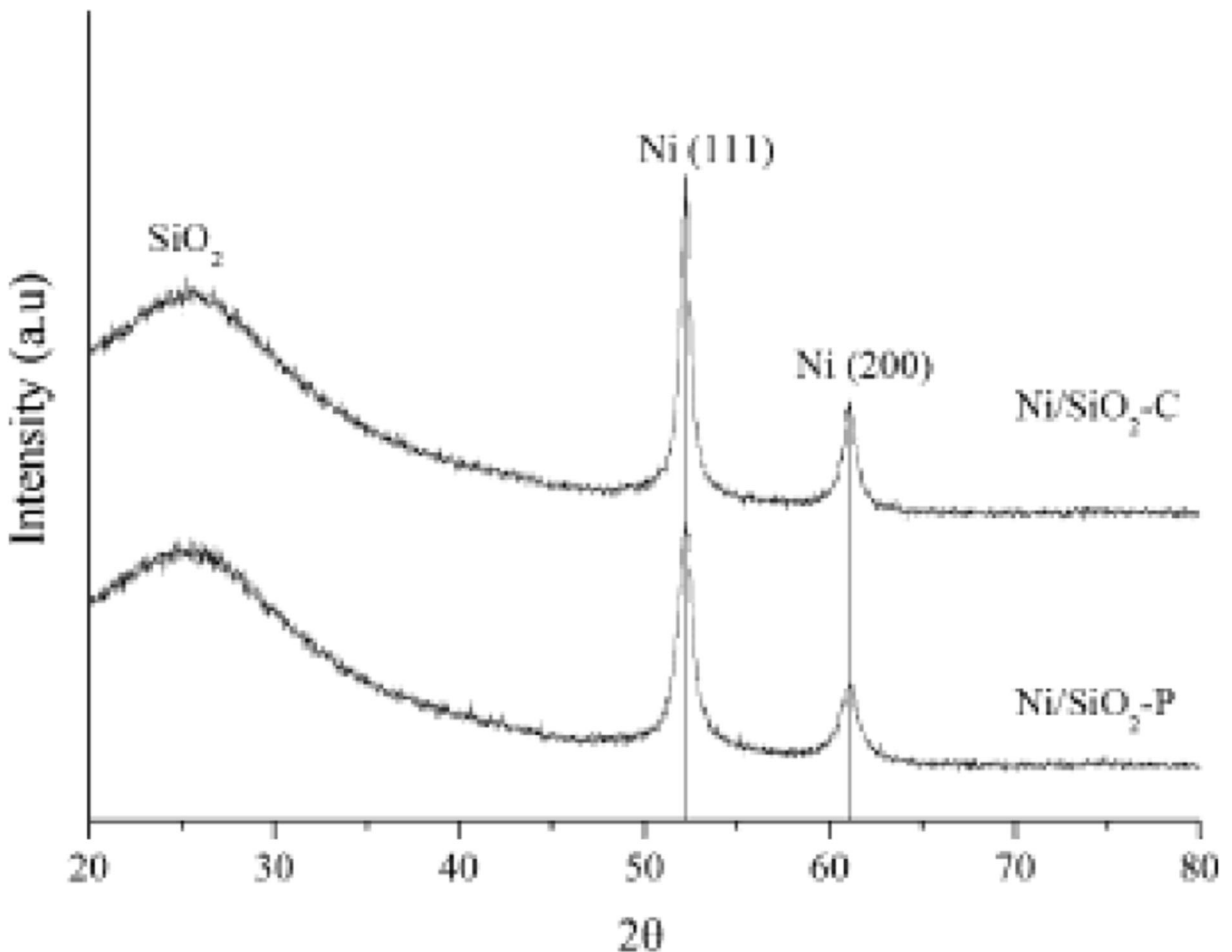


Fig. 53 XRD patterns of fresh samples after reduction at 500 °C for 2 h. Ni/SiO₂-P: plasma treated sample. Ni/SiO₂-C: thermal treated sample

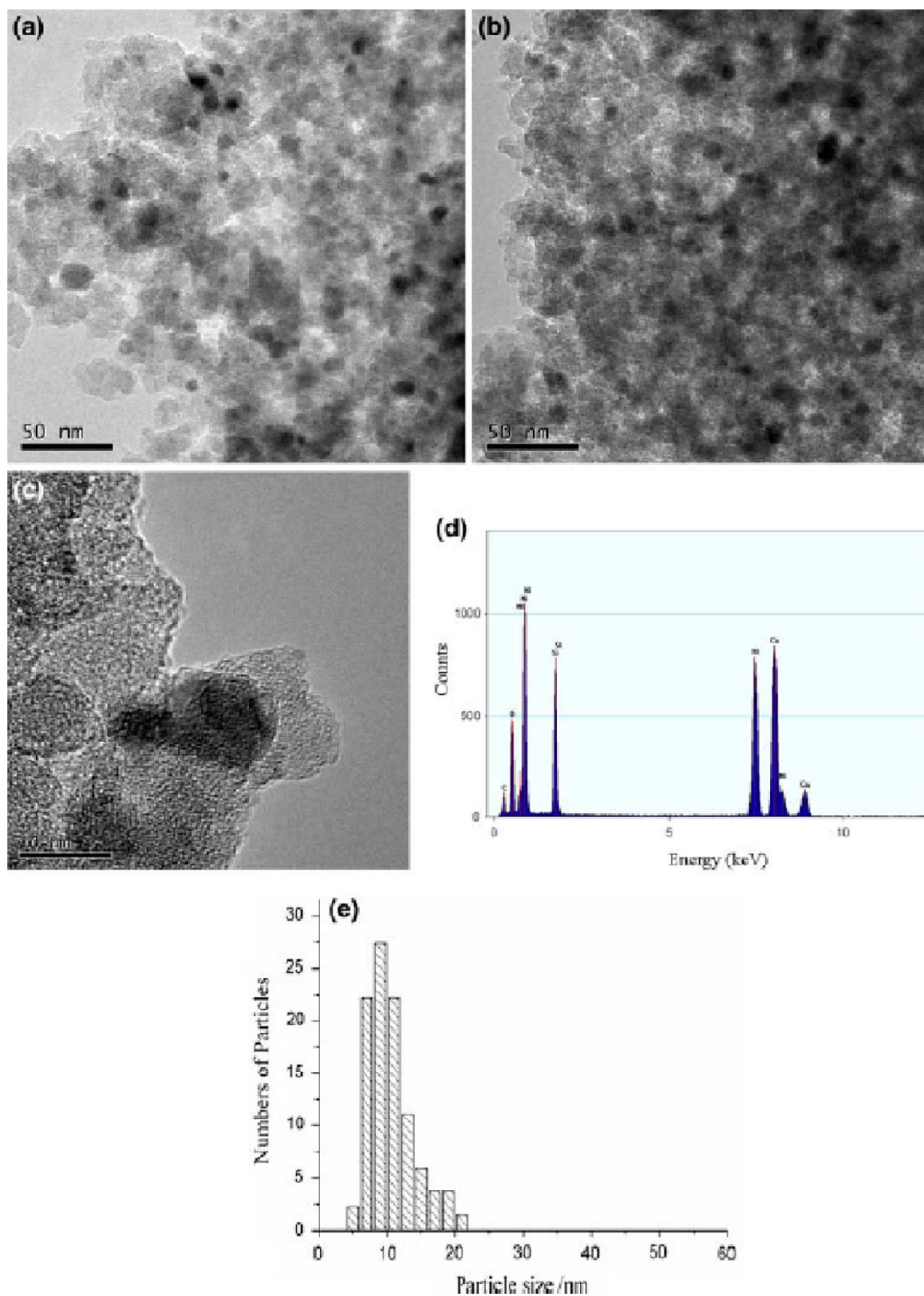


Fig. 54 TEM images of nickel particles of Ni/SiO₂-P after reaction at 350 °C for 4 h (a, b, c) with EDX of image c (d) and size distribution (e)

were highly dispersed with smaller particle size and narrow size distribution at around 9.7 nm, compared to 17.5 nm for the material prepared without plasma treatment, with wide particle size distribution (Figs. 51 and 52).

The prepared material was analysed by XRD to identify the chemical structure of the nickel particles,

and to calculate their size. XRD patterns of fresh samples are presented in Fig. 53. Two peaks assigned to Ni (111) at 52.2° and Ni (200) at 61.1°, respectively, appeared on the XRD patterns confirming the metallic nature of nickel particles. The average particle size calculated from Scherrer formula was about 14 nm for

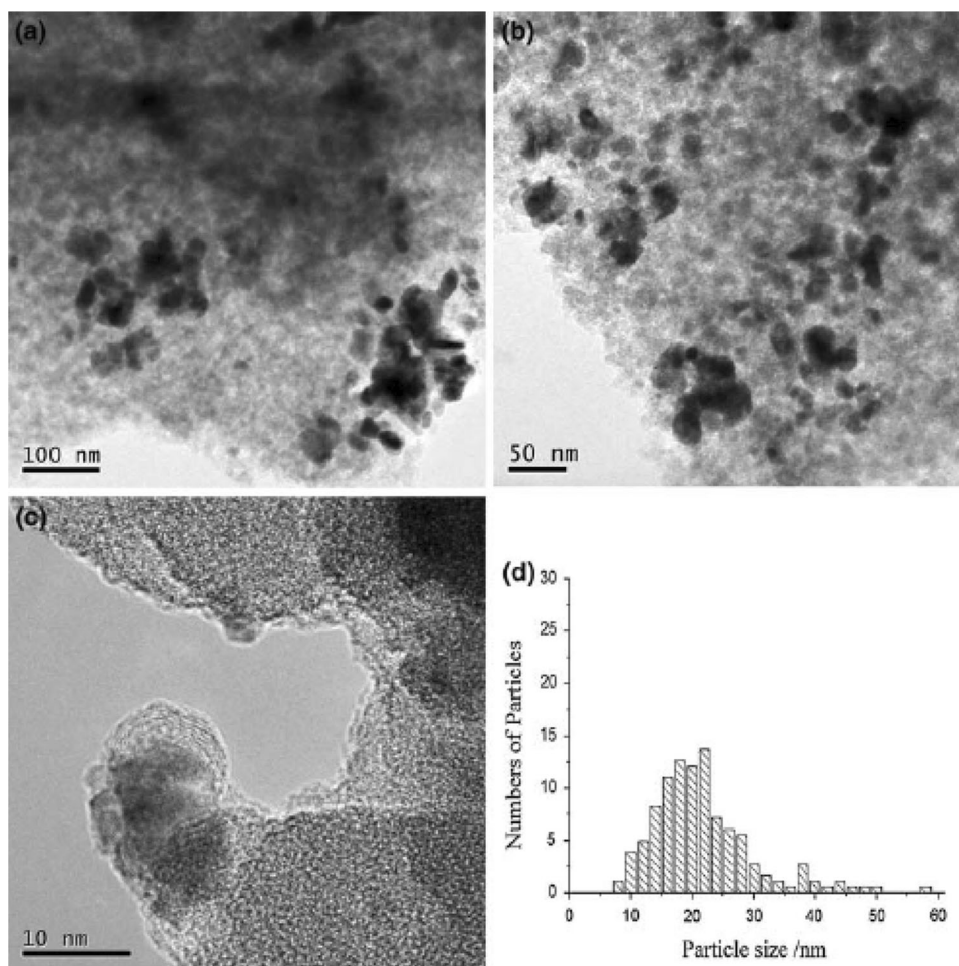


Fig. 55 TEM images of nickel particles of Ni/SiO₂-C after reaction at 350 °C for 4 h (a, b, c) and size distribution (d)

Ni/SiO₂-C and around 10 nm for Ni/SiO₂-P, which is in agreement with the results observed in TEM. The XRD and TEM analyses confirmed that smaller metal particles were obtained in the plasma treated sample.

The obtained catalysts were evaluated in the methanation reaction of carbon monoxide. The catalyst exhibited high conversion of carbon monoxide and hydrogen with less carbon deposition.

As shown in TEM images of Ni/SiO₂-P and Ni/SiO₂-C samples (Figs. 54 and 55, respectively), the plasma treated catalyst showed enhanced nickel–silica interaction with good dispersion after reaction. While aggregation of nickel was observed on Ni/SiO₂-C after reaction, with broad partition distribution of nickel particles (from 7.7 to 57.4 nm, with an average of 21.8 nm). In addition, nickel particles on Ni/SiO₂-C were covered by carbon species, with no visible carbon species found on Ni/SiO₂-P.

A new method to prepare ultra fine nickel NPs in mesoporous silica, called templating assemble method, was reported by Yang et al. (Yang et al. 2017). This process is based on the complexation of the nickel sources (precursor) by the amine groups attached to the surfactant followed by addition of TEOS then calcination (Fig. 56). In this process, dodecyl amine was used as a neutral structure directing agent for silica and as a complexing agent to capture the nickel ions which were added with different loadings (1, 2, 3 and 4 mmol for 10.73 mL of TEOS). The samples corresponding to different nickel amounts were labeled as H-*x*Ni (*x* = 1, 2, 3, and 4), in which *x* stands for the nickel amount (number of moles of Ni(NO₃)₂·6H₂O mmol) of different samples.

After the calcination step, highly dispersed and fine NiO NPs were observed in TEM images (Fig. 57).

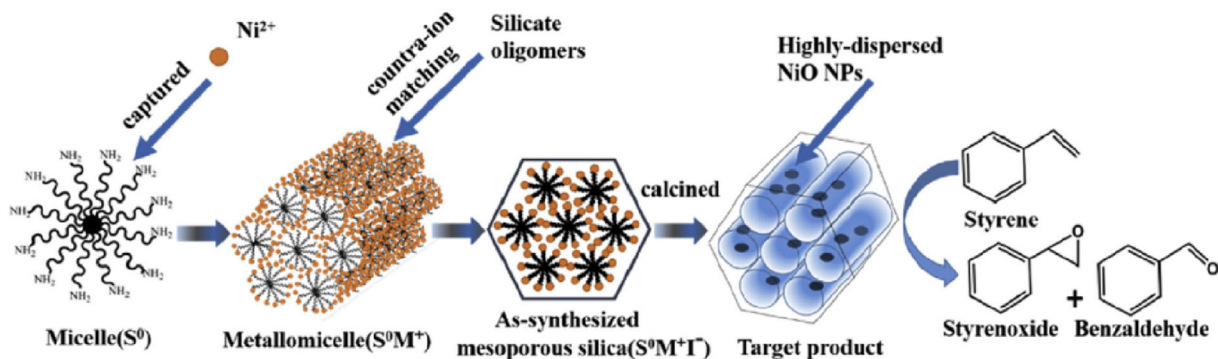


Fig. 56 Preparation of mesoporous silica-supported NiO NPs using a templating assembly route (Yang et al. 2017)

TEM images showed a sponge-like framework mesoporous structure with wormhole pore for the prepared samples. In addition, these images demonstrated the presence of fine Ni NPs (2–5 nm) with high dispersion in mesoporous silica. However, some Ni aggregates have been observed in high Ni loading material. As expected, the surface area, pore size, and pore volume were decreased by increasing the Ni loading.

Because nickel oxide nanoparticles prepared by the templating route (H-*x*Ni series) were mono-dispersed in the silica framework, only broad peaks were observed in XRD patterns (Fig. 58). In this work, the loadings of

nickel in catalysts were measured using the inductively coupled plasma spectrometer (ICP).

The obtained nanocatalyst exhibited a good catalytic activity for the epoxidation reaction of styrene. The maximum conversion of styrene (67%) and high styrene oxide selectivity (94%) were obtained using the catalyst with high Ni loading (4 mmol of nickel nitrate) which was named H-4Ni.

However, using functionalized surfactant to interact with the metal sources can affect the silica structure and its porosity. In addition, this method is limited by the use of some specific and expensive surfactants which carry

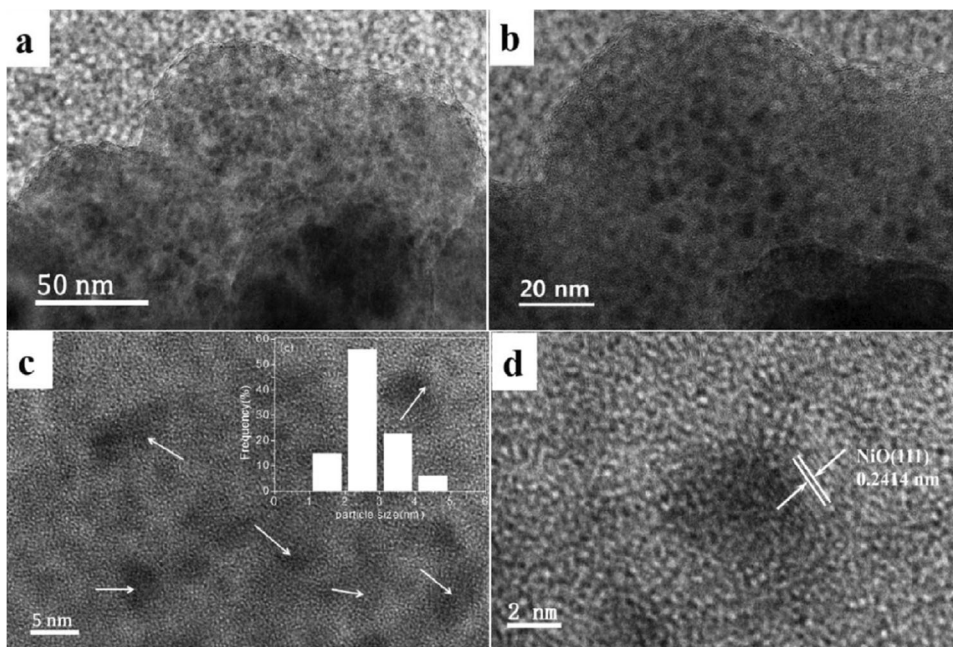


Fig. 57 TEM images of sample of H-4Ni and size distribution of NiO NPs (inset) (Yang et al. 2017)

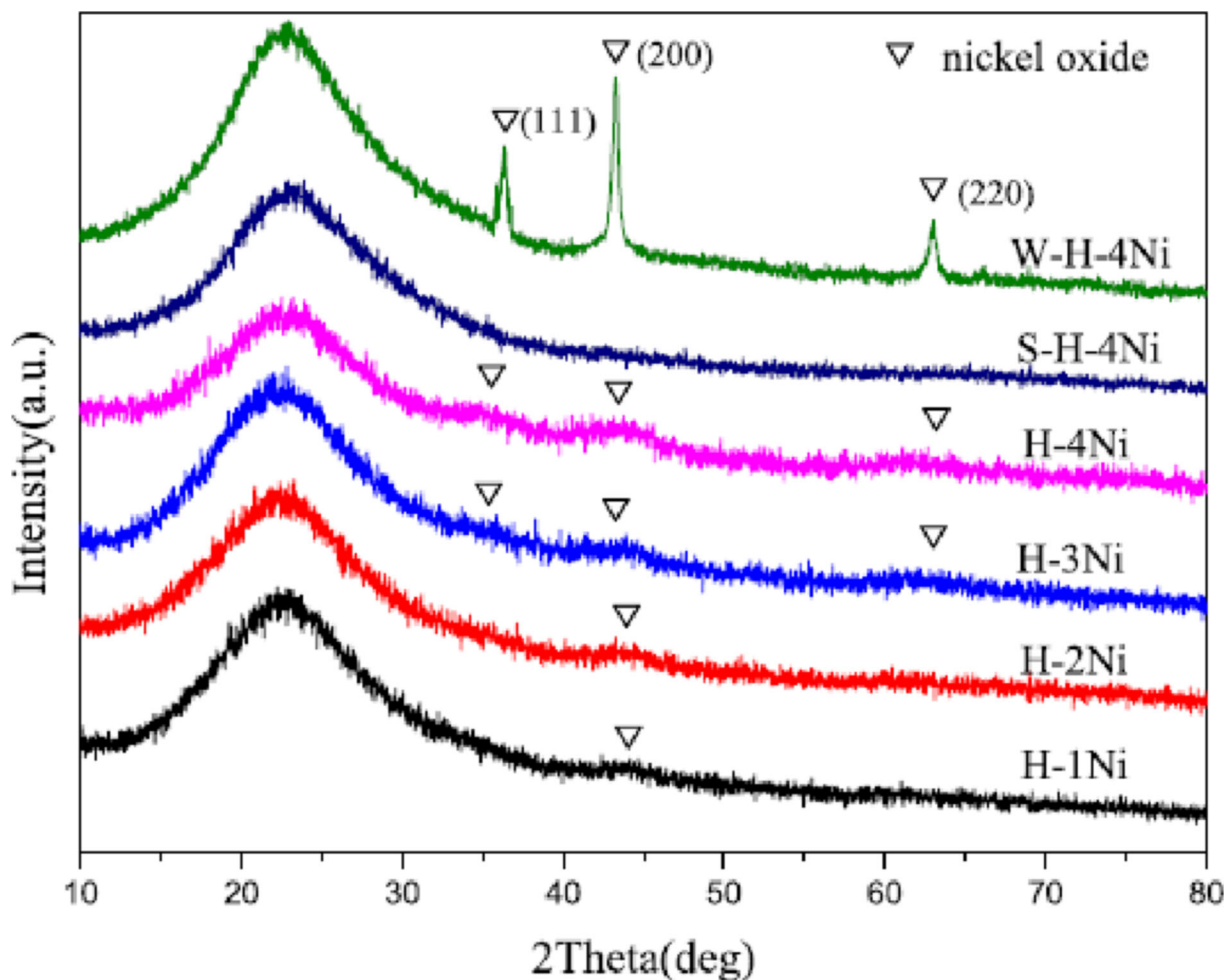


Fig. 58 High-angle patterns of the series samples of H- x Ni (samples prepared by templating route), S-H-4Ni (sample prepared via a single-step procedure), and W-H-4Ni (sample prepared by wetness impregnation)

amine groups; thus, the access to commercial mesoporous silica such as SBA-15 and MCM-41 is not possible.

Nickel-based bimetallic NPs incorporated in mesoporous silica material have been also prepared and used in catalysis. Recently, Pandey et al. (Pandey et al. 2021) reported the synthesis of Pd–Ni bimetallic NPs incorporated in mesoporous silica and the utilisation of the obtained material as an efficient and cheaper photocatalyst for the degradation of anionic and cationic dyes.

Mesoporous silica nanoparticles (MSNPs) supported Pd–Ni NPs were prepared in situ using an organo trialkoxysilane as a template and stabilizer for efficient reduction. Briefly, in the first step, silica-supported palladium NPs were prepared by impregnation of tetrachloropalladate in MSNPs using ethylene glycol.

The obtained palladium cations dispersed MSNPs were suspended in a solution of 3-aminopropyltrimethoxysilane (template) in ethylene glycol. After addition of formaldehyde and microwave treatment, PdNP-inserted MSNPs was obtained. A similar method was used to prepare mesoporous silica-supported PdNPs. In the second step, PdNP-inserted MSNPs was suspended in an aqueous solution of nickel sulphate containing 1% PVP under stirring followed by the addition of NaBH₄ aqueous solution under stirring resulting the formation of Pd–Ni NP-inserted MSNPs and collected by centrifugation.

In this method, 3-aminopropyltrimethoxysilane had an active role in efficient reduction of palladium cations along with in situ providing a template for efficient reduction and stabilisation of Pd–Ni nanocrystallite. In addition, this

organotrialkoxysilane enabled controlled insertion of bi-

Pd–Ni particle size and structure of the prepared

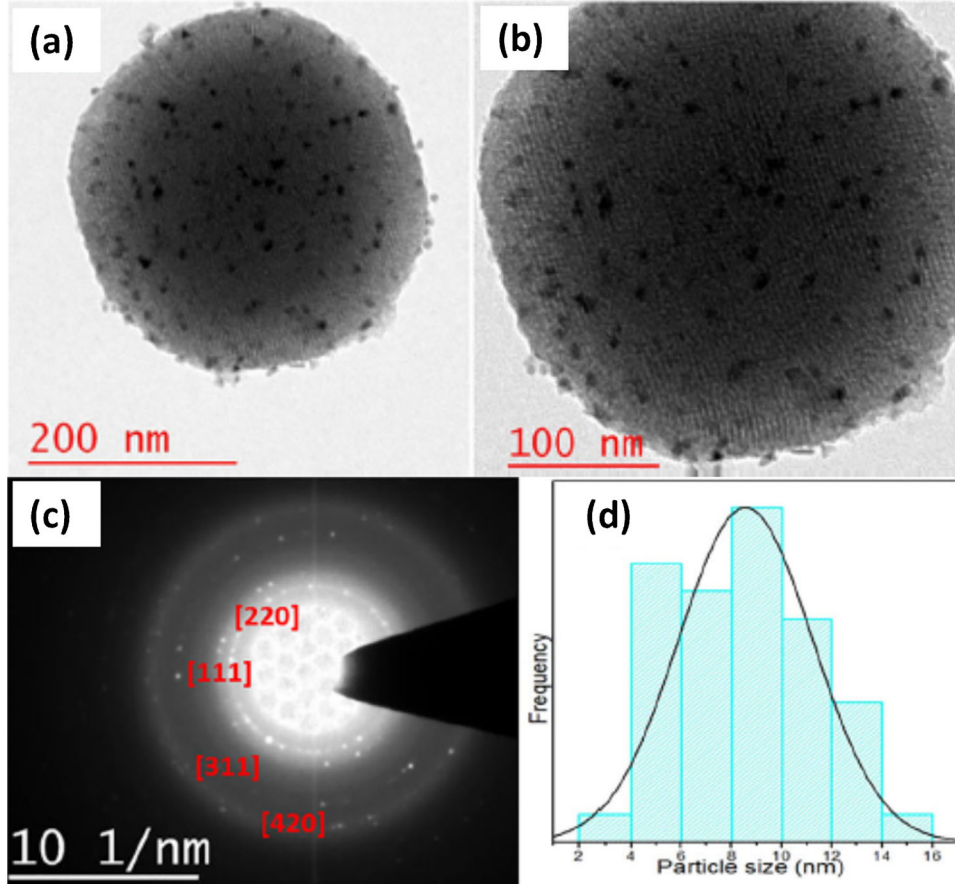


Fig. 59 (a, b) TEM images of Pd–Ni NP–inserted MSNPs; (c) selected area diffraction pattern; (d) particle size distribution curve

metallic Pd–Ni nanocrystallite within mesoporous silica support.

material were investigated by TEM and selected area electron diffraction pattern (SAED) (Fig. 59). The TEM

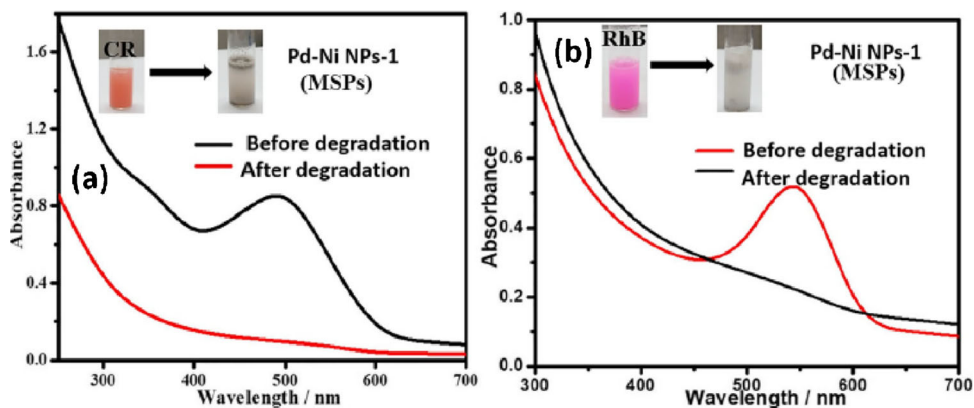


Fig. 60 UV–Vis absorption spectra of the real textile sample in the absence and the presence of Pd–Ni NPs-1 inserted MSPs, (a) for Congo red and (b) for Rh B. The samples were collected from

the washout of stencil used in fabric printing using dye embedded with binder and thinner

images of Pd–Ni NP inserted MSNPs are shown in Fig. 59a and b. SAED as shown in Fig. 59c confirms the presence of 111, 311 planes assigned to nickel, whereas 220, 420 planes are assigned the presence of palladium nanocatalyst. Figure 59d shows the average size of Pd–Ni NPs nanocrystallite to the order of 8 nm.

Compared to Pd–Ni bimetallic nanocatalyst (made at Pd:Ni ratio of 1:1), the use of Pd–Ni NP–inserted MSNPs yielded faster degradation of both Rh B and Congo red dyes to the order of 50 s and 150 s, respectively (Fig. 60), justifying potent catalytic behaviour for real-time degradation of toxic industrial dye. In addition, this nanocatalytic system showed high stability and excellent reusability.

Conclusion

Throughout this review, the most commonly used techniques to prepare unsupported Ni NPs and their recent applications in heterogeneous catalysis, including photocatalysis, have been discussed.

Despite the importance of Ni NPs as efficient economic and eco-friendly nanocatalysts, characteristics such as optical and catalytic activity may be lost if the dispersion of these particles is not adequately modulated. Several efforts have been deployed to overcome their aggregation problem, low durability, low dispersibility, and electrons and holes recombination by incorporating them into solid matrices such as porous silica materials.

In this review, we have discussed the most commonly used methods to incorporate Ni NPs into different types of porous silica materials (e.g. SBA-15, MCM-41, MCM-48, TUD-1, and other silica) and their applications in heterogeneous catalysis. The most used technique to prepare Ni NPs@silica is the impregnation, with nickel nitrate as nickel precursor, and reforming of methane as the most used application.

However, the use of different approaches to prepare Ni NPs@silica is still limited by the Ni NP size and aggregation, particles sintering, low dispersion, Ni loading, and the complicated, expensive, and time-consuming techniques.

The synthesis of stable Ni NPs@silica with quantized size and high dispersion tended to be difficult. This explains why the investigation of Ni NP catalytic activity is relatively scarce compared with other transition

metal NPs. Hence, the development of more efficient approaches remains a fecund area of research.

Acknowledgements The authors would like to express their gratitude to King Khalid University, Abha, Saudi Arabia, for providing administrative and technical support.

Funding The Deanship of Scientific Research at King Khalid University provided funding for this work through a general research project under grant number GP 89–42.

Declarations

Conflict of interest The authors declare no competing interests.

References

- Sheldon RA, Dakka J (1994) Heterogeneous catalytic oxidations in the manufacture of fine chemicals. *Catal Today* 19(2):215–245. [https://doi.org/10.1016/0920-5861\(94\)80186-X](https://doi.org/10.1016/0920-5861(94)80186-X)
- Sachdeva, H., Dwivedi, D., Bhattacharjee, R. R., Khaturia, S., & Saroj, R. (2013). NiO nanoparticles: an efficient catalyst for the multicomponent one-pot synthesis of novel spiro and condensed indole derivatives. *Journal of Chemistry*, 2013. <https://doi.org/10.1155/2013/606259>
- Clark J, Macquarrie D (1998) Catalysis of liquid phase organic reactions using chemically modified mesoporous inorganic solids. *Chem Commun* 8:853–860. <https://doi.org/10.1039/A709143E>
- Liu L, Corma A (2018) Metal catalysts for heterogeneous catalysis: from single atoms to nanoclusters and nanoparticles. *Chem Rev* 118(10):4981–5079. <https://doi.org/10.1021/acs.chemrev.7b00776>
- Kung, H. H. (1989). *Transition metal oxides: surface chemistry and catalysis*. Elsevier
- Henrich, V. E., & Cox, P. A. (1996). *The surface science of metal oxides*. Cambridge university press
- Noguera, C. (1996). *Physics and chemistry at oxide surfaces*. Cambridge University Press
- Salem I (2003) Recent studies on the catalytic activity of titanium, zirconium, and hafnium oxides. *Catalysis Reviews* 45(2): 205–296. <https://doi.org/10.1081/CR-120015740>
- Ornelas C, Méry D, Blais JC, Cloutet E, Ruiz Aranzaes J, Astruc D (2005) Efficient mono- and bifunctionalization of polyolefin dendrimers by olefin metathesis. *Angew Chem Int Ed* 44(45):7399–7404. <https://doi.org/10.1002/anie.200502848>
- Astruc D (2007) Palladium nanoparticles as efficient green homogeneous and heterogeneous carbon–carbon coupling precatalysts: a unifying view. *Inorg Chem* 46(6):1884–1894. <https://doi.org/10.1021/ic062183h>
- Zhong LS, Hu JS, Cui ZM, Wan LJ, Song WG (2007) In-situ loading of noble metal nanoparticles on hydroxyl-group-rich titania precursor and their catalytic applications. *Chem Mater* 19(18):4557–4562. <https://doi.org/10.1021/cm071403z>

- Moreno-Manas M, Pleixats R (2003) Formation of carbon–carbon bonds under catalysis by transition-metal nanoparticles. *Acc Chem Res* 36(8):638–643. <https://doi.org/10.1021/ar020267y>
- Li Y, Boone E, El-Sayed MA (2002) Size effects of PVP–Pd nanoparticles on the catalytic Suzuki reactions in aqueous solution. *Langmuir* 18(12):4921–4925. <https://doi.org/10.1021/la011469q>
- Astruc, D. (Ed.). (2008). *Nanoparticles and catalysis*. John Wiley & Sons.
- Djakovitch, L., Köhler, K., & Vries, J. G. D. (2007). The role of palladium nanoparticles as catalysts for carbon–carbon coupling reactions. *Nanoparticles and Catalysis*, 303–348. <https://doi.org/10.1002/9783527621323.ch10>
- Durand J, Teuma E, Gómez M (2008) An overview of palladium nanocatalysts: surface and molecular reactivity. *Eur J Inorg Chem* 2008(23):3577–3586. <https://doi.org/10.1002/jeic.200800569>
- Yang F, Zhou S, Gao S, Liu X, Long S, Kong Y (2017) In situ embedding of ultra-fine nickel oxide nanoparticles in HMS with enhanced catalytic activities of styrene epoxidation. *Microporous Mesoporous Mater* 238:69–77. <https://doi.org/10.1016/j.micromeso.2016.03.007>
- Astruc D (2020) Introduction: nanoparticles in catalysis. *Chem Rev* 120(2):461–463. <https://doi.org/10.1021/acs.chemrev.8b00696>
- Bian Z, Das S, Wai MH, Hongmanorom P, Kawi S (2017) A review on bimetallic nickel-based catalysts for CO₂ reforming of methane. *ChemPhysChem* 18(22):3117–3134. <https://doi.org/10.1002/cphc.201700529>
- Jaji N-D, Lee HL, Hussin MH, Akil HM, Zakaria MR, Othman MBH (2020) Advanced nickel nanoparticles technology: from synthesis to applications. *Nanotechnol Rev* 9:1456–1480. <https://doi.org/10.1515/ntrev-2020-0109>
- Vollath, D., & Szabó, D. V. (2009). Nonmetallic bulk nanomaterials. *Bulk nanostructured materials*, (eds MJ Zehetbauer and YT Zhu), 49–85.
- Schubert, U., & Hüsing, N. (2019). *Synthesis of inorganic materials*. John Wiley & Sons
- Ozin, G. A., Arsenault, A. C., & Cademartiri, L. (2009). Nanorod, nanotube, nanowire self-assembly. *Nanochemistry: A Chemical Approach to Nanomaterials*, 215.
- Lai TL, Lee CC, Wu KS, Shu YY, Wang CB (2006) Microwave-enhanced catalytic degradation of phenol over nickel oxide. *Appl Catal B* 68(3–4):147–153. <https://doi.org/10.1016/j.apcatb.2006.07.023>
- Lai TL, Lee CC, Huang GL, Shu YY, Wang CB (2008) Microwave-enhanced catalytic degradation of 4-chlorophenol over nickel oxides. *Appl Catal B* 78(1–2): 151–157. <https://doi.org/10.1016/j.apcatb.2007.09.015>
- Christoskova ST, Stoyanova M (2001) Degradation of phenolic waste waters over Ni-oxide. *Water Res* 35(8):2073–2077. [https://doi.org/10.1016/S0043-1354\(00\)00469-3](https://doi.org/10.1016/S0043-1354(00)00469-3)
- Ashik UPM, Daud WW, Hayashi JI (2017) Governance of the porosity and of the methane decomposition activity sustainability of NiO/SiO₂ nanocatalysts by changing the synthesis parameters in the modified Stöber method. *C R Chim* 20(9–10):896–909. <https://doi.org/10.1016/j.crci.2017.06.007>
- Guo XF, Kim YS, Kim GJ (2011) Synthesis of mesoporous metal oxides and their efficient property for super capacitor application. *J Nanosci Nanotechnol* 11(2):1672–1675. <https://doi.org/10.1166/jnn.2011.3321>
- Solsona B, Concepción P, Nieto JL, Dejos A, Cecilia JA, Agouram S, Castellón ER (2016) Nickel oxide supported on porous clay heterostructures as selective catalysts for the oxidative dehydrogenation of ethane. *Catal Sci Technol* 6(10):3419–3429. <https://doi.org/10.1039/C5CY01811K>
- Vikraman D, Park HJ (2016) Shape-selective synthesis of NiO nanostructures for hydrazine oxidation as a nonenzymatic amperometric sensor. *RSC Adv* 6(89):86101–86107. <https://doi.org/10.1039/C6RA12805J>
- Sasaki T, Ichikuni N, Hara T, Shimazu S (2018) Study on the promoting effect of nickel silicate for 1-phenylethanol oxidation on supported NiO nanocluster catalysts. *Catal Today* 307:29–34. <https://doi.org/10.1016/j.cattod.2017.05.076>
- Gao X, Mao H, Lu M, Yang J, Li B (2012) Facile synthesis route to NiO–SiO₂ intercalated clay with ordered porous structure: intragallery interfacially controlled functionalization using nickel–ammonia complex for deep desulfurization. *Microporous Mesoporous Mater* 148(1):25–33. <https://doi.org/10.1016/j.micromeso.2011.07.022>
- El-Safty SA, Kiyozumi Y, Hanaoka T, Mizukami F (2008) Heterogeneous catalytic activity of NiO-silica composites designated with cubic Pm3n cage nanostructures. *Appl Catal B* 82(3–4):169–179. <https://doi.org/10.1016/j.apcatb.2008.01.027>
- Adil SF, Assal ME, Kuniyil M, Khan M, Shaik MR, Alwarthan A, Siddiqui MRH (2017) Synthesis and comparative catalytic study of zinc oxide (ZnO_x) nanoparticles promoted MnCO₃, MnO₂ and Mn₂O₃ for selective oxidation of benzylic alcohols using molecular oxygen. *Mater Express* 7(2):79–92. <https://doi.org/10.1166/mex.2017.1357>
- Arora AK, Kumar P, Kumar S (2017) Synthesis of ZnO nanoparticle and its application in catalytic hydrolysis of p-acetoxynitrobenzene. *Int J Nanosci* 16(04):1750005. <https://doi.org/10.1142/S0219581X17500053>
- Pike SD, García-Trenco A, White ER, Leung AH, Weiner J, Shaffer MS, Williams CK (2017) Colloidal Cu/ZnO catalysts for the hydrogenation of carbon dioxide to methanol: investigating catalyst preparation and ligand effects. *Catal Sci Technol* 7(17):3842–3850. <https://doi.org/10.1039/C7CY01191A>
- Chand, S., & Sandhu, J. S. (2015). ZnO Nanoparticles: an efficient green reusable catalyst for the synthesis of 3-formyl benzopyranones chalcones by Claisen-Schmidt reaction under solvent-free condition. <https://hdl.handle.net/123456789/33037>
- Sun X, Zhang X, Cao X, Zhao X (2016) Optimization of reaction conditions for cyclohexane to cyclohexanone with t-butylhydroperoxide over CuCl₂ loaded with activated carbon. *J Braz Chem Soc* 27(1):202–208. <https://doi.org/10.5935/0103-5053.20150271>
- Grosso C, Boissiere BS, Brezesinski T, Pierre N, Albouy P, Amenitsch H, Antonietti M, Sanchez C (2004) Periodically ordered nanoscale islands and mesoporous films composed of nanocrystalline multimetallic oxides. *Nat Mater* 3(11): 787–92. <https://doi.org/10.1038/nmat1206>
- Zou X, Conradsson T, Klingstedt M, Dadachov MS, O’Keeffe M (2005) A mesoporous germanium oxide with crystalline pore walls and its chiral derivative. *Nature* 437(7059):716–719. <https://doi.org/10.1038/nature04097>

- Ying JY, Mehnert CP, Wong MS (1999) Synthesis and applications of supramolecular-templated mesoporous materials. *Angew Chem Int Ed* 38(1–2):56–77. [https://doi.org/10.1002/\(SICI\)1521-3773\(19990115\)38:1/2%3C56::AID-ANIE56%3E3.0.CO;2-E](https://doi.org/10.1002/(SICI)1521-3773(19990115)38:1/2%3C56::AID-ANIE56%3E3.0.CO;2-E)
- Jia J, Wang Y, Tanabe E, Shishido T, Takehira K (2003) Carbon fibers prepared by pyrolysis of methane over Ni/MCM-41 catalyst. *Microporous Mesoporous Mater* 57(3):283–289. [https://doi.org/10.1016/S1387-1811\(02\)00598-X](https://doi.org/10.1016/S1387-1811(02)00598-X)
- Basha SS, Sasirekha NR, Maheswari R, Shanthi K (2006) Mesoporous H-AlMCM-41 supported NiO-MoO₃ catalysts for hydrodenitrogenation of o-toluidine: I. Effect of MoO₃ loading. *Appl Catal A* 308:91–98. <https://doi.org/10.1016/j.apcata.2006.04.013>
- Moreno-Tost R, Santamaría-González J, Maireles-Torres P, Rodríguez-Castellón E, Jiménez-López A (2002) Nickel oxide supported on zirconium-doped mesoporous silica for selective catalytic reduction of NO with NH₃. *J Mater Chem* 12(11):3331–3336. <https://doi.org/10.1039/B204041G>
- Polshettiwar V, Baruwati B, Varma RS (2009) Nanoparticle-supported and magnetically recoverable nickel catalyst: a robust and economic hydrogenation and transfer hydrogenation protocol. *Green Chem* 11(1):127–131. <https://doi.org/10.1039/B815058C>
- Kalbasi RJ, Mosaddegh N (2011) Suzuki-Miyaura cross-coupling reaction catalyzed by nickel nanoparticles supported on poly(N-vinyl-2-pyrrolidone)/TiO₂-ZrO₂ composite. *Bull Korean Chem Soc* 32:2584–2592
- Alonso F, Riente P, Yus M (2011) Nickel nanoparticles in hydrogen transfer reactions. *Acc Chem Res* 44(5):379–391. <https://doi.org/10.1021/ar1001582>
- Sriram S, Thayumanavan A, Ravichandran K (2016) Influence of nitrogen doping on properties of NiO films. *Surf Eng* 32(3): 207–211. <https://doi.org/10.1179/1743294414Y.0000000380>
- Kumar R, Singh RK, Singh DP, Savu R, Moshkalev SA (2016) Microwave heating time dependent synthesis of various dimensional graphene oxide supported hierarchical ZnO nanostructures and its photoluminescence studies. *Mater Des* 111: 291–300. <https://doi.org/10.1016/j.matdes.2016.09.018>
- Wang Y, Ma J, Xu Q, Zhang J (2017) Fabrication of antibacterial casein-based ZnO nanocomposite for flexible coatings. *Mater Des* 113:240–245. <https://doi.org/10.1016/j.matdes.2016.09.082>
- Jin Y, Li A, Hazelton SG, Liang S, John CL, Selid PD, Zhao JX (2009) Amorphous silica nanohybrids: synthesis, properties and applications. *Coord Chem Rev* 253(23–24):2998–3014. <https://doi.org/10.1016/j.ccr.2009.06.005>
- Martín-Jimeno FJ, Suarez-García F, Paredes JI, Martínez-Alonso A, Tascon JMD (2021) Nickel nanoparticle/carbon catalysts derived from a novel aqueous-synthesized metal-organic framework for nitroarene reduction. *J Alloys Compd* 853: 157348. <https://doi.org/10.1016/j.jallcom.2020.157348>
- Lin XZ, Terepka AD, Yang H (2004) Synthesis of silver nanoparticles in a continuous flow tubular microreactor. *Nano Lett* 4(11):2227–2232. <https://doi.org/10.1021/nl0485859>
- Tsunoyama H, Ichikuni N, Tsukuda T (2008) Microfluidic synthesis and catalytic application of PVP-stabilized, ~ 1 nm gold clusters. *Langmuir* 24(20):11327–11330. <https://doi.org/10.1021/la801372j>
- Glasnov TN (2013) Highlights from the flow chemistry literature 2013 (part 3). *J Flow Chem* 3(4):132–140. <https://doi.org/10.1556/JFC-D-13-00026>
- Rogers, S. M. (2017). Designing metal nanoparticles for catalysis (Doctoral dissertation, UCL (University College London)). <https://core.ac.uk/download/pdf/111015385.pdf>
- Baumgard J, Vogt AM, Kragl U, Jähnisch K, Steinfeldt N (2013) Application of microstructured devices for continuous synthesis of tailored platinum nanoparticles. *Chem Eng J* 227: 137–144. <https://doi.org/10.1016/j.cej.2012.08.066>
- Woehl TJ, Evans JE, Arslan I, Ristenpart WD, Browning ND (2012) Direct in situ determination of the mechanisms controlling nanoparticle nucleation and growth. *ACS Nano* 6(10):8599–8610. <https://doi.org/10.1021/nn303371y>
- Demello AJ (2006) Control and detection of chemical reactions in microfluidic systems. *Nature* 442(7101):394–402. <https://doi.org/10.1038/nature05062>
- Bönnemann H, Richards RM (2001) Nanoscopic metal particles – synthetic methods and potential applications. *Eur J Inorg Chem* 2001(10):2455–2480. [https://doi.org/10.1002/1099-0682\(200109\)2001:10%3C2455::AID-EJIC2455%3E3.0.CO;2-Z](https://doi.org/10.1002/1099-0682(200109)2001:10%3C2455::AID-EJIC2455%3E3.0.CO;2-Z)
- Polte J, Erler R, Thunemann AF, Sokolov S, Ahner TT, Rademann K, Kraehnert R (2010a) Nucleation and growth of gold nanoparticles studied via in situ small angle X-ray scattering at millisecond time resolution. *ACS Nano* 4(2): 1076–1082. <https://doi.org/10.1021/nn901499c>
- McKenzie LC, Haben PM, Kevan SD, Hutchison JE (2010) Determining nanoparticle size in real time by small-angle X-ray scattering in a microscale flow system. *J Phys Chem C* 114(50):22055–22063. <https://doi.org/10.1021/jp1077533>
- Polshettiwar V, Cha D, Zhang X, Basset JM (2010) High-surface-area silica nanospheres (KCC-1) with a fibrous morphology. *Angew Chem Int Ed* 49(50):9652–9656. <https://doi.org/10.1002/anie.201003451>
- Gniewek A, Ziółkowski JJ, Trzeciak AM, Zawadzki M, Grabowska H, Wrzyszczyk J (2008) Palladium nanoparticles supported on alumina-based oxides as heterogeneous catalysts of the Suzuki-Miyaura reaction. *J Catal* 254(1):121–130. <https://doi.org/10.1016/j.jcat.2007.12.004>
- Polte J, Kraehnert R, Radtke M, Reinholz U, Rieseemeier H, Thünemann A. F., & Emmerling, F. (2010). New insights of the nucleation and growth process of gold nanoparticles via in situ coupling of SAXS and XANES. In *Journal of Physics: Conference Series* (Vol. 247, No. 1, p. 012051). IOP Publishing. <https://iopscience.iop.org/article/>. <https://doi.org/10.1088/1742-6596/247/1/012051/pdf>
- Polte J, Ahner TT, Delissen F, Sokolov S, Emmerling F, Thünemann AF, Kraehnert R (2010c) Mechanism of gold nanoparticle formation in the classical citrate synthesis method derived from coupled in situ XANES and SAXS evaluation. *J Am Chem Soc* 132(4):1296–1301. <https://doi.org/10.1021/ja906506j>
- Pacioni, N. L., Borsarelli, C. D., Rey, V., & Veglia, A. V. (2015). Synthetic routes for the preparation of silver nanoparticles. In *Silver nanoparticle applications* (pp. 13–46). Springer, Cham. <https://link.springer.com/book/>. <https://doi.org/10.1007/978-3-319-11262-6>
- Swathy, B. (2014). A review on metallic silver nanoparticles. *IOSR J Pharm*, 4(7), 2250–3013. <https://iosrphr.org/papers/v4i07/F047038044.pdf>

- Horikoshi, S., & Serpone, N. (Eds.). (2013). *Microwaves in nanoparticle synthesis: fundamentals and applications*. John Wiley & Sons. <https://books.google.com.sa/books?id=6D2ZC3qjYCoC&printsec=frontcover>
- Ahmed S, Ahmad M, Swami BL, Ikram S (2016) A review on plants extracts mediated synthesis of silver nanoparticles for antimicrobial applications: a green expertise. *J Adv Res* 7(1): 17–28. <https://doi.org/10.1016/j.jare.2015.02.007>
- Jamkhande PG, Ghule NW, Bamer AH, Kalaskar MG (2019) Metal nanoparticles synthesis: an overview on methods of preparation, advantages and disadvantages, and applications. *J Drug Deliv Sci Technol* 53:101174. <https://doi.org/10.1016/j.jddst.2019.101174>
- Meyers MA, Mishra A, Benson DJ (2006) Mechanical properties of nanocrystalline materials. *Prog Mater Sci* 51(4):427–556. <https://doi.org/10.1016/j.pmatsci.2005.08.003>
- Nadagouda MN, Speth TF, Varma RS (2011) Microwave-assisted green synthesis of silver nanostructures. *Acc Chem Res* 44(7):469–478. <https://doi.org/10.1021/ar1001457>
- Balamurugan S, Philip AJ, Kiruba V, Veluraja K (2015) Simple and efficient way of synthesizing NiO nanoparticles by combustion followed by ball milling method. *Nanosci Nanotechnol Lett* 7(2):89–93. <https://doi.org/10.1166/nnl.2015.1889>
- Ahmadioltansaraei K, Moghaddam J (2014) Preparation of NiO nanoparticles from Ni(OH)₂·NiCO₃·4H₂O precursor by mechanical activation. *Int J Miner Metall Mater* 21(7):726–735. <https://doi.org/10.1007/s12613-014-0964-z>
- Fiss BG, Vu NN, Douglas G, Do TO, Friščić T, Moores A (2020) Solvent-free mechanochemical synthesis of ultrasmall nickel phosphide nanoparticles and their application as a catalyst for the hydrogen evolution reaction (HER). *ACS Sustain Chem Eng* 8(32):12014–12024. <https://doi.org/10.1021/acssuschemeng.0c02762>
- Tang A, Li X, Zhou Z, Ouyang J, Yang H (2014) Mechanochemical synthesis of Ni(OH)₂ and the decomposition to NiO nanoparticles: thermodynamic and optical spectra. *J Alloy Compd* 600:204–209. <https://doi.org/10.1016/j.jallcom.2014.02.120>
- Gondal MA, Saleh TA, Drmash QA (2012) Synthesis of nickel oxide nanoparticles using pulsed laser ablation in liquids and their optical characterization. *Appl Surf Sci* 258(18):6982–6986. <https://doi.org/10.1016/j.apsusc.2012.03.147>
- Khashan KS, Sulaiman GM, Hamad AH, Abdulameer FA, Hadi A (2017) Generation of NiO nanoparticles via pulsed laser ablation in deionised water and their antibacterial activity. *Appl Phys A* 123(3):190. <https://doi.org/10.1007/s00339-017-0826-4>
- Mahdi, R. O., Hadi, A. A., Taha, J. M., & Khashan, K. S. (2020, March). Preparation of nickel oxide nanoparticles prepared by laser ablation in water. In *AIP Conference Proceedings* (Vol. 2213, No. 1, p. 020309). AIP Publishing LLC. <https://doi.org/10.1063/5.0000116>
- Safa M, Dorrnian D, Masoudi AA, Matin LF (2019) Characterizing nickel oxide nanostructures produced by laser ablation method: effects of laser fluence. *Appl Phys A* 125(10):1–9. <https://doi.org/10.1007/s00339-019-2986-x>
- Karpinski A, Ferrec A, Richard-Plouet M, Cattin L, Djouadi MA, Brohan L, Jouan PY (2012) Deposition of nickel oxide by direct current reactive sputtering: effect of oxygen partial pressure. *Thin Solid Films* 520(9):3609–3613. <https://doi.org/10.1016/j.tsf.2011.12.068>
- Li G, Jiang Y, Deng S, Tam A, Xu P, Wong M, Kwok HS (2017) Overcoming the limitations of sputtered nickel oxide for high-efficiency and large-area perovskite solar cells. *Advanced Science* 4(12):1700463. <https://doi.org/10.1002/advsc.201700463>
- Salunkhe P, Ali AVM, Kekuda D (2020) Investigation on tailoring physical properties of nickel oxide thin films grown by dc magnetron sputtering. *Mater Res Express* 7(1):016427. <https://doi.org/10.1088/2053-1591/ab69c5>
- Peng, J., Xu, Z., Wang, S., Jie, Q., & Chen, C. (2010). Preparation and performance of nickel oxide thin films by ion beam sputtering deposition and oxidation annealing. *Sensors and Materials*, 22(8), 409–416. https://myukk.org/SM2017/sm_pdf/SM820.pdf
- Lin CW, Chung WC, Zhang ZD, Hsu MC (2017) P-channel transparent thin-film transistor using physical-vapor-deposited NiO layer. *Jpn J Appl Phys* 57(1S):01AE01. <https://doi.org/10.7567/JJAP.57.01AE01>
- Moravec, P., Keskinen, H., Jyrki, M. M., Bakardjieva, S., & Levinský, V. V. (2011). NiO x nanoparticle synthesis by chemical vapor deposition from nickel acetylacetonate. *Materials Sciences and Applications*, 2(04), 258. <https://www.scirp.org/html/4360.html>
- Napari M, Huq TN, Hoye RL, MacManus-Driscoll JL (2020) Nickel oxide thin films grown by chemical deposition techniques: potential and challenges in next-generation rigid and flexible device applications. *InfoMat*. <https://doi.org/10.1002/inf2.12146>
- Pooyandeh, S., Shahidi, S., Khajehnezhad, A., & Ghoranneviss, Z. (2020) Synthesizing and deposition of nickel oxide nanoparticles on glass mat using sol–gel method (morphological and magnetic properties) *J Text Inst* 1–9. <https://doi.org/10.1080/00405000.2020.1785606>
- Shamim, A., Ahmad, Z., Mahmood, S., Ali, U., Mahmood, T., & Ahmad, Z. (2019). Synthesis of nickel nanoparticles by sol-gel method and their characterization. *Open J. Chem.* 2(1), 16–20. <https://pdfs.semanticscholar.org/0c75/3ea0c2700b6f6449f17873f8b713fbec9f7f.pdf><https://>
- Zorkipli NNM, Kaus NHM, Mohamad AA (2016) Synthesis of NiO nanoparticles through sol-gel method. *Procedia Chemistry* 19:626–631. <https://doi.org/10.1016/j.proche.2016.03.062>
- Abboud M, Haija MA, Bel-Hadj-Tahar R, Mubarak AT, Ismail I, Hamdy MS (2020) Highly ordered mesoporous flower-like NiO nanoparticles: synthesis, characterization and photocatalytic performance. *New J Chem* 44(8):3402–3411. <https://doi.org/10.1039/C9NJ04955J>
- Ebin B (2018) Simple preparation of Ni and NiO nanoparticles using raffinate solution originated from spent NiMH battery recycling. *J Inorg Organomet Polym Mater* 28(6):2554–2563. <https://doi.org/10.1007/s10904-018-0926-4>
- Bahari Molla Mahaleh, Y., Sadmezzaad, S. K., & Hosseini, D. (2008). NiO nanoparticles synthesis by chemical precipitation and effect of applied surfactant on distribution of particle size *J Nanomater* 2008 <https://doi.org/10.1155/2008/470595>
- El-Kemary M, Nagy N, El-Mehasseb I (2013) Nickel oxide nanoparticles: synthesis and spectral studies of interactions with glucose. *Mater Sci Semicond Process* 16(6):1747–1752. <https://doi.org/10.1016/j.mssp.2013.05.018>

- Cao S, Peng L, Han T, Liu B, Zhu D, Zhao C, He S (2020) Hydrothermal synthesis of nanoparticles-assembled NiO microspheres and their sensing properties. *Physica E* 118: 113655. <https://doi.org/10.1016/j.physe.2019.113655>
- Zhou Q, Lu Z, Wei Z, Xu L, Gui Y, Chen W (2018) Hydrothermal synthesis of hierarchical ultrathin NiO nanoflakes for high-performance CH₄ sensing. *Front Chem* 6:194. <https://doi.org/10.3389/fchem.2018.00194>
- Ahire, D. V., Patil, G. E., Jain, G. H., & Gaikwad, V. B. (2012, December). Synthesis of nanostructured NiO by hydrothermal route and its gas sensing properties. In 2012 Sixth International Conference on Sensing Technology (ICST) (pp. 136–141). IEEE. <https://doi.org/10.1109/ICST.2012.6461656>
- Gu Y, Sun S, Liu Y, Dong M, Yang Q (2019) Solvent effect on the solvothermal synthesis of mesoporous NiO catalysts for activation of peroxymonosulfate to degrade organic dyes. *ACS Omega* 4(18):17672–17683. <https://doi.org/10.1021/acsomega.9b01883>
- Beach ER, Shqau K, Brown SE, Rozeveld SJ, Morris PA (2009) Solvothermal synthesis of crystalline nickel oxide nanoparticles. *Mater Chem Phys* 115(1):371–377. <https://doi.org/10.1016/j.matchemphys.2008.12.018>
- Ukoba KO, Eloka-Eboka AC, Inambao FL (2018) Review of nanostructured NiO thin film deposition using the spray pyrolysis technique. *Renew Sustain Energy Rev* 82:2900–2915. <https://doi.org/10.1016/j.rser.2017.10.041>
- Desai JD (2016) Nickel oxide thin films by spray pyrolysis. *J Mater Sci Mater Electron* 27(12):12329–12334. <https://doi.org/10.1007/s10854-016-5617-8>
- Dillon F, Copley M, Koós AA, Bishop P, Grobert N (2013) Flame spray pyrolysis generated transition metal oxide nanoparticles as catalysts for the growth of carbon nanotubes. *RSC Adv* 3(43):20040–20045. <https://doi.org/10.1039/C3RA40773J>
- Seo DJ, Park SB, Kang YC, Choy KL (2003) Formation of ZnO, MgO and NiO nanoparticles from aqueous droplets in flame reactor. *J Nanopart Res* 5(3):199–210. <https://doi.org/10.1023/A:1025563031595>
- Salvadori MR, Ando RA, Oller Nascimento CA, Corrêa B (2015) Extra and intracellular synthesis of nickel oxide nanoparticles mediated by dead fungal biomass. *PLoS ONE* 10(6): e0129799. <https://doi.org/10.1371/journal.pone.0129799>
- Yang P, Gu H, Zhao Z, Wang W, Cao B, Lai C, Wang X (2014) Angiotensin-converting enzyme 2 (ACE2) mediates influenza H7N9 virus-induced acute lung injury. *Sci Rep* 4(1):1–6. <https://doi.org/10.1038/srep07027>
- Habtemariam AB, Oumer M (2020) Plant extract mediated synthesis of nickel oxide nanoparticles. *Mater Int* 2:205–209. <https://doi.org/10.33263/Materials22.205209>
- Z Sabouri N Fereydouni A Akbari HA Hosseini A Hashemzadeh MS Amiri M Darroudi 2019 Plant-based synthesis of NiO nanoparticles using salvia macrosiphon Boiss extract and examination of their water treatment *Rare Met* 1–11 <https://doi.org/10.1007/s12598-019-01333-z>
- Helan V, Prince JJ, Al-Dhabi NA, Arasu MV, Ayeshamariam A, Madhumitha G, Jayachandran M (2016) Neem leaves mediated preparation of NiO nanoparticles and its magnetization, coercivity and antibacterial analysis. *Results Phys* 6:712–718. <https://doi.org/10.1016/j.rinp.2016.10.005>
- Ramalingam R, Fazil MHUT, Verma NK, Arunachalam KD (2019) Green synthesis, characterization and antibacterial evaluation of electrospun nickel oxide nanofibers. *Mater Lett* 256:1266–16. <https://doi.org/10.1016/j.matlet.2019.126616>
- Zhang Y, Xiao X, Sun Y, Shi Y, Dai H, Ni P, Wang L (2013) Electrochemical deposition of nickel nanoparticles on reduced graphene oxide film for nonenzymatic glucose sensing. *Electroanalysis* 25(4):959–966. <https://doi.org/10.1002/elan.201200479>
- Moghaddam AB, Ganjali MR, Saboury AA, Moosavi-Movahedi AA, Norouzi P (2008) Electrodeposition of nickel oxide nanoparticles on glassy carbon surfaces: application to the direct electron transfer of tyrosinase. *J Appl Electrochem* 38(9):1233–1239. <https://doi.org/10.1007/s10800-008-9541-3>
- Azhagu Raj R, AlSalhi MS, Devanesan S (2017) Microwave-assisted synthesis of nickel oxide nanoparticles using Coriandrum sativum leaf extract and their structural-magnetic catalytic properties. *Materials* 10(5):460. <https://doi.org/10.3390/ma10050460>
- Jena, A., & Shivashankar, S. A. (2008, October). Microwave-assisted synthesis of NiO nanoparticles. In AIP Conference Proceedings (Vol. 1063, No. 1, pp. 211–216). American Institute of Physics. <https://doi.org/10.1063/1.3027161>
- Vargas E, Romero-Sáez M, Denardin JC, Gracia F (2016) The ultrasound-assisted synthesis of effective monodisperse nickel nanoparticles: magnetic characterization and its catalytic activity in CO₂ methanation. *New J Chem* 40(9):7307–7310. <https://doi.org/10.1039/C6NJ01574C>
- A Alshammari VN Kalevaru 2016 Supported gold nanoparticles as promising catalysts *Catalytic Application of Nano-Gold Catalysts* 57–81
- Barhoum A, Van Assche G, Rahier H, Fleisch M, Bals S, Delplanck MP, Bahnemann D (2017) Sol-gel hot injection synthesis of ZnO nanoparticles into a porous silica matrix and reaction mechanism. *Mater Des* 119:270–276. <https://doi.org/10.1016/j.matdes.2017.01.059>
- Badari CA, Lónyi F, Drotár E, Kaszonyi A, Valyon J (2015) A study of the hydrodenitrogenation of propylamine over supported nickel phosphide catalysts using amorphous and nanostructured silica supports. *Appl Catal B* 164:48–60. <https://doi.org/10.1016/j.apcatb.2014.09.001>
- Rudko, G. Y., Kovalenko, S. A., Gule, E. G., Bobyk, V. V., Solomakha, V. M., & Bogoslovskaya, A. B. (2015). Zinc oxide nanoparticles fabricated in the porous silica matrix by the sublimation method. *Semiconductor physics quantum electronics & optoelectronics*, (18, № 1), 20–25. <https://dspace.nbu.gov.ua/handle/123456789/119991>
- Ashik UPM, Daud WW (2015) Probing the differential methane decomposition behaviors of n-Ni/SiO₂, n-Fe/SiO₂ and n-Co/SiO₂ catalysts prepared by co-precipitation cum modified Stöber method. *RSC Adv* 5(82):67227–67241. <https://doi.org/10.1039/C5RA10997C>
- Corma A (1997) From microporous to mesoporous molecular sieve materials and their use in catalysis. *Chem Rev* 97(6): 2373–2420. <https://doi.org/10.1021/cr960406n>
- Vadia, N., Desai, D., & Rajput, S. (2013). Hydrothermal treatment and mesoporosity of MCM-41 mesoporous nanocomposite. *Journal of Applied Pharmaceutical Science*, 3(3), 24. https://japsonline.com/admin/php/uploads/812_pdf.pdf

- Look DC, Claffin B (2004) P-type doping and devices based on ZnO. *Physica Status Solidi (b)* 241(3):624–630. <https://doi.org/10.1002/pssb.200304271>
- Rioux, R. (2010). *Model Systems in Catalysis*. Springer, Ed. 1, New York, NY. pp XIX, 526. <https://doi.org/10.1007/978-0-387-98049-2>
- Rodríguez JA, García MF (2007) The world of oxide nanomaterials. John Wiley & Sons Inc, Hoboken, NJ, p 15
- Penner S (2014) Pure and mixed-oxide thin film model systems grown on sodium chloride templates for structural and catalytic studies. *Thin Solid Films* 562:1–15. <https://doi.org/10.1016/j.tsf.2014.03.001>
- Finiels A, Fajula F, Hulea V (2014) Nickel-based solid catalysts for ethylene oligomerization—a review. *Catal Sci Technol* 4(8):2412–2426. <https://doi.org/10.1039/C4CY00305E>
- Schubert, U., & Hüsing, N. (2005). *Synthesis of inorganic materials*, 2nd. *Synthesis of Inorganic Materials*, 429.
- Ozin, G. A., Arsenault, A. C., & Cademartiri, L. (2009). Nanocrystal synthesis and self-assembly. *Nanochemistry: A Chemical Approach to Nanomaterials*, 335. <https://books.google.com.sa/books?id=CdrUwo3HvPwC&printsec=frontcover>
- Frey AS, Hinrichsen O (2012) Comparison of differently synthesized Ni (Al) MCM-48 catalysts in the ethene to propene reaction. *Microporous Mesoporous Mater* 164:164–171. <https://doi.org/10.1016/j.micromeso.2012.07.015>
- S He L, Zhang S He L Mo X Zheng H Wang Y Luo 2015 Ni/SiO2 catalyst prepared with nickel nitrate precursor for combination of CO2 reforming and partial oxidation of methane: characterization and deactivation mechanism investigation *J Nanomater* 2015 <https://doi.org/10.1155/2015/659402>
- Nakagawa Y, Nakazawa H, Watanabe H, Tomishige K (2012) Total hydrogenation of furfural over a silica-supported nickel catalyst prepared by the reduction of a nickel nitrate precursor. *ChemCatChem* 4(11):1791–1797. <https://doi.org/10.1002/cctc.201200218>
- Yao T, Sun Z, Li Y, Pan Z, Wei H, Xie Y, Wei S (2010) Insights into initial kinetic nucleation of gold nanocrystals. *J Am Chem Soc* 132(22):7696–7701. <https://doi.org/10.1021/ja101101d>
- Zhao K, Hu Y, Tian Y, Chen D, Feng Y (2020) Chlorine removal from MSWI fly ash by thermal treatment: effects of iron/aluminum additives. *J Environ Sci* 88:112–121. <https://doi.org/10.1016/j.jes.2019.08.006>
- Spagnolo S, Spolaore M, Dalla Palma M, Pasqualotto R, Sartori E, Serianni G, Veltri P (2016) Preliminary design of electrostatic sensors for MITICA beam line components. *Rev Sci Instrum* 87(2):02B931. <https://doi.org/10.1063/1.4935612>
- Bianchi CL, Canton P, Dimitratos N, Porta F, Prati L (2005) Selective oxidation of glycerol with oxygen using mono and bimetallic catalysts based on Au, Pd and Pt metals. *Catal Today* 102:203–212. <https://doi.org/10.1016/j.cattod.2005.02.003>
- Patil GA, Bari ML, Bhanvase BA, Ganvir V, Mishra S, Sonawane SH (2012) Continuous synthesis of functional silver nanoparticles using microreactor: effect of surfactant and process parameters. *Chem Eng Process* 62:69–77. <https://doi.org/10.1016/j.cep.2012.09.007>
- Mehrabadi BA, Eskandari S, Khan U, White RD, Regalbutto JR (2017) A review of preparation methods for supported metal catalysts. *Adv Catal* 61:1–35. <https://doi.org/10.1016/bs.acat.2017.10.001>
- Kennedy J, Jones W, Morgan DJ, Bowker M, Lu L, Kiely CJ, Dimitratos N (2015) Photocatalytic hydrogen production by reforming of methanol using Au/TiO2, Ag/TiO2 and Au-Ag/TiO2 catalysts. *Catal Struct React* 1(1):35–43. <https://doi.org/10.1179/2055075814Y.0000000006>
- Jia CJ, Schüth F (2011) Colloidal metal nanoparticles as a component of designed catalyst. *Phys Chem Chem Phys* 13(7):2457–2487. <https://doi.org/10.1039/C0CP02680H>
- Yoshida, H., Nonoyama, S., Yazawa, Y., & Hattori, T. (2005). Quantitative determination of platinum oxidation state by XANES analysis. *Physica Scripta*, 2005(T115), 813. <https://iopscience.iop.org/article/.https://doi.org/10.1238/Physica.Topical.115a00813/meta>
- Chen S, Yang Q, Wang H, Zhang S, Li J, Wang Y, Song L (2015) Initial reaction mechanism of platinum nanoparticle in methanol–water system and the anomalous catalytic effect of water. *Nano Lett* 15(9):5961–5968. <https://doi.org/10.1021/acs.nanolett.5b02098>
- Zhou QF, Bao JC, Xu Z (2002) Shape-controlled synthesis of nanostructured gold by a protection–reduction technique. *J Mater Chem* 12(2):384–387. <https://doi.org/10.1039/B103767F>
- Paulose R, Mohan R, Parihar V (2017) Nanostructured nickel oxide and its electrochemical behaviour—a brief review. *Nano-Struct Nano-Objects* 11:102–111
- Aboud M (2020) Immediate epoxidation of cyclohexene at room temperature using mesoporous flower-like NiO nanoparticles. *RKM Cat* 131:781–792. <https://doi.org/10.1007/s11144-020-01864-y>
- Behnajady MA, Bimeghdar S (2014) Synthesis of mesoporous NiO nanoparticles and their application in the adsorption of Cr(VI). *Chem Eng J* 239:105–113. <https://doi.org/10.1016/j.cej.2013.10.102>
- Sahlabji T, Aboud M, Bel-Hadj-Tahar R, Hamdy MS (2020) Spontaneous epoxidation of styrene catalyzed by flower-like NiO nanoparticles under ambient conditions. *J Nanopart Res* 22(12):1–10. <https://doi.org/10.1007/s11051-020-05098-w>
- Nasseri MA, Ahrari F, Zakerinasab B (2015a) Nickel oxide nanoparticles: a green and recyclable catalytic system for the synthesis of diindoloxindole derivatives in aqueous medium. *RSC Adv* 5(18):13901–13905. <https://doi.org/10.1039/C4RA14551H>
- Nasseri MA, Kamali F, Zakerinasab B (2015b) Catalytic activity of reusable nickel oxide nanoparticles in the synthesis of spirooxindoles. *RSC Adv* 5(34):26517–26520. <https://doi.org/10.1039/C5RA02825F>
- Arrigo R, Gallarati S, Schuster ME, Seymour J, Gianolio D, da Silva I, Held G (2020) Influence of synthesis conditions on the structure of nickel nanoparticles and their reactivity in selective asymmetric hydrogenation. *ChemCatChem* 12(5):1491–1503. <https://doi.org/10.1002/cctc.201901955>
- Bashir AKH, Razanamahandry LC, Nwanya AC, Kaviyarasu K, Saban W, Mohamed HEA, Maaza M (2019) Biosynthesis of NiO nanoparticles for photodegradation of free cyanide solutions under ultraviolet light. *J Phys Chem Solids* 134:133–140. <https://doi.org/10.1016/j.jpcs.2019.05.048>
- Amin MH (2020) Relationship between the pore structure of mesoporous silica supports and the activity of nickel

- nanocatalysts in the CO₂ reforming of methane. *Catalysts* 10(1):51. <https://doi.org/10.3390/catal10010051>
- Weiping, C., & Lide, Z. (1997). Synthesis and structural and optical properties of mesoporous silica containing silver nanoparticles. *Journal of Physics: Condensed Matter*, 9(34), 7257. [https://iopscience.iop.org/article/](https://iopscience.iop.org/article/.). <https://doi.org/10.1088/0953-8984/9/34/015/meta>
- Lai, C. Y. (2013). Mesoporous silica nanomaterials applications in catalysis. *J Thermodyn Catal*, 5(1), 1000e124. <https://www.longdom.org/open-access/mesoporous-silica-nanomaterials-applications-in-catalysis-2157-7544.1000e124.pdf>
- Dixit M, Mishra M, Joshi PA, Shah DO (2013) Study on the catalytic properties of silica supported copper catalysts. *Procedia Engineering* 51:467–472. <https://doi.org/10.1016/j.proeng.2013.01.066>
- Luque R, Balu AM, Campelo JM, Gracia MD, Losada E, Pineda A, Serrano-Ruiz JC (2012) Catalytic applications of mesoporous silica-based materials. *Catalysis* 24:253–280. <https://doi.org/10.1039/9781849734776-00253>
- Jadhav KS, Dumbare PS, Pande VV (2015) Mesoporous silica nanoparticles (MSN): a nanonetwork and hierarchical structure in drug delivery. *J Nanomed Res* 2(5):1–8. <https://doi.org/10.15406/jnmr.2015.02.00043>
- Baharudin KB, Taufiq-Yap YH, Hunns J, Isaacs M, Wilson K, Derawi D (2019) Mesoporous NiO/Al-SBA-15 catalysts for solvent-free deoxygenation of palm fatty acid distillate. *Microporous Mesoporous Mater* 276:13–22. <https://doi.org/10.1016/j.micromeso.2018.09.014>
- Baktash E, Littlewood P, Pfrommer J, Schomäcker R, Driess M, Thomas A (2015) Controlled formation of nickel oxide nanoparticles on mesoporous silica using molecular Ni₄O₄ clusters as precursors: enhanced catalytic performance for dry reforming of methane. *ChemCatChem* 7(8):1280–1284. <https://doi.org/10.1002/cctc.201402983>
- Lu B, Ju Y, Kawamoto K (2014) Conversion of producer gas using NiO/SBA-15 obtained with different synthesis methods. *Int J Coal Sci Technol* 1(3):315–320. <https://doi.org/10.1007/s40789-014-0037-y>
- Ahmed RA, Pang YX, Olea M, Hodgson SNB (2012) Preparation and structural characterisation of SBA-15 supported nickel catalysts via sol-gel nickel oxide coatings for dry reforming of methane. *WIT Trans Eng Sci* 81:71–82
- Liu D, Quek XY, Wah HHA, Zeng G, Li Y, Yang Y (2009) Carbon dioxide reforming of methane over nickel-grafted SBA-15 and MCM-41 catalysts. *Catal Today* 148(3–4): 243–250. <https://doi.org/10.1016/j.cattod.2009.08.014>
- Schumacher K, Ravikovitch PI, Du Chesne A, Neimark AV, Unger KK (2000) Characterization of MCM-48 materials. *Langmuir* 16(10):4648–4654. <https://doi.org/10.1021/la991595i>
- Roosta Z, Izadbakhsh A, Sanati AM, Osfour S (2018) Synthesis and evaluation of NiO@MCM-41 core-shell nanocomposite in the CO₂ reforming of methane. *J Porous Mater* 25(4): 1135–1145. <https://doi.org/10.1007/s10934-017-0525-8>
- Zhang Q, Zhang T, Shi Y, Zhao B, Wang M, Liu Q, Wang J, Long K, Duan Y, Ning P (2017) A sintering and carbon-resistant Ni-SBA-15 catalyst prepared by solid-state grinding method for dry reforming of methane. *J CO₂ Utilization* 17:10–19. <https://doi.org/10.1016/j.jcou.2016.11.002>
- Zhang J, Li F (2015) Coke-resistant Ni@SiO₂ catalyst for dry reforming of methane. *Appl Catal B* 176:513–521. <https://doi.org/10.1016/j.apcatb.2015.04.039>
- Kresge CT, Leonowicz ME, Roth WJ, Vartuli JC, Beck JS (1992) Ordered mesoporous molecular sieves synthesized by a liquid-crystal template mechanism. *Nature* 359(6397):710–712. <https://doi.org/10.1038/359710a0>
- Mokri, N. A., Ching, O. P., Mukhtar, H., & Leng, C. T. (2019). Tailoring Particle Size and Agglomeration State of Mesoporous MCM-48 via Optimisation of Sol-gel Silica Process. *Journal of Physical Science*, 30(1). <https://doi.org/10.21315/jps2019.30.1.11>
- M Shaban A Hamd RR Amin MR Abukhadra AA Khalek AAP Khan AM Asiri 2020 Preparation and characterization of MCM-48/nickel oxide composite as an efficient and reusable catalyst for the assessment of photocatalytic activity *Environ Sci Pollut Res* 1–13. <https://doi.org/10.1007/s11356-020-09431-7>
- Jansen JC, Shan Z, Marchese L, Zhou W, Puil N v d, Maschmeyer T (2001) A new templating method for three-dimensional mesopore networks. *Chem Comm* 8:713–714. <https://doi.org/10.1039/B101000J>
- Telalović S, Ramanathan A, Mul G, Hanefeld U (2010) TUD-1: synthesis and application of a versatile catalyst, carrier, material. *J Mater Chem* 20(4):642–658. <https://doi.org/10.1039/B904193A>
- Gorsd MN, Sosa AA, Frenzel RA, Pizzio LR (2018) Synthesis and characterization of tungstophosphoric acid-modified mesoporous sponge-like TUD-1 materials. *J Sol-Gel Sci Technol* 87(1):204–215. <https://doi.org/10.1007/s10971-018-4677-z>
- Tanglumlert W, Yang ST, Jeong KE, Jeong SY, Ahn WS (2011) Facile synthesis of Ti-TUD-1 for catalytic oxidative desulfurization of model sulfur compounds. *Res Chem Intermed* 37(9):1267–1273. <https://doi.org/10.1007/s11164-011-0393-9>
- Quek XY, Liu D, Cheo WNE, Wang H, Chen Y, Yang Y (2010) Nickel-grafted TUD-1 mesoporous catalysts for carbon dioxide reforming of methane. *Appl Catal B* 95(3–4):374–382. <https://doi.org/10.1016/j.apcatb.2010.01.016>
- Malleshm B, Sudarsanam P, Venkata Shiva Reddy B, Govinda Rao B, Reddy BM (2018) Nanostructured nickel/silica catalysts for continuous flow conversion of levulinic acid to γ -valerolactone. *ACS omega* 3(12):16839–16849. <https://doi.org/10.1021/acsomega.8b02008>
- Shi P, Liu CJ (2009) Characterization of silica supported nickel catalyst for methanation with improved activity by room temperature plasma treatment. *Catal Lett* 133(1):112–118. <https://doi.org/10.1007/s10562-009-0163-0>
- Pandey PC, Mitra MD, Tiwari AK, Singh S (2021) Synthetic incorporation of palladium-nickel bimetallic nanoparticles within mesoporous silica/silica nanoparticles as efficient and cheaper catalyst for both cationic and anionic dyes degradation. *J Environ Sci Health A* 56(4):460–472. <https://doi.org/10.1080/10934529.2021.1886793>

Publisher's Note Springer Nature remains neutral with regard to jurisdictional claims in published maps and institutional affiliations.